Data-driven Methods for Reliable Energy Performance Characterisation of Occupied Buildings

Rasmussen, Christoffer

Publication date:
2020

Document Version
Publisher's PDF, also known as Version of record

DTU Compute
Department of Applied Mathematics and Computer Science

Data-driven Methods for Reliable Energy Performance Characterisation of Occupied Buildings

PhD Thesis

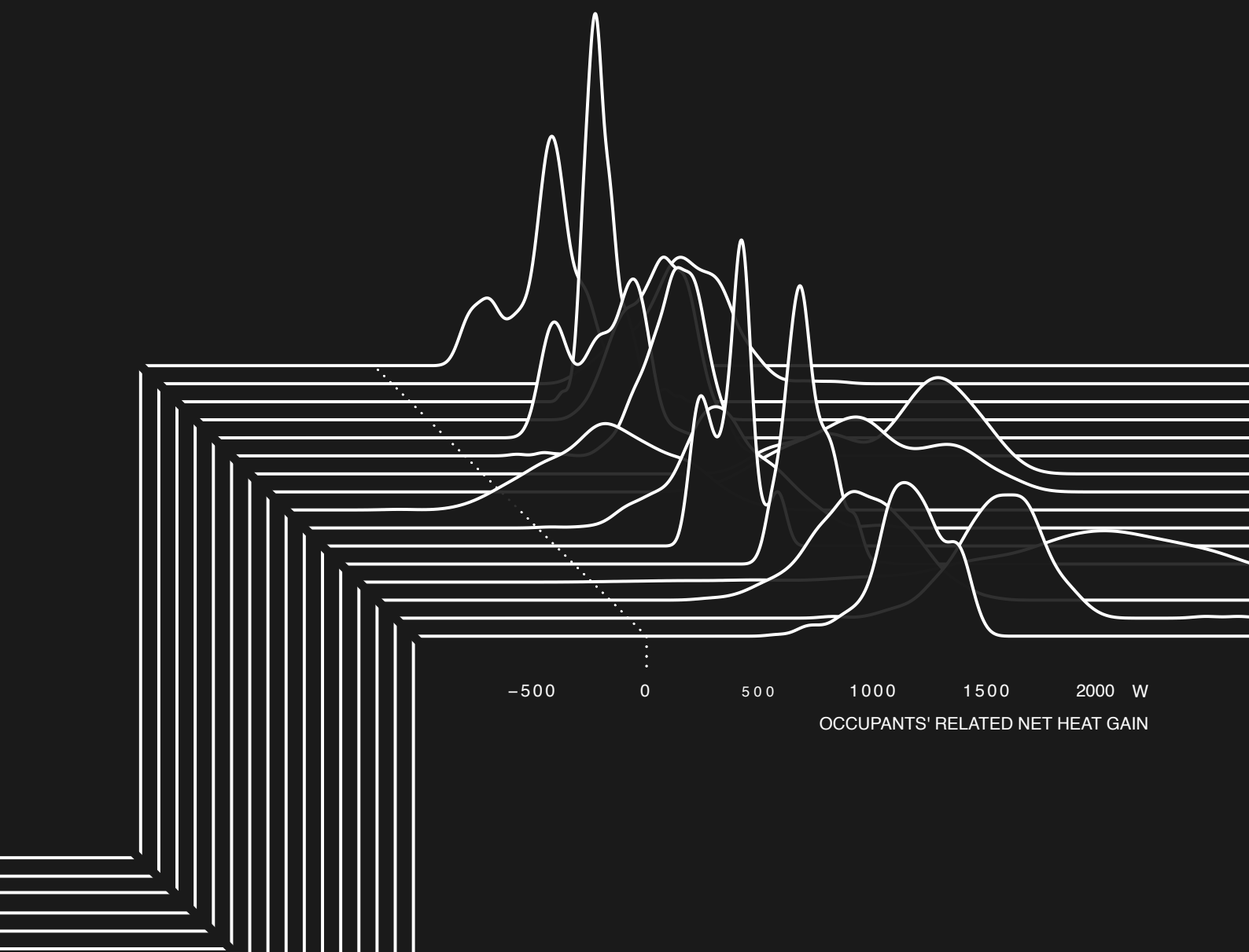

Data-driven Methods for Reliable Energy Performance Characterisation of Occupied Buildings

PhD Thesis
May, 2020

By: Christoffer Rasmussen
Supervisor: Henrik Madsen (DTU Compute)
Co-supervisor: Carsten Rode (DTU Civil Engineering)

Cover illustration: Christoffer Rasmussen, 2020
Histogram of occupants' related net heat gain in 16 single-family houses. The net heat gain comprises electricity use, metabolism, and ventilation loss under the assumption that an indoor temperature of 20 °C is maintained. The results originates from Paper C, *Method for Scalable and Automatised Thermal Building Performance Documentation and Screening*, contained in this thesis.

Published by: DTU, Department of Applied Mathematics and Computer Science, Richard Petersens Plads, Building 324, 2800 Kgs. Lyngby Denmark
www.compute.dtu.dk
ISSN: [0909-3192]

Preface

This PhD thesis was prepared at the Department of Applied Mathematics and Computer Science at the Technical University of Denmark in fulfilment of the requirements for acquiring a PhD degree in Applied Mathematics and Computer Science.

This PhD study is supported financially by the partnership REBUS – Renovating Buildings Sustainably [5151-00002B]. REBUS is funded by Innovation Fund Denmark, Realdania, and the Landowners Investment Fund by 60 %. The remaining financing is established by the partners.

Christoffer Rasmussen

.....

Signature

.....

Date

Summary (English)

Global and increased awareness of climate changes are apparent, and within the EU, strengthened energy policies are put in force to reduce greenhouse gas emissions. By accounting for 40 % of the total energy end-use, buildings are the single most energy-intensive consumer, and the residential sector alone, accounts for 25 % with space heating as the dominant share.

With the current EU Energy Performance in Buildings Directive (EPBD), each member state is instructed to establish a national building renovation plan and conduct an energy performance screening of the building stock. The aim is to increase the building renovation rate and the effect of the renovations.

Despite all the initiatives, there exists a well documented and rather large discrepancy between anticipated and actual energy consumption in buildings. Furthermore, the gap can hardly be quantified by evaluating the energy consumption alone. The reason is that occupants, weather, and the building quality affect it. The focus of this PhD thesis is therefore to develop methods to quantify the performance of buildings and to separate the reasons for the energy use.

Earlier research has shown promising results in terms of identifying thermal building performance characteristics based on data-driven quasi-stationary and dynamical mathematical models. A special focus has been on the transition of modelling techniques applied on unoccupied and thermally controlled test buildings, to reliable modelling techniques applied on occupied buildings.

It has been shown in **Paper C** that methods relying on only heat consumption measurements and weather data are capable of quantifying the heat loss coefficient, solar transmittance, influence of wind, transition period etc. Indications of the occupants' effect on energy use have been estimated as well.

Paper D showed that time constants and the building's energy flexibility (i.e. energy demand-shifting capabilities) can be obtained from measurements of only the indoor and outdoor temperature.

For more detailed dynamical grey-box modelling techniques, a novel approach to sun position dependent solar gain estimation has been proposed in **Paper B**.

The thesis discusses the importance of handling the disturbances caused by the occupants' interaction with the building. In **Paper A**, a method for estimating the occupancy status in dwellings has been proposed, with the intention of describing model noise in grey-box models in a more detailed manner.

The work of this thesis outlines new scalable approaches for documentation and screening of thermal building performance and energy flexibility. New modelling techniques have been presented and discussed in order to increase the reliability of data-driven models. The combination of the intensified energy data collection within the EU and reliable methods for thermal building performance assessments is believed to bring us closer to targeted building renovation strategies, and evidence-based energy performance documentation of buildings.

Resumé (Danish)

En global og øget opmærksomhed på klimaændringer ses tydelig, og inden for EU er skærpede energipolitikker blevet introduceret med det formål at reducere udledningen af drivhusgasser. Med 40 % af det totale energi slut-forbrug, er det bygninger, der har det mest intensive energiforbrug. Boliger alene står for 25 %, hvor rumopvarmning er den dominerende andel.

Med det nuværende EU-direktiv for bygningers energimæssige ydeevne (EPBD), skal hver medlemsstat formulere en national bygningsrenoveringsplan og kortlægge energiydeevnen af bygningsmassen. Målet er at øge bygningsrenoveringsraten og effekten af renoveringerne.

Trods alle initiativerne findes der et veldokumenteret og stort spænd mellem forventet og faktisk energiforbrug i bygninger. I tillæg til det er spændet svært at kvantificere ved alene at evaluere energiforbruget. Dette skyldes, at både brugere, vejr og byggekvalitet påvirker det. Fokusset i denne PhD-afhandling er derfor at udvikle metoder til at kvantificere bygningers ydeevne og at separere årsagerne til energiforbruget.

Tidligere forskning har vist lovende resultater ift. identifikation af termiske bygningsydeevne-karakteristikker baseret på datadrevne kvasi-stationære og dynamiske matematiske modeller. Der har været et særligt fokus på overgangen fra modelleringsteknikker anvendt på ubeboede og termisk kontrollerede testbygninger til pålidelige modelleringsteknikker anvendt på beboede bygninger.

Det er vist i **Artikel C**, at metoder der kun bygger på varmeforbrugsmålinger og vejrdata kan kvantificere varmetabskoefficienten, solindstrålingen, vindens effekt, overgangsperioden m.m. Indikationer af brugernes påvirkning af energiforbruget er ligeledes estimeret.

Artikel D viser, at tidskonstanter og bygningens energifleksibilitet (evnen til at tidsforskyde energibehovet) kan bestemmes ud fra målinger af kun inde- og udetemperatur.

For mere detaljerede dynamiske grey-box-modelleringsteknikker, er der i **Artikel B** forestået en ny tilgang til estimering af solpositionsafhængigt solvarmetilskud.

Afhandlingen diskuterer vigtigheden af at håndtere forstyrrelser forårsaget af brugernes interaktion med bygningen. I **Artikel A** er der fremlagt en metode til at estimere brugerstatussen i boliger. Intentionen er at beskrive modelstøj i grey-box-modeller mere detaljeret.

Afhandlingen udlægger nye skalerbare metoder til at dokumentere og kortlægge termisk bygningsydeevne og energifleksibilitet. Nye modelleringsteknikker er blevet præsenteret og diskuteret med det formål at øge troværdigheden af datadrevne modeller. Kombinationen af den intensiverede energidataindsamling i EU og troværdige metoder til at bestemme bygningers ydeevne vil antageligt bringe os tættere på målrettede bygningsrenoveringsstrategier og evidensbaseret dokumentation af bygningers energimæssige ydeevne.

Acknowledgements

I would like to thank my two supervisors Henrik Madsen (DTU Compute) and Carsten Rode (DTU Civil Engineering) for giving a building engineer like me, the opportunity to dig into the world of statistics and mathematical modelling. It has been challenging, but an extremely worth-while experience. A special thanks to Henrik Madsen for giving me time and headspace to grasp all the new concepts I have been introduced to — it is appreciated.

I would also like to thank my colleagues and those I share office and have the everyday conversations with: Hjörleifur Bergsteinsson, Jaume Palmer Real, Dominik Dominkovic, and Rune Grønborg Junker. Especially Rune Grønborg Junker deserves big thanks. You have strong fundamental knowledge about statistics and mathematical modelling and an exceptional ability to explain it in an extremely clear manner. All the hours we have talked about statistics and mathematical modelling have taught me a lot.

Thank you Rune Grønborg Junker and Niclas Brabrand Brok for taking your time to read and give me feedback on this thesis.

I would also like to thank my unofficial supervisor, Peder Bacher. You have been a great help during the last years, and it is always a pleasure to work and travel to different meetings all across Europe with you.

A special thank to my former colleague Rishi Relan is suitable a well. Thank you for all of your help and good conversations on everything from A to Z.

A big thank to KU Leuven, Department of Building Physics, in Belgium for hosting me for three months during the Autumn, 2018. And special thank to Staf Roels and Dirk Saelens for being my supervisors during my stay, and for many fruitful conversations afterwards.

The countless discussions with the participants of the IEA-EBC Annex 71 project and the REBUS partners are much appreciated as well.

A final thank is given to my former colleagues at VELUX, Department of Daylight, Energy and Indoor Climate, and especially Thorbjørn Færing Asmussen for introducing me to VBA programming and data science. That is what led me to the DTU course on introduction to statistics, a series of online courses on machine learning and data science, and ultimately a PhD at the Department of Applied Mathematics and Computer Science, DTU.

List of Works

During the period from January 2017 to May 2020, the work of this PhD study has been disseminated in a total number of four articles and 18 presentations as listed below. The letters assigned to each of the articles are used throughout this report, including in the List of Figures.

Publications

Peer-Reviewed

A Christoffer Rasmussen, Rishi Relan and Henrik Madsen. "Identification of Occupancy Status by Statistical Change Point Detection of CO_2 Concentration". *2018 IEEE Conference on Control Technology and Applications (CCTA)*, August 21-24, 2018.

B Christoffer Rasmussen, Linde Frölke, Peder Bacher, Henrik Madsen and Carsten Rode. "Semi-parametric Modelling of Sun Position Dependent Solar Gain Using B-splines in Grey-box Models". *Solar Energy*, Volume 195, January 1, 2020.

Submitted

C Christoffer Rasmussen, Peder Bacher, Davide Calì, Henrik Aalborg Nielsen and Henrik Madsen. "Method for Ccalable and Automatised Thermal Building Performance Documentation and Screening". *Energies*, May, 2020.

D Jaume Palmer Real, Christoffer Rasmussen, Rongling Li, Kenneth Leerbeck, Ole Michael Jensen, Kim B. Wittchen and Henrik Madsen. "Characterization of Energy Dynamics of Residential Buildings with Scarce Data", *Energy and Buildings*, May, 2020.

Presentations

1. Christoffer Rasmussen. "Bridging the Building Performance Gap". Pitch at the PhD Bazaar 2017, May 10, 2017, Technical University of Denmark, Denmark.

2. Christoffer Rasmussen. "Bridging the Building Performance Gap – Tools for Reliable Energy Performance Characterisation of Buildings". 4th CITIES consortium meeting, Poster session, May 30-31, 2017, The Danish Technological Institute, Aarhus, Denmark.

3. Christoffer Rasmussen, Peder Bacher, Henrik Madsen. "ARX Models for Building Energy Performance Assessment Based on In-Situ Measurements". IEA-EBC Annex 71 – 3rd Expert meeting, October 24, 2017, Université Savoie Mont Blanc, Chambéry, France.

4. Davide Calì and Christoffer Rasmussen, "Smart Buildings Retrofit Accelerator: Making Housing Energy Renovation an Investment Opportunity", Nordic Ideation Day 2018, January, 2018, Aalto University, Helsinki, Finnland.

5. Christoffer Rasmussen, Peder Bacher, Henrik Madsen. "Grey-box Models For Building Energy Performance Assessment Based on In-situ Measurements". IEA-EBC Annex 71 – 4th Expert meeting, April 9, 2018, Faculté d'Architecture LOCI, Bruxelles, Belgium.

6. Christoffer Rasmussen, Giulia De Zotti, Henrik Madsen. "Bridging the Building Performance Gap". Lecture at PhD summer school, August 20, 2018, EnergyLab Nordhavn, Copenhagen, Denmark.

7. Christoffer Rasmusen, Rishi Relan and Henrik Madsen. "Identification of Occupancy Status by Statistical Change Point Detection of CO_2 Concentration". 2018 IEEE Conference on Control Technology and Applications (CCTA), August 21-24, 2018, Scandic, Copenhagen, Denmark.

8. Christoffer Rasmusen, Henrik Madsen and Carsten Rode. "Data-Driven Approaches for Reliable Energy Labelling of Buildings". INSPIRE Conference 2018, September 18-21, 2018, Koningin Elisabethzaal, Antwerp, Belgium.

9. Christoffer Rasmussen, Peder Bacher, Henrik Madsen. "ARX and Grey-box Models For Building Energy Performance Assessment Based on In-situ Measurements (Continued)". IEA-EBC Annex 71 – 5th Expert meeting, October 18, 2018, University of Innsbruck, Campus Technology, Innsbruck, Austria.

10. Christoffer Rasmussen, Henrik Madsen, Sebastian Wolf. "Tools for Reliable Energy Performance Characterisation of Buildings". REBUS workshop – Tools for Reliable Energy Performance Characterisation of Buildings, January 18, 2019, The Technical University of Denmark, Kgs. Lyngby, Denmark.

11. Christoffer Rasmussen, Andrea Mazzucco and Renato Ezban. "Kan data give bedre renoveringer? Seks bud på, hvordan vi med nytænkning af bygningsdata kan opnå bedre renoveringer. (Can data provide better building renovations? Six suggestions of how we can utilise building data in new ways to achieve better building renovations.)". Video, January 18, 2019, Online: http://rebus.nu/aktuelt/kan-data-give-bedre-renoveringer/.

12. Christoffer Rasmussen, Peder Bacher, Henrik Madsen. "Grey-box Modelling and Validation – First Steps Towards Identification of Occupants Effect on Heat Consumption". IEA-EBC Annex 71 – 6th Expert meeting, April 8, 2019, University of the Basque Country, Bilbao, Spain.

13. Christoffer Rasmussen, Henrik Madsen, Carsten Rode and Sebastian Wolf. "Energy Efficiency of Buildings (CITIES + REBUS)". CITIES Presentation, June 3, 2019, The Technical University of Denmark, Kgs. Lyngby, Denmark.

14. Christoffer Rasmussen, Carsten Rode, Henrik Madsen. "Er Data det Nye Guld i Renoveringer? (Are Data the New Gold in Building Renovations?)". Presentation and Q&A at REBUS partner group meeting, June 6, 2019, The Danish Technological Institute, Taastrup, Denmark.

15. Christoffer Rasmussen, Rune Juhl, Peder Bacher, Henrik Madsen. "REBUS – Renovating Buildings Sustainably". Lecture at Summer School 2019 - Dynamic Calculation Methods for Building Energy Assessment, September 16-20, 2019, Granada, Spain.

16. Christoffer Rasmussen, Rune Juhl, Peder Bacher, Henrik Madsen. "Semi-parametric Modelling of Solar Gain in Energy Systems". Lecture at Summer School 2019 – Dynamic Calculation Methods for Building Energy Assessment, September 16-20, 2019, Granada, Spain.

17. Christoffer Rasmussen, Peder Bacher, Henrik Madsen. "Modelling of Sun-position-dependent Solar Gain Using B-splines in Grey-box Models". IEA-EBC Annex 71 – 7th Expert meeting, October 21, 2019, Technische Hochschule Rosenheim, Rosenheim, Germany.

18. Christoffer Rasmussen and Henrik Madsen. "REBUS – Renovating Buildings Sustainably". Workshop, October 30, 2019, Skanska Office, Oslo, Norway.

Contents

List of Figures

Part I

Summary Report

1 Introduction

1.1 Motivation

Humans are rather sensitive to outdoor environmental conditions, such as temperature, rain, and wind. For that reason, humans have lived in caves, huts or buildings for thousands of years

During the same period, the requirements to the indoor environment have increased. Temperatures are only accepted in an interval of around 5 °C, and humidity, CO_2 concentrations and even air movements are only accepted for rather narrow intervals as well. Consequently, the buildings are equipped with an increasing amount of technical equipment, monitoring systems, etc., to maintain the desired comfort levels, while keeping the energy consumption at a minimum.

Today, around 40 % of the total end-use energy consumption is related to building operation in EU [1], and similar numbers are expected to be found globally. Furthermore, the vast majority of the buildings which exist today will still be in function in 2050 [2]. Consequently, the focus on building renovation has increased significantly to decrease the greenhouse gas emission, as seen in the latest EU Energy Performance in Buildings Directive [3, 4].

Even though the share of renewable energy is increasing [1], renovation of the building stock is still of first priority in order to reduce the energy consumption. In relation to the Smart Readiness Indicator (SRI) definition in the EPBD [4], *10 principles to deliver real benefits for Europe's citizens* are listed in [5]. Principle number one is: *maximise the buildings' energy efficiency first*.

The reason is stated rather clear by Jørgen Nørgaard, associate professor, emeritus at DTU Civil Engineering: *One unit of energy saved, is better than any unit of energy produced*. The message is that any produced unit of energy — no matter how green — is initially associated with emission of greenhouse gases.

As a consequence of the need for reduction of greenhouse gas emissions on a global scale, and the fact that the majority of the existing buildings will remain for many years to come, different initiatives to increase the building renovation rate has appeared. Among others is the renovation goals established in the EPBD; initiatives such as energy performance certifications (EPCs); and consortiums such as BetterHome [6].

However, the renovation rate is still below 1 % for non-residential buildings, and the aim is 3 % [7]. In addition to the low renovation rate, the EPCs, which should work as a security for the buildings energy performance, seems to have flaws as well. In 2018, between 20 and 30 % of the Danish EPCs were estimated to be wrong [8]. It seems more like the rule than the exception, that buildings consume more energy than anticipated as discussed in Chapter 3.

In light of that, reliable tools for pinpointing big potential energy savings and documenting buildings thermal performance seem to be missing.

Today there does not exist any tools, which on a large scale can identify, quantify and analyse the reasons for the performance gap. Consequently, there is no efficient opportunities to identify and tailor renovation strategies for the worst performing share of the building stock. Additionally, there are no operational methods to document the energy performance of the renovations.

In the building design phase, several assumptions are made in order to estimate the future energy consumption and to ensure that the building fulfils the energy frame. A typical misconception is however that the calculations, and especially the dynamical building simulations, provide the future energy consumption of a given building. This is far from the case. Instead, the energy calculations of the EPCs meant for comparisons across the building stock, and dynamical building simulations are meant for design optimisation. None of the methods are therefore intended for actual prediction of the future energy consumption.

That fact has an inexpedient consequence. The thermal building performance can hardly be validated as it is practically infeasible to distinguish between heat consumption related to the building, the weather, and especially the occupants' behaviour.

In the project, REBUS – Renovating Buildings Sustainably, the focus on quantifying the actual energy performance of buildings has emerged. REBUS is a partnership representing the entire value chain of the building construction industry [9]. The partners are COWI A/S, the Danish Technological Institute, Enemærke & Petersen A/S, Frederikshavn Housing Association, Henning Larsen A/S, Himmerland Housing Association, Saint-Gobain Denmark A/S, Aalborg University/SBi, and the Technical University of Denmark (DTU).

REBUS aims at making facade renovation solutions for 1960s to 1970s social housing apartments, and by that reducing the energy consumption by 50 %, the resources by 30 %, and increase the productivity by 20 %. The specific task of this PhD thesis — which is part of the REBUS project — has been to develop methods for screening for potential energy savings and document the thermal energy performance after renovations. Special focus has been on the conversion of existing modelling techniques applied on unoccupied test buildings, to reliable modelling techniques applied to occupied dwellings.

1.2 Research Objectives

The foundation of this PhD thesis is defined by the following research objectives:

Data-driven methods for quantifying the thermal energy performance of buildings has been studied for several years. The objective of this thesis is, therefore:

1. To make existing methods for thermal building performance analysis on unoccupied thermally controlled test buildings, applicable to actual occupied buildings.

2. To identify typical pitfalls when working with data-driven models on occupied buildings, and formulate and test new approaches to tackle these issues.

3. To refine existing data-driven methods for thermal building performance analysis to obtain more robust assessment of the building performance.

The occupants' behaviour of the energy consumption cannot be neglected, two key objective are, therefore:

4. To develop methods for identification of occupants' presence, which can be used to refine the treatment of disturbances related to occupants in various building performance models.

5. To develop methods for separating and quantifying the causes of heat consumption. That being occupants, weather and the building envelope related causes.

1.3 Thesis Structure

This thesis consists of two parts. In Part 1 the summary of the thesis is presented. In the following chapter, Chapter 2, the current state of the European building stock's energy performance, as well as the trends, visions, and politics concerning energy performance in buildings are presented. In Chapter 3 the performance gap is described and probable reasons for it is occurrence is stated. In Chapter 4 an overview of the dominating data-driven methods for quantifying the thermal performance of buildings are described and the main issues and concerns by applying these models are stated. Chapter 5 summarises the contribution of this PhD study and discuss the results, findings, limitations, etc. Chapter 6 suggests where further research should go and draws the last conclusion on this PhD thesis.

Finally, Part 2 includes pre-prints of the articles contained in this study.

2 Building Energy Conservation in the European Union

2.1 Energy Use in the European Building Stock

Within the European Union around 45 % of the building stock is built before requirements and standards to the thermal performance of buildings were common. Thermal performance requirements started to appear more widely around in 1970 [7]. Since the first thermal performance requirements came in force, the requirements to the energy efficiency have been intensified. However, only 3 % of the building stock in the EU has energy label A, which corresponds to the level of new buildings [10].

With the release of the energy performance of buildings directive (EPBD) recast in 2010, building renovation with the aim of improving the energy efficiency came to light. For major renovation projects, the building parts involved should fulfil the minimum energy performance requirement to the extent that it was technically, functionally and economically feasible [3].

In 2012 the Energy Efficiency Directive (EED) started to encourage the EU member states to make long term renovation plans for the building stock and increase the annual rate of building renovation for the first time [11].

The EU project ZEBRA2020 [12] estimated some of the member state's renovation rate in 2013 and 2014. France and Germany were the countries with the highest rate (1.75 % and 1.49 %, respectively), and Spain and Poland had the lowest (0.08 % and 0.12 %, respectively).

The EED also stated that state-owned buildings should undergo energy renovation with an annual rate of 3 % of the heated or cooled floor area as of January 1, 2014. Also in this case the monitoring was lacking, which meant that the fulfilment of the 3 % target was impossible to evaluate. The EU concluded that the *renovation monitoring is poor and for the moment there is no data to assess if the 3 % target has been reached. However, some studies reveal that the current average building energy renovation rate in the EU for non-residential is below 1 %* [7].

The need for renovations is important as the majority of the building stock which exists today, still, will exist in 2050. In [2] it is estimated that 85 % of today's buildings still are in function in 2050.

In the residential sector on average around 65 % of the end-use energy consumption is used for space heating in the European Union. Furthermore, more than 25 % of the total end-use energy across all sectors is consumed in residential buildings, and the total energy use in all buildings accounts for 40 % [1]. This makes the building stock the single most energy-intensive consumer in Europe.

The average total energy consumption for the residential sector is 184 kWh/m^2 per year, where non-residential buildings consume around 40 % more.

Based on these numbers, the end-use energy conservation potential is probably one of the largest when looking at a single energy end-use category. Reducing the space heating for the residential buildings alone by approximately 6 %, corresponds to a reduction of the total end-use energy in the EU of 1 %.

According to the ZEBRA2020 consortium, the heating demand for buildings can be reduced by 50 to 80 % by technical and economically feasible means. That corresponds to a reduction of around 20 to

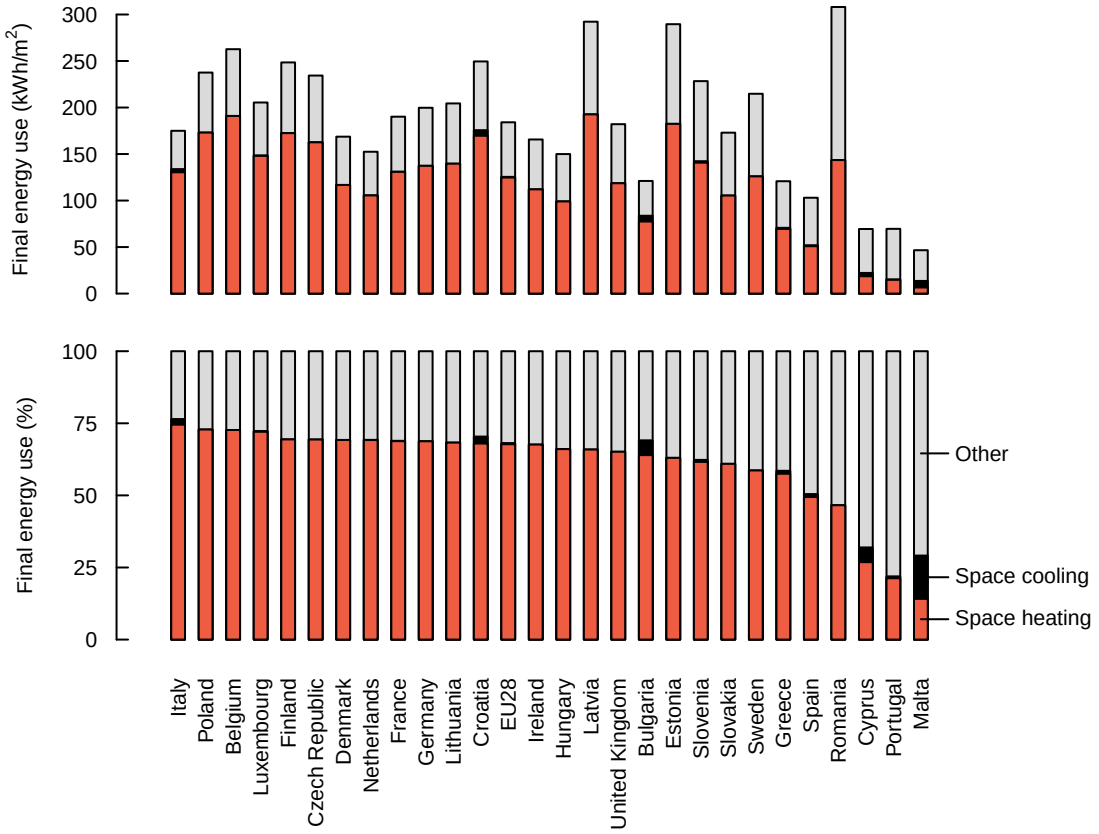

Figure 2.1: Final energy consumption in residential buildings in the European Union. Space heating, space cooling and other energy consumption are specified. Source: *EU Buildings Factsheets* [7].

30 % in the total European end-used energy consumption, or — if those numbers are representative for the residential buildings on their own — a reduction in the total end-use energy consumption within EU of approximately 10 to 20 % considering residential buildings alone.

In [13] it was estimated that Denmark could achieve 31 % cost-effective reduction in space heating for the existing national building stock before 2050. The number, however, does not consider a potential extra heat consumption due to increased thermal comfort after a renovation. A similar number (33 %) was found by the Danish Building Research Institute (SBi) according to [2].

2.1.1 Energy Performance Certificates

In the EPBD recast from 2010, a set of strengthened requirements to the building energy performance certificates (EPCs) were introduced. All new buildings, renovated buildings, and buildings over 250 m^2 owned and occupied by a public authority were required to have an EPC.

The EPC should include information about the energy performance of the building and recommendation for feasible improvements. Additionally, spot checks should be made of a certain percentage of the yearly issued EPCs to validate if the certificate is made under reasonable assumptions.

The Danish Energy Agency who are responsible for the validation of the Danish EPCs, published in 2018 a report stating that around 20 to 30 % of the building energy labels were wrong that year. That corresponds to between 12 000 and 18 000 EPCs. The two previous years (2016 and 2017) the error percentages were 31 and 21 %, respectively.

The Danish Energy Agency stated in 2018 that new data-driven methods for EPC validation will be

implemented in 2019 to 2021 [8], similar to what Sweden is doing already [14]. Recently, an initiative for establishing a building energy atlas was announced in [15].

2.2 EU Directives

In 2015 the European Commission agreed on committing to a common energy strategy for the union [16]. The commission stated five key points regarding energy security; a fully integrated energy market; energy efficiency; a decarbonised economy; and research, innovation and competitiveness. The strategy is manifested in the *Clean Energy for all Europeans Package*, with the most recent version from 2019 [17].

Two main directives which lay out the path of energy reduction and decarbonisation of the building energy use are the Energy Efficiency Directive (EED 2012/27/EU) [11], and the Energy Performance in Buildings Directive (EPBD 2010/31/EU) [3], as well as the amendments in Directive (EU) 2018/844 [4].

2.2.1 Energy Efficiency Directive (EED)

The Energy Efficiency Directive (EED) has among others, two important requirements to make building performance monitoring possible and shed light on potential building performance issues to ensure energy efficiency in the European building stock.

1. The requirements to measure the building energy consumption in such a manner that the temporal energy use is reflected in measurements.

2. Measuring on a level that corresponds to each building unit as long as it is technically and economically feasible. For multi-apartment and multi-purpose buildings, the heat consumption specifically, may, therefore, be measured on a central level, and divided among the consumers through individual heat cost allocators.

Furthermore, as of October 25, 2020, all energy meters and heat cost allocators need to be remotely readable devices. For meters and heat cost allocators which are installed before October 25, 2020, it is required that they are remotely readable before January 1, 2027.

Finally, as stated in the EED 2012/27/EU, article 10a, paragraph 2, the member states are required to ensure that information on historical consumption or heat cost allocator readings is available upon request by the end-user, or made available to an energy service provider designated by the end-user. Furthermore, article 11 states that *end-use customers should have access to their consumption data in an appropriate way and free of charge*.

The EED used to outline the national requirements for developing building renovations strategies, which was first introduced in the EED from 2012. However, the requirements have now moved to the Energy Performance in Buildings Directive with the introduction of Directive (EU) 2018/844 [4].

2.2.2 Energy Performance in Buildings Directive (EPBD)

The Energy Performance in Buildings Directive (EPBD) builds on the EED. The current EPBD, which was updated in 2018 with the Directive (EU) 2018/844 [3, 4], paces the EU member states' building stock toward nearly zero-energy buildings by 2050 by setting up definitions, policies and requirements.

The EU member states were required to make an updated renovation strategy by March 2020 and evaluate on the previous strategy from 2017. The strategy should be revised by the second quarter of 2024, and again by January 2029 as part of the national energy and climate plan [18].

Additionally, the member states are required to outline policies and actions to target the worst-performing buildings as well as public buildings; identify cost-effective approaches to building renovation: promote smart building technologies to strengthen the interconnection of buildings and societies; provide evidence-based estimates of the expected savings; and establish actions and policies which promote building renovations. A building performance passport with step-wise renovation road maps for individual buildings is suggested regarding the latter point.

The EPBD outlines the requirements for national energy performance certificates, spot checks of their validity, etc. Furthermore, the EPSs of at least public buildings are required to be stored in such a way that evaluations of the energy performance on the EU building stock are possible and more transparent.

Currently, 24 member states already have national or regional EPC databases and the Czech Republic and Latvia are currently developing such storage systems.

The EPBD makes room for different EPCs, such that it can be based on measured or calculated energy performance. For example, in Sweden the energy performance certificates are partly based on measured energy consumption, rather than calculated consumption alone. After a measurement campaign of 12 months, the energy consumption is registered in a national database and normalised according to weather conditions, indoor temperature set-points, and hot water consumption [18].

The Smart Readiness Indicator (SRI) definition set by the European Commission is mentioned in the EPBD as well. The SRI serves as an indicator for the building readiness of utilising new renewable energy sources; adapting the user needs to provide a comfortable and healthy environment in a user-friendly manner; and to contribute to energy grid operation by e.g. utilising the thermal flexibility of the building thermal mass as conceptualised in e.g. [19].

All-in-all, the current EPBD has a very strong focus on intelligent energy use, transparency, and documentation of the union and nations initiatives, as well as the aids to achieve a highly energy-efficient building stock. This includes requirements of databases with information on the national building stock's energy efficiency; data collection and accessibility for the end-user, Smart Readiness Indicators, etc.

Finally, the EPBD refines the approach of energy performance calculation to *reduce the energy needed to meet the energy demand associated with the typical use of buildings* [20]. However, there is no guarantee that the calculated energy performance is tenable as it has been shown for several years by the Danish Energy Agency [8]. Additionally, there is certainly not a reason to believe that the energy performance calculations reflect the actual energy use as it will be shown in Chapter 3.

However, the current EED and EPBD have established a path towards data-driven building energy performance assessment and monitoring approaches. This will potentially give a more accurate picture of the energy performance in the European building stock, and result in better advise on building renovation strategies.

3 The Performance Gap

The performance gap of buildings is typically referring to the discrepancy between anticipated and realised energy use (or CO_2 emission) in the operational phase.

A comprehensive British study on residential buildings from 2016 on 29 new low-energy homes showed that the actual CO_2 emission was two to three times higher than expected [22]. Another British study on 18 new build houses showed that not a single one of them was insulated as well as the design prescribed. The results from the study are illustrated in Figure 3.1. The evaluation was done by co-heating tests and discrepancies between 9 and 126 % were found [21].

90 refurbished dwellings in Southern Germany were studied, and the findings were published in 2016. As part of the renovation, the dwellings were equipped with different technical heating and ventilation solutions. Furthermore, comprehensive building monitoring systems were installed to be able to estimate the in-use building performance. The study found that the average performance gap varied by 117, 107, 41, and 60 % in the years from 2011 to 2014. A maximum discrepancy of 287 % was found [23].

In the literature review in [24] it is stated that the average difference between the predicted and realised energy consumption is 34 %. Furthermore, the dominating reasons for the discrepancy are estimated to be related to specification uncertainties, occupant behaviour, and poor workmanship. Each of the three reasons have an estimated effect of 20-60 %, 10-80 %, and 15-80 % on energy use.

One study states that buildings with Green Star sustainability ratings perform fairly good. In [25] 70 Green Star rated buildings were investigated by the Green Star association itself. The study found that

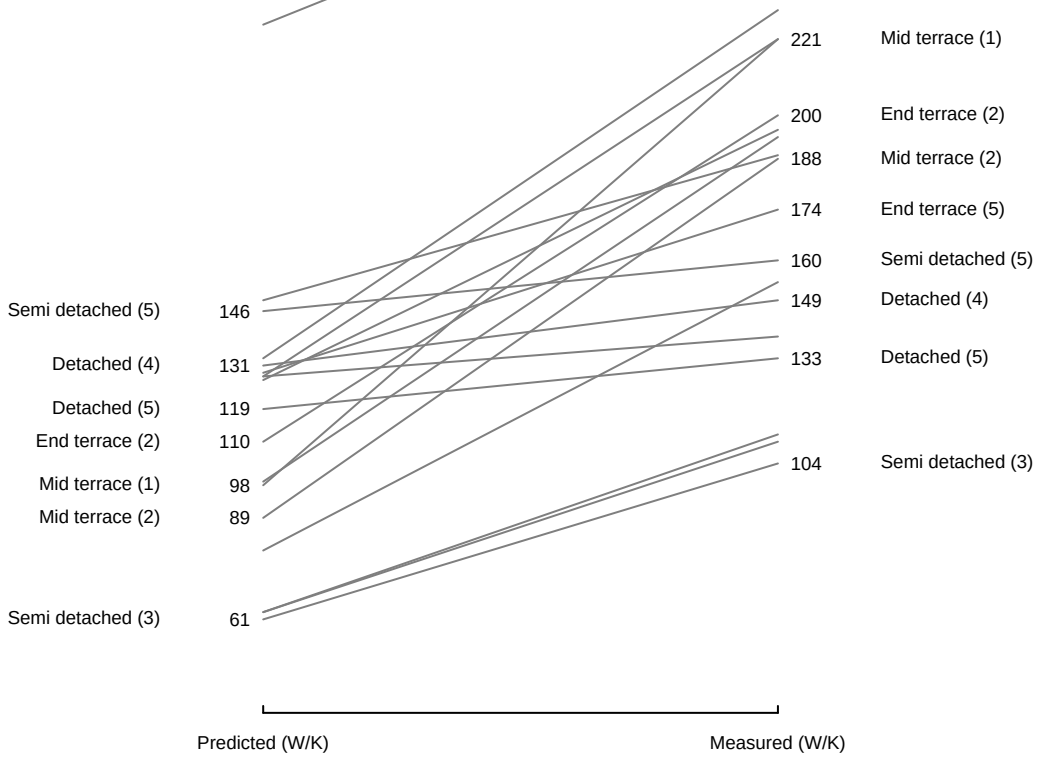

Figure 3.1: Predicted and measured whole-house heat loss coefficients (W/K) of 18 new British houses. Not a single house lives up to the design, and discrepancies between 9 and 126 % were found. Data are obtained from [21] and post-processed to make this chart.

the majority of the buildings (57 %) performed as predicted or better measured by their greenhouse gas performance rating.

The magnitude of the gap between predicted and realised greenhouse gas performance was, however, higher for the under-performing buildings, than the magnitude of the gap for the well- or over-performing buildings. This was measured by the performance parameter *greenhouse gas performance gap in NABERS energy stars* — whatever that means. The actual discrepancy for the 70 buildings was not stated, but by visual inspection of the figures in the publication [25], the buildings under-perform on average by 0.4 stars. In can therefore be concluded that the majority of the customers (assumingly) are satisfied with their Green Star certificated building, but the average greenhouse gas emission across the 70 buildings is higher than promised, which should be of concern for the society.

Based on the findings in the literature, most buildings show signs of a performance gap. It should, however, be noticed that different methods are used in different studies, which makes the comparison between studies difficult. I.e. different energy consumptions may or may not be included in the calculations. A literature review on energy performance gaps in buildings from 2019 list 10 articles with different performance gap definitions [26]. This might also be part of the reason for the various performance gaps found in the literature.

It has not been possible to find any literature where the general pattern shows that buildings perform as well, or better than anticipated. The performance gap is therefore concluded to be an evident and existing phenomenon. Furthermore, the reasons for the performance gap are typically due to uncertainties in the model specifications; the occupants' behaviour; and the workmanship [24, 27].

The importance of documenting the performance gap is therefore clear. Without the certainty of the reasons for the discrepancy, there is no certainty about the realised reduction in energy consumption and greenhouse gas emission, which is of relevance on a national and global scale. Furthermore, there is no guarantee that building owners get anything similar to what they have ordered when they build or renovate — except a bill from the energy consultant.

3.1 The Uncertainty in Building Design and Construction

From the literature on building performance gap, one thing seems to be clear. The buildings rarely perform better than anticipated. Time after time, investigations have shown that buildings use more energy than stated in the design.

One could expect that the deviations from the design would be more symmetrically distributed, rather than this seemingly skewed distribution. With a heavy over-representation of under-performing building one might ask questions like:

- Does occupants' behaviour always cause a higher energy consumption than expected, and if so, why have the design practice not adapted?
- Is the weather always causing the realised energy consumption to be higher than predicted?
- Do contractors, in general, deliver a lower quality product than what is on the blueprints?

In the following sections an attempt to answer each of these questions is given.

3.1.1 Occupants' Effect on the Performance Gap

In [28] an investigation on the occupants' effect on the energy consumption was carried out. Eight almost similar red-brick semi-detached houses located in the western part of Denmark were studied. The

calculated energy consumption was compared with the measured energy use, which revealed deviations in the most extreme cases of more than 100 %.

A sensitivity study on 13 parameters was investigated. It was found that the vast majority of the differences were caused by variations in temperature set-points and occupants' heat loads. The contribution of the four most influencing factors were the set-point indoor temperature (37 %); occupants heat loads (22 %); natural ventilation and infiltration (20 %); and heat loads from appliances (15 %).

Another study concluded that the occupants' behaviour had a significant impact on the buildings energy consumption as well [29], and that the differences between various individuals were a major contributor to the variation. Similarly, in [30] the behavioural effect on the energy consumption was found to be 51, 37, and 11 % of the variance in space heating, electricity, and hot water consumption.

Whether the occupants, in general, give rise to higher energy consumption is hard to say. However, the studies on this topic agree that occupants have a significant impact on energy consumption. Since the set-point temperature according to [28] has the highest influence on the energy consumption, it might be so if they tend to maintain an indoor temperature higher than the design temperature. Also, there seems to be an overweight of occupants' related heat losses compared to free heat gains.

It is, however, strongly believed that the common practice of using static occupancy profiles in building simulation and calculation tools should be avoided. Doing energy performance calculations and building performance simulation, the building designers should avoid to do "occupancy designing", i.e. the act of optimising occupancy behaviour for particular buildings, and instead focus on the building design. Instead, occupancy profiles should be treated as stochastic processes determined by the building type. Recent work on stochastic occupants' profiles and a corresponding occupancy simulator for non-residential buildings is found in [31, 32]. For dwellings, a similar online occupancy simulator exists [33, 34].

In **Paper C**, a scalable method for quantifying occupants' related heat consumption is proposed. Furthermore, a method to estimate the occupancy status (i.e. sleeping, present and away) intended for a more accurate description of the occupants' related model noise in grey-box models is found in **Paper A**.

3.1.2 Weather's Effect on the Performance Gap

Another factor which will cause a difference between the predicted and actual energy consumption is the weather. During the building design, a single synthetic weather file is typically used for the specific location. This weather data may be designed with particular warm and cold periods, intended to stress test the building design. The simulation consequently acts as a validation of the buildings capability to maintain the required comfort levels and keep the peak energy loads at the desired levels.

Even though a lot of work has been carried out on weather data generation, the synthetic weather files still have pitfalls. For instance they do not represent extreme weather scenarios and are not capable of describing future climatic changes and microclimates such as urban heat islands [37].

In a study from 2017, two commonly used *typical meteorological year* (TMY) [38] weather data files used for building simulations were tested on a social housing block located in Milan, Italy. The first data set was based on historic weather data from 1951 to 1970, whereas the other was based on more recent data from 2015 to 2016.

The results showed that the same dynamical building simulation model provided significantly different results by applying the two different TMY files. Furthermore, the heat demand reduced by approximately 50 % by applying the most recent TMY data, and the cooling demand almost tripled [39].

In [40] the weather-related variations of the total energy consumption among other things were investigated. A series of dynamical simulations were carried out for three types of office buildings, each with two levels of energy efficiencies. All buildings were tested in all of the 17 ASHRAE climate zones [41], as well as with one year of synthetic data (TMY3) and the actual weather from 1980 to 2009.

The analysis showed that the energy use for heat, ventilation and air conditioning (HVAC) was influenced the most by using different weather data. The energy consumption for HVAC was in the worst cases over- or underestimated by 18 and 37 %, respectively. For the total energy use the variation was between 8 and −10 %, where the largest deviations were found in the colder climates.

From the results, it seems like the synthetic weather data do a rather good job at estimating the mean energy consumption for both HVAC and the overall energy consumption.

Another study on a Danish kindergarten has shown that the effect of the weather data can result in a variation of the heat demand of roughly ±20 % [42].

Both studies indicate that the deviations between predicted and realised energy consumption are symmetric. That means that in some cases the models will underestimate the energy consumption, and in other cases, they will overestimate the energy consumption. Conclusively, even though the weather is a source of significant errors, there is no indication of synthetic weather data in general should lead to underestimated energy consumption.

The actual weather condition's influence on the heat consumption is fairly easy to account for by normalising the measured energy consumption. Estimating building physical parameters by data-driven models may, on the other hand, be biased due to the model formulations. This is shown and accounted for in the quasi-stationary model in **Paper C**. Additionally, **Paper B** presents a novel sun position dependent method for obtaining better solar gain estimations in dynamical data-driven models.

3.1.3 Building Design and Workmanship

A third reason for the performance gap is related to the actual design specifications and the workmanship.

In a study on insulation of brick cavity walls, it was demonstrated how the heat loss through several identical designed walls varied [44]. The study investigated six walls over two winter seasons. Half of the walls were insulated as intended in the design — i.e. proper contact between the insulation material and the inner wall inside the cavity — and the other half were constructed with intentional air gaps between the insulation and the inner wall. The same walls were tested with and without air tightening of the inner wall.

A post-processing of the results in [44] is shown in Figure 3.2. The results show two things which are relevant for understanding the performance gap. First, the workmanship is of crucial importance to obtain the design requirements. Second, the actual insulation levels of the walls are *not symmetrically distributed* around the design value. The latter is important to understand the differences between energy optimisation, design, and buildability.

In the field of structural engineering, the term tolerances is crucial. It serves the simple purpose of allowing smaller deviation between the technical drawings and the actual physical structure on the building site. The reasoning is that it is more difficult to make bolts and nuts fit on the building site than it is in a CAD (computer-aided design) software.

Looking at the results in Figure 3.2 again, 11 out of the 12 U values representing good workmanship are equal to or higher (worse) than anticipated. Only in one case is the U value lower. That means that only

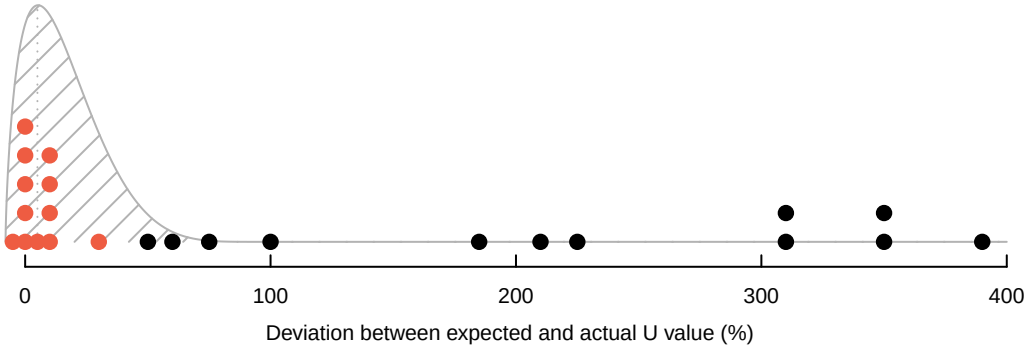

Figure 3.2: Strip chart of deviation between expected and actual U values obtained from lab tests. The numbers are rounded to the nearest 5 %. The red dots indicate realised U values of proper workmanship, whereas the black dots indicate realised U values obtained by poor workmanship. The beta distribution overlay shows a conceptual distribution of the expected deviation. Data are obtained from [44] and post-processed to make this chart.

exact workmanship will lead to the design requirements, and the probability of achieving better performance than specified in the design is negligible — or in other words: *the actual thermal performance of building envelopes are condemned to fail due to a designer optimism bias.*

An obvious way of solving this issue is to introduce a measure of uncertainty in the energy performance calculations, analogue to tolerances used in structural engineering. One approach to this has already been developed and tested on real buildings by Aarhus University in Denmark [45]. The method (called BeREAL) is an add-on to the current mandatory energy performance calculation tool, Be18, used in Denmark [46]. BeREAL is used for making corrections to the standard Be18 calculation by applying more realistic usage schedules, actual weather data for the location, more realistic energy use for various devices like computers, servers, lighting, etc [45]. Finally, BeREAL uses a 3-point estimation technique for constructing an approximate distribution of reasonable building thermal properties. The 3-point estimation technique was originally proposed in [47], and works by setting a pessimistic, an optimistic, and the most likely estimate for a certain building parameter. Based on those numbers, a distribution of the parameter is obtained — typically by assuming that the parameter is beta distributed as shown in Figure 3.2.

Based on the rather simple inputs, the output of the BeREAL calculation is an estimate of the energy consumption with an associated uncertainty measure. Such results are very much in line with the outcome of data-driven models as those described in **Paper B**, **Paper C**, and **Paper D**.

At last, a more concerning reason for the performance gap is related to the building modellers potential lack of fundamental understanding of the building physics and the importance of different building parameters. A study on 108 building modellers with different educations and experience showed that their ability to determine the most important building physical parameters of a specific building were surprisingly low. 25 % of the building modellers made judgements which were worse than random responses. Furthermore, no correlation between experience or educational level and the percentage of correct answers were found [48].

3.1.4 Conclusions on the Performance Gap

The documentation of the performance gap found in the literature shows time after time that there is: either a systematic error in the energy performance calculations which makes predictions look better than reality; or a negligible focus on well and over-performing buildings. Based on the considerations in the previous sections, the former seems to be the case.

There are several pitfalls which may lead to a discrepancy between anticipated and realised energy performance of buildings as explained in the previous sections. However, one issue is believed to be the main drivers for the performance gap: the discrepancy between the building designer's objectives and what is practically achievable on the building site.

The building designer is working on an idealised building, without uncertainties, whereas craftsmen are working under real and uncertain conditions. By reflecting the uncertain conditions in the design practice, the performance gap is believed to shrink significantly. To do that, a few specific things can be done:

- Be realistic about the design parameters and their distributions.
- Design buildings rather than occupancy profiles. Rely instead on stochastic alternatives.
- Do not estimate the energy performance based on a single calculation or simulation — and definitely not on the realisation obtained from the most optimistic set of building physical parameters. Instead, several simulations should be made from models with small variations in thermal properties, weather, and occupancy profiles.
- Accept that the calculated energy performance is uncertain and state it.

4 Data-driven Methods for Quantifying Thermal Performance – State-of-the-art

As design tools are based on several assumptions and idealised considerations as described in Chapter 3, other methods are needed to quantify the actual building performance. One approach is to rely on data, statistical modelling and knowledge on the physics driving the heat dynamics.

For data-driven models, the description of the thermal dynamics needs to be reduced to estimate all the parameters. Furthermore, only a fraction of the relevant input variables can be measured. The aim is, therefore, to describe the most significant thermal dynamics with the data at hand. Typically, this would be weather data, heat consumption and some data on the indoor climate, such as air temperatures and CO_2 concentrations. Other variables such as the temperatures of the thermal masses, internal heat gains, and window openings are definitely not irrelevant, but infeasible to measure, and therefore are rarely included in data-driven thermal models.

As a consequence of the limited data and the simplified models, there will be discrepancies between observations and predictions. Or as Tor Nørretranders wrote with reference to Kurt Gödel: *A formal description has its limitations; a map can never contain all the details of the terrain without being the terrain itself and is therefore not a map* [49]. This is an incontrovertible fact one has to deal with — one way or another.

Statistical approaches to model physical systems introduce a convenient way of doing that. The physical model is associated with a measure of uncertainty. Depending on the model and the estimation technique, system and observation noise can be estimated separately or as a combined term.

In the following, it is assumed that the reader has some knowledge of time series analysis and mathematical modelling.

4.1 Quasi-stationary Methods

When time series data are smoothed or filtered, some information in the data — e.g. dynamical characteristics such as time constants and heat capacities or short term effects like a window openings — will be lost.

The class of quasi-stationary models relies on such data processing in order to determine for instance heat loss coefficients. By averaging the data for sufficiently long periods, the building conditions can be treated as stationary, and stationary considerations can be applied.

In the following sections, some common quasi-stationary methods are described.

4.1.1 Average Method

Probably one of the most widely accepted methods for assessing the heat loss coefficient is the average method defined in ISO 9869 [50]. The method simply determines the heat loss U by the relation between the heat flow through the building envelope, $\dot{q}$, and the average temperature difference between inside, T_i, and outside, T_e,

$$\mathrm{U} = \frac{\sum_{t=0}^{N} \dot{q}_t}{\sum_{t=0}^{N} (T_{\mathrm{i},t} - T_{\mathrm{e},t})} + e\,, \tag{4.1}$$

where N is the number of observations, t is the time step, and $e \sim \mathrm{N}(0,\ \sigma^2)$ is the normally distributed error.

The method is simple and builds on steady-state assumptions. This is of course not possible to obtain for real buildings. Instead the method relies on the assumption that all dynamics are averaged out when data is obtained for sufficiently long periods.

In [51] a comparison of several steady-state and dynamical models is made. Applying the average method on winter data, showed rather good results despite its simplicity. For periods with high outdoor temperatures, the model tends, however, to fail. For these periods the dynamical models such as those presented in Section 4.2 did a significantly better job at estimating the heat loss coefficient.

Despite the reasonable results obtained in [51] on winter data, the long measurement period and the additional measurement equipment (heat flow meter) are both drawbacks of this method. Furthermore, the method can only be used to obtain the U value. The information extracted from the data is therefore rather limited.

Another issue is that a heat flow meter only measures the heat flow in one spot. For that reason, it can be hard to deduct the total U value when dealing with heterogeneous walls with multi-dimensional heat transfer.

Substituting the heat flow $\dot{q}$ in Equation (4.1) with the heat inputs to the building, another average method is obtained for which the whole-house UA value can be obtained.

4.1.2 Co-heating Methods

The co-heating method, which seems to originate from the late 1970s and early 1980s [52, 53], utilises quasi-stationary temperature conditions and linear regression to estimate the whole-house heat loss coefficient (HLC). The method works by increasing the indoor temperature to a level which makes the effect of e.g. wind and solar irradiation negligible. From time series measurements of the heating power and the temperature difference between inside and outside the HLC can be determined. As the overall HLC comprise of both ventilation and transmission heat loss, it is sometimes separated by estimating the infiltration rate by means of blower door tests.

The co-heating method has been applied and studied several times. In [54] a review of the published work on co-heating methods is outlined and the state-of-the-art of co-heating methods is presented.

Some work has also been done to shorten the measurement period. E.g. as done in the QUB and QUB/e method [55–57]. The methods work by performing one cooling and one heating experiment for which the rate of temperature change is determined through linear regression. With the two estimates the heat loss coefficient and the heat capacity is obtained. During the two experiments, the outdoor temperature is assumed constant, and the indoor temperature is kept uniform by mixing the indoor air.

The co-heating method requires an experimental setup and that the building is unoccupied. As it is an on-site experiment-based method, it cannot be used for large scale thermal performance screening and documentation.

4.1.3 Linear Regression Models

A certain group of methods used to estimate thermal characteristics of buildings are the linear regression models. The linear regression models differ from the co-heating methods by the fact that they rely on in-use data rather than experimental data. On the other hand, significantly longer measurement periods are required to obtain reliable results.

The methods are based on the steady-state heat balance

$$\Phi_{\mathrm{h}} - \Phi_{\mathrm{tr}} + \Phi_{\mathrm{sol}} + \Phi_{\mathrm{int}} - \Phi_{\mathrm{vent}} + \Phi_{\mathrm{mass}} + \Phi_{\mathrm{latent}} = 0\,, \tag{4.2}$$

where Φ_{h} is the space heating, Φ_{tr} is the transmission losses, Φ_{sol} is the solar gain, Φ_{int} is the internal heat gains, Φ_{vent} is the ventilation loss, Φ_{mass} is the absorption and release of thermal energy in the thermal mass, and Φ_{latent} is the energy absorption and release due to evaporation and condensation in the thermal zone.

By lumping the five last terms into Φ_{x}, and using the simplification that Φ_{tr} only consists of transmission loss to the ambient air, Equation (4.2) can be formulated as the model

$$\Phi_{\mathrm{h}} = \mathrm{UA}\,(T_{\mathrm{i}} - T_{\mathrm{e}}) - \Phi_{\mathrm{x}} + e\,, \tag{4.3}$$

where UA is the heat loss coefficient, T_{e} and T_{i} is the ambient outdoor temperature and the indoor temperature, respectively, and $e \sim \mathrm{N}(0,\, \sigma^2)$ is the error term.

The model in Equation (4.3) can be extended and refined. However, a returning concern when modelling dynamical systems such as buildings is to get proper data. Especially accurate weather and indoor climatic data can be troublesome to obtain. Special weather conditions such as heat islands and turbulent wind conditions may result in discrepancies between the weather data and the actual conditions. Furthermore, a seemingly simple task such as measuring the indoor temperature involves major pitfalls, which can corrupt the reliability of the estimated model parameters, such as the heat loss coefficient.

In Figure 4.1 the temperature differences between inside and outside obtained from two different buildings are shown. In the first case, four temperature sensors were installed in the living room in different heights (0.1, 10, 110, and 170 cm above the floor). The data is obtained from an unoccupied test building at the Fraunhofer Institute in Holzkirchen, Germany. The building is heated by electrical radiators. For the two most extreme measurements shown in the upper plot of the figure, the average difference between them is 2.5 °C. The average outdoor temperature for the five days shown was -0.1 °C.

In the second plot of Figure 4.1 the temperature differences obtained from an occupied apartment in Aalborg, Denmark is shown. The apartment is a two-room apartment of approximately 55 m^2 occupied by an elderly couple. Eight temperature sensors were installed in the apartment in different rooms. Some rooms had multiple sensors installed. The outdoor temperature for the five days shown in the plot was -6.0 °C. If the two most extreme temperature differences measured are considered as before, the average difference between them is 9.6 °C.

Looking at the simple steady-state heat balance in Equation (4.3), it is seen that an error of e.g. 10 % in the temperature difference between inside and outside, will result in an error in the estimated thermal resistance (UA^{-1}) of 10 % as well.

By considering the temperature differences in Figure 4.1, the implications can be rather serious. For the first case, the mean difference between the measurements in the most severe case is 12 %, and for the second case, the difference is 55 %. If a single temperature is used for determining the thermal resistance, an error of similar order can, therefore, be expected.

With that in mind, it is obvious that a representative temperature can be troublesome to determine.

But what is the true representative indoor temperature after all? For characterisation of thermal building performance, this must be the temperature which in combination with the true exterior conditions and heat consumption, reveals the true thermal building properties.

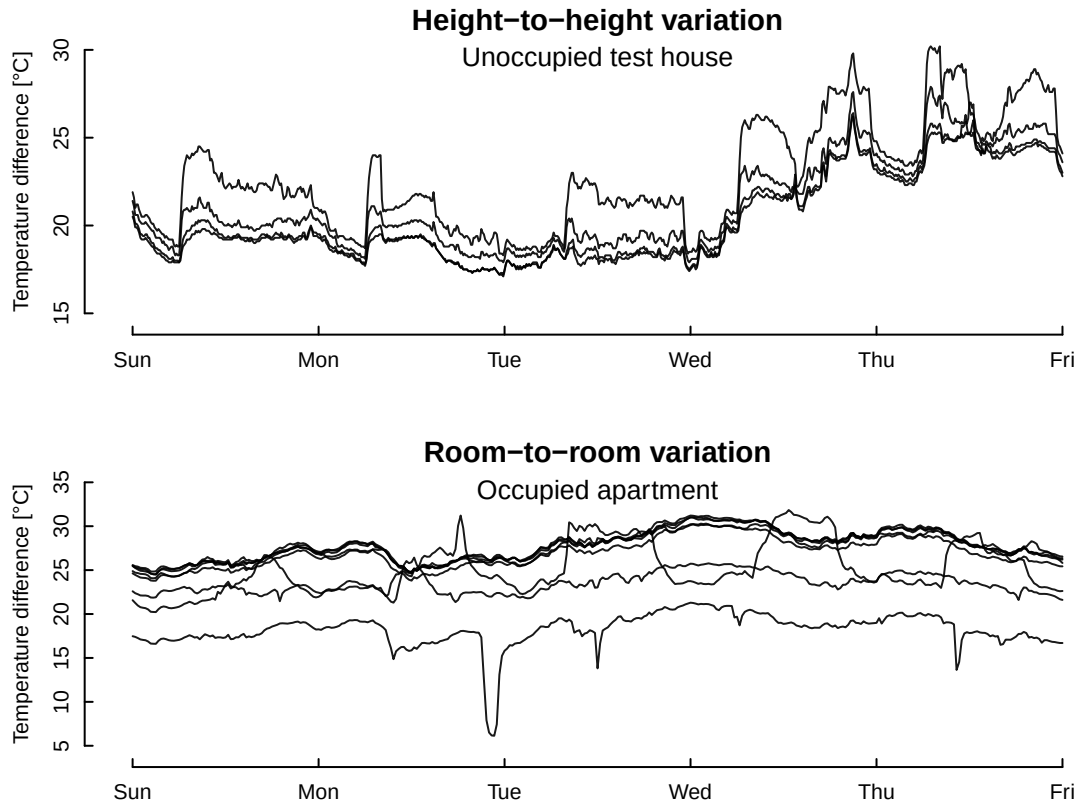

Figure 4.1: Illustration of variations in measured temperature difference between indoor and outdoor in two different buildings. The first plot shows the temperature difference between the living room (measured in heights of 0.1, 10, 110, and 170 cm above the floor) and the outside form a Fraunhofer Institute test building. The second plot shows the temperature differences obtained by measuring the indoor temperature in different locations and rooms in an occupied apartment in Denmark.

Different approaches to estimate such a temperature (or temperatures) can be considered or found in the literature. Some examples could be: the arithmetic mean temperature at each time step as done in **Paper B**; different kinds of weighted means, such as space volume-weighted mean used as in [58]; principal component analysis as in [59–61] etc.

Unless detailed knowledge about the building and the locations of the sensors are known, as in [61], each approach is a qualified guess of a representative indoor temperature, which might or might not give reasonable parameter estimates.

Instead of relying on indoor temperature measurements, another approach is to estimate it from data. Besides eliminating the issue of measuring the representative indoor temperature, this kind of methods also needs less measured variables from the building. This is naturally an advantage if the methods are intended to be applied on a large scale.

The energy signature methods are one kind of models which often disregard the indoor temperature and relies on an estimated base temperature at which the building is in thermal balance.

Energy Signature

Some of the earliest work on the energy signature models is found in [62–64]. In the basic form, the models have the outdoor temperature as the dependent variable and the heat consumption as the independent variable. A linear relationship between them is then found. The slope and intersection with the x-axis is the estimated UA value and the base temperature, respectively, as seen from the following.

By rewriting Equation (4.3), the space heat demand can be expressed by the base temperature $T_\mathrm{b} = T_\mathrm{i} - \Phi_\mathrm{x}\mathrm{UA}^{-1}$.

$$\Phi_\mathrm{h} = \mathrm{UA}\,(T_\mathrm{i} - \Phi_\mathrm{x}\mathrm{UA}^{-1} - T_\mathrm{e}) + e \tag{4.4}$$

$$= \mathrm{UA}\,(T_\mathrm{b} - T_\mathrm{e}) + e\,, \tag{4.5}$$

where T_b and UA are constants and $e \sim \mathrm{N}(0,\ \sigma^2)$ is the combined observation and systems noise.

Expanding Equation (4.5) such that

$$\Phi_\mathrm{h} = \mathrm{UA}\,T_\mathrm{b} - \mathrm{UA}\,T_\mathrm{e} + e\,, \tag{4.6}$$

it can be seen that the model can be estimated as a first-order linear model with UA as the slope and $\mathrm{UA}\,T_\mathrm{b}$ as the intercept.

In the early literature on energy signatures — e.g. [63] — linear models, such as the one just presented, were suggested due to limited data and computational power. However, the linear models seem still to be dominating the energy signatures. This is seen in some of the more recent studies from 2013 to 2020 [65–69]. Furthermore, the energy signature models are often treated as univariate models as Equation (4.5). Other times, multivariate models with solar irradiation as a second explanatory variable are used.

Equation (4.5) is of course only valid for periods with heating demand. For periods without heating demand the building enters another regime. The regime is typically treated as a linear relation between heat consumption and the outdoor temperature. In *ASHRAE Guideline 14-2002 – Measurement of Energy and Demand Savings* different model proposals are listed for buildings with different kinds of heating, cooling, and heat recovery systems [70]. For buildings without cooling and heat recovery, the second regime can be modelled as a constant Φ_0 corresponding to the base heat use related to e.g. hot water consumption. The full model then becomes

$$\Phi_\mathrm{h} = \begin{cases} \mathrm{UA}\,(T_\mathrm{b} - T_\mathrm{e}) + e & \text{for} \quad T_\mathrm{e} \leq T_\mathrm{b} \\ \Phi_0 + e & \text{otherwise}\,. \end{cases} \tag{4.7}$$

By neglecting substantial heat flows such as infiltration and solar gain as in (4.7), the estimates might end up being biased as stated in [63] and shown in **Paper C**. For example, particularly windy and cold weather results in higher estimated UA values than cold and less windy weather. This is seen in the left plot in Figure 4.2. Likewise, a sunny period around the transition point of the two regimes in Equation (4.7) will result in an overestimated UA value as well. This is illustrated in the right plot in Figure 4.2.

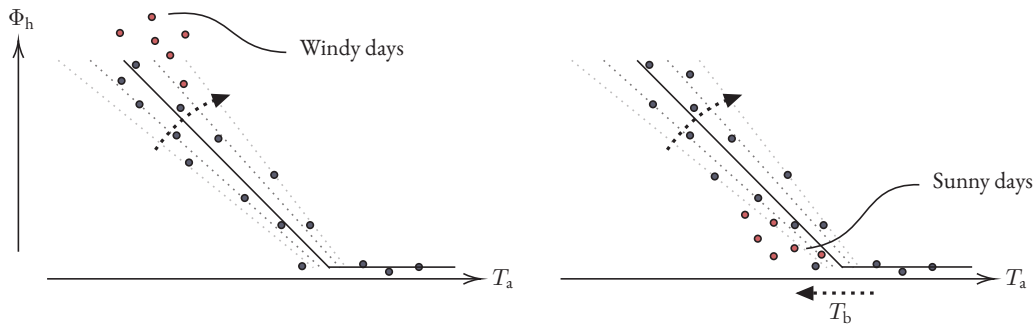

Figure 4.2: Illustration of energy signature bias. The left plot shows how the slope of the linear heat demand formulation (i.e. the UA value) will increase if particularly windy and cold days occur (red dots). In the plot to the right, the UA value is increasing as well, but this time due to particularly sunny days (red dots) which will a reduced the heat demand.

4.2 Dynamical Methods

Dynamical models are used to describe the transient behaviour of dynamical systems, such as buildings. This kind of models does, therefore, not assume or rely on steady-state or quasi-stationary conditions. Actually, they require that the data contains a sufficient amount of variation, for the dynamics to be practically identifiable [71].

As a result of applying dynamical models on time series building data, time constants and heat capacities can be estimated, as well as steady-state thermal performance parameters such as heat loss coefficients.

In the the following sections two types of dynamical models are presented. The linear auto-regressive and moving-average models (i.e. the ARX and the ARMAX models) and the stochastic state-space models described by stochastic differential equations.

For introduction to both classes of models the reader is referred to the report of IEA-EBC Annex 58, *IEA-EBC Annex 58 – Reliable Building Energy Performance Characterisation Based on Full Scale Dynamic Measurements. Report of Subtask 3, Part 2: Thermal Performance Characterisation Using Time Series Data – Statistical Guidelines* [59].

More detailed description of linear auto-regressive models can be found in the book *Time Series Analysis* by Henrik Madsen [72], and for in-depth literature on stochastic differential equations and non-linear modelling the reader is referred to *Modelling Non-linear and Non-stationary Time Series* by Henrik Madsen, Jan Holst and Erik Lindström [71].

4.2.1 Auto-regressive Models

A subcategory of the linear regression models is the linear auto-regressive models — the AR models. The AR model simply regresses on lagged (i.e. previous) values of the independent variable Y_t, such that

$$Y_t + \phi_1 Y_{t-1} + \cdots + \phi_p Y_{t-p} = e_t \,, \tag{4.8}$$

where t is the discrete time, ϕ_1 to ϕ_p are the model parameters, and p is the order of the AR model. The model in Equation (4.8) is consequently called the AR(p) model.

Two extensions of the AR model are the ARX model (auto-regressive models with exogenous inputs) and the ARMAX model (auto-regressive moving-average models with exogenous inputs). Other variations of the auto-regressive models exist as well, but will not be discussed here.

The ARX and ARMAX models are different from the normal linear regression models mentioned previously, by their capabilities of describing a system's dynamics. They do so by regressing on lagged input variables and hence describe the response to a change in the inputs.

The family of auto-regressive models is typically linear, discrete-time models, which are useful for modelling many weakly stationary stochastic processes. I.e. processes with time-invariant mean and variance [72]. Since the models are discrete-time models the parameters depend on the time step in the data. Consequently, it is required that the time steps in the time series are equidistant.

Modelling either the heat demand or the indoor temperature of a building, the data are typically not stationary when looking at the yearly variation. Instead, a seasonal trend is seen. Because the models need to be excited as much as possible to be identifiable, periods with high temperature differences between inside and outside are typically used for model estimation. This naturally shortens the data period to maybe a few weeks or months during the winter, and the stationarity requirement is fulfilled.

ARX

The AR(p) model can easily be extended to include one or more exogenous inputs, u, as seen in Equation (4.9).

$$Y_t + \phi_1 Y_{t-1} + \cdots + \phi_p Y_{t-p} = \omega_0 u_t + \omega_1 u_{t-1} + \cdots + \omega_r u_{t-r} + e_t \,, \tag{4.9}$$

where ϕ and ω are the model parameters, and r is the lag of the inputs.

Introducing the backshift operator B, where

$$B^k \, X_t = X_{t-k} \,, \tag{4.10}$$

with X as a random variable, and k as the lag, Equation (4.9) can be now be written as

$$(1 + \phi_1 B + \cdots + \phi_p B^p) Y_t = (\omega_0 + \omega_1 B + \cdots + \omega_r B^r) u_t + e_t \,. \tag{4.11}$$

For further simplification, two backshift polynomials in B are introduced:

$$\phi(B) = (1 + \phi_1 B + \cdots + \phi_p B^p) \,, \tag{4.12}$$

$$\omega(B) = (\omega_0 + \omega_1 B + \cdots + \omega_r B^r) \,. \tag{4.13}$$

The ARX model can now be written as

$$\phi(B) Y_t = \omega(B) u_t + e_t \,. \tag{4.14}$$

ARMAX

Whereas the ARX model only relies on correlations between current and present inputs (u_t) and observations (Y_t), the ARMAX model has an additional moving average (MA) term, which describes the auto-correlation in the model residuals. The ARMAX model is therefore

$$(1 + \phi_1 B + \cdots + \phi_p B^p) Y_t = (\omega_0 + \omega_1 B + \cdots + \omega_r B^r) u_t \; + (1 + \theta_1 B + \cdots + \theta_q B^q) e_t \,, \tag{4.15}$$

where the θ_1 to θ_q are the parameters of the lagged model errors.

Introducing the third backshift polynomial in B,

$$\theta(B) = (1 + \theta_1 B + \cdots + \theta_q B^q) \,, \tag{4.16}$$

the ARMAX model can be written as

$$\phi(B) Y_t = \omega(B) u_t + \theta(B) e_t \,, \tag{4.17}$$

which on transfer function form is

$$Y_t = \underbrace{\frac{\omega(B)}{\phi(B)}}_{H(B)} u_t + \frac{\theta(B)}{\phi(B)} e_t \,. \tag{4.18}$$

In Equation (4.18), $H(B)$ is the transfer function of the inputs variables, which will later be used for calculation of the time constants of the system.

Least Squares and Prediction Error Method Estimation

One possible way of estimating the ARX models is by the least squares (LS) method [59, 72]. It has a closed-form solution and is easy to calculate. If β is the full set of parameters, the estimate $\hat{\beta}$ is

$$\hat{\beta} = \arg\min_{\beta} \frac{1}{N} \sum_{i=1}^{N} e_i(\beta)^2 \,, \tag{4.19}$$

where N is the number of observations.

The ARMAX model, on the other hand, relies on the model errors. That means that the output at time t is dependent on the model error at time $t-1$ to $t-q$. However, the model errors are only known after predictions have been made, and the predictions can only be done when the errors are known.

As the Box-Jenkins approach of estimating transfer function models does not apply for most multiple input models, the recursive prediction error method can be used instead. A description of the method is given in [72].

It should be noticed that different software use different methods for fitting ARMAX models. For example do the *arima* function in base *R* [73], as well as the *Arima* and *auto.arima* from the *forecast* package [74] in *R*, fit a linear regression model with ARIMA errors. The exact implications on the model estimates are unknown, but it is suspected that the interpretability, which will further described in Section 4.2.2, will be lost.

If a custom implementation of the ARMAX estimation process is not done, there might be other interesting packages in *R*. E.g. the *Multivariate ARIMA and ARIMAX Analysis (marima)* package and the *Time Series Analysis (TSA)* package [75, 76].

Alternatively, other software can be used. E.g. *Matlab* and the *System Identification Toolbox* which rely on the prediction error method [77, 78].

Physical Interpretation

The family of auto-regressive models is often used to model various types of dynamical systems, such as physical, biological and financial systems. However, in its pure form it may be a good model for predictions, but it is seemingly a black-box model which can be hard to interpret physically.

In e.g. [79–81] the interpretability of ARX and ARMAX models applied on building data has been shown. It is done by setting up a dynamic state-space model in continuous time and showing the link between that and the discrete-time ARX or ARMAX model.

As in the example from [80], it is shown that the following dynamic continuous-time model can be rewritten as an ARMAX model:

$$C_1 \frac{\mathrm{d}T_1}{\mathrm{d}t} = \frac{T_\mathrm{e} - T_1}{R_1} + \frac{T_2 - T_1}{R_2} + \frac{\mathrm{d}W_1}{\mathrm{d}t} \,, \tag{4.20}$$

$$C_2 \frac{\mathrm{d}T_2}{\mathrm{d}t} = \frac{T_1 - T_2}{R_1} + \frac{T_i - T_2}{R_2} + \frac{\mathrm{d}W_2}{\mathrm{d}t} \,, \tag{4.21}$$

$$\Phi_\mathrm{h} = \mathrm{UA}(T_\mathrm{i} - T_2) - \mathrm{gA}\, I + e \,, \tag{4.22}$$

where C is the heat capacities, R is the thermal resistances, Φ_h is the space heating, UA is the heat loss coefficient, gA is the solar transmittance, and I is the solar irradiation. Furthermore, T_i and T_e are the indoor and outdoor temperatures, while T_1 and T_2 are temperature states in the separation layer (e.g. a building envelope) between inside and outside. Finally, W is the Wiener processes, $e \sim \mathrm{N}(0,\, \sigma^2)$ is the

independent and identically distributed (i.i.d.) white noise with zero mean and variance σ^2, and t is the time.

It was shown that the system in Equation (4.20)–(4.22) can be expressed as the ARMAX model with heating as output:

$$\phi(B)\Phi_{\mathrm{h},t} = \omega_1(B)T_{\mathrm{e},t} + \omega_2(B)T_{\mathrm{i},t} + \omega_3(B)I_t + \theta(B)e_t\,, \tag{4.23}$$

or with the indoor temperature as output:

$$\phi(B)T_{\mathrm{i},t} = \omega_1(B)T_{\mathrm{e},t} + \omega_2(B)\Phi_{\mathrm{h},t} + \omega_3(B)I_t + \theta(B)e_t\,, \tag{4.24}$$

where the number of temperature states in the continuous-time state-space model corresponds to the number of lags in the discrete ARMAX model. This further translates into the number of time constants of the system.

To obtain the steady-state parameters of the system like the heat loss coefficient UA and the solar transmittance gA, Equation (4.23) and (4.24) can be brought on steady-state form by setting $B = 1$, and comparing it to the steady-state heat balance

$$\Phi_{\mathrm{h}} = \mathrm{UA}(T_{\mathrm{i}} - T_{\mathrm{e}}) - \mathrm{gA}\, I_{\mathrm{g}} + e\,. \tag{4.25}$$

Remembering that $B^k\, X_t = X_{t-k}$ it can be seen that for $B = 1$, the steady-state, where inputs and outputs are constant, is reached.

As this procedure results in two estimates of the heat loss coefficient, it is suggested in [80] that the two values are weighted such that the variance of the resulting HLC has the least possible variance. The variance of the individual parameters can be established by error propagation — see e.g. [59].

Other important parameters which describe the dynamics of a dynamical system are the time constants. The time constant for a first-order system expresses the time it takes for the system to reach approximately 63 % of the ultimate new state after the system has been exposed to a step-change in the inputs.

In the continuous-time models, the time constants are found by multiplication of resistances and heat capacities. However, in the discrete-time models like the ARMAX models, the time constants, τ, are determined by the *poles* of the system — i.e. the *roots* of the denominator of $H(B)$ in Equation (4.18). The number of lagged values of the dependent variable p is therefore equal to the maximum number of time constants [72].

$$\tau_i = \frac{1}{\ln|\mathrm{pole}_i|}\,, \quad \forall\, i \in [1,\, p]. \tag{4.26}$$

ARX and ARMAX Models Used in Practice

Single-output ARX models have been compared with multi-output ARX models with significant improvements in [82]. Based on several tests on a test cell in real weather conditions across different periods, it is stated that the multi-output ARX model showed significant improvements. Both in terms of consistent estimations of the U value and in good agreement with other estimation methods tested.

Another study on several different data-driven models tested on both simulated data and data from a test cell at KU Leuven, Belgium, showed all good results during winter periods with high heat demands. Both quasi-stationary and dynamic models (the Anderlind's regression method, an ARX model, and a stochastic differential equation model) were tested. By testing the models on summer data, the dynamic models outperformed the quasi-stationary models, but performed worse on winter data [51].

In a third study presented in [83], an ARX model was derived from a thermal resistance-capacity network. An experiment was conducted on a test cell at Plataforma Solar de Almeria in south-east Spain. The tested wall was a homogeneous lightweight wall without windows. The estimated heat loss, solar transmittance, and heat capacity were rather consistent for the winter data, but less for the summer data.

In [58], ARX models for thermal parameter identification were tested on a British occupied apartment. The results obtained with a rather simple ARX model using only total heat consumption, indoor and outdoor temperature showed that the confidence interval and the estimate of the heat loss coefficient stabilised for measurement periods of around 16 weeks. Slightly more complex models reduced the convergence time by approximately three weeks.

The same study showed that the choices made by the modeller can result in variations of the estimated heat loss of up to 90 %. Alone by using either one of the two temperatures measured (the temperature measured in the living room) or the volume-weighted mean temperature of the two sensors, the difference on the estimated heat loss coefficient was close to 70 %.

Both ARX and ARMAX models have been tested in the International Energy Agency, Energy in Buildings and Communities Programme (IEA-EBC), *IEA-EBC Annex 58: Reliable Building Energy Performance Characterisation Based on Full-scale Dynamic Measurements* as well [59, 84, 85]. The methods are still investigated in the current *IEA-EBC Annex 71: Building Energy Performance Assessment Based on In-situ Measurements* [86].

As the ARX models are typically estimated by means of the least squares method. It is clear that the optimisation of the model parameters is done by minimising the one-step model errors.

In [87] a different estimation technique for ARX models has been tested on an 80 m^2 apartment in Berkeley, California. While ARX models might be good for one-step predictions, they are typically not as good for multi-step predictions. To overcome this, they formulated an ARX model as a neural network and fitted it by applying backward error propagation of multiple prediction horizons. That way the estimated parameters are optimised to perform the best on several prediction horizons, rather than on one-step predictions alone. The aim of the article was, however, focused on control, rather than parameter estimation.

Yet another study has implemented fractional-order ARX models to model the thermal dynamics of a simulated test house [88]. The *fractional-order models* differ from typical *integer-order models* by allowing the model order to be any number larger than zero.

Naturally, it is difficult to understand the meaning and implication of fractional-order models. However, one of the key benefits is stated to be that the model has extended memory compared to integer-order models. Consequently, as shown in [88] the model order can be significantly reduced while still capturing the dynamics of the system.

Even though the work of the article focuses on control and not physical parameter identification, the method has interesting and potentially useful features regarding the random nature of occupants' behaviour. The exact use of fractional-order models with the aim of characterising thermal properties of buildings is not clear. However, if the models can be physically interpreted, it might be useful for modelling systems with random disturbances like occupants' behaviour.

4.2.2 ARX and ARMAX Models Continued – Implications of the MA Term

As mentioned earlier, the data-driven models are simplified representations of the physical system one wants to model. It is often assumed that two or three time constants are adequate to describe a building

treated as a lumped resistance-capacity (RC) model — see e.g. Section 4.2.3.

However, several of the studies mentioned previously in Section 4.2.1 show that exceptionally high number of lags were needed to describe the dynamics of buildings. In the most extreme case 100 lags of the inputs were needed to achieve similar accuracy as a 6^{th}-order FARX model [88]. In [87], ARX models with up to 100 lags in the inputs were tested as well. It was, however, stated that no significant improvements were observed for more than a 30 lags.

It should be noted that both methods were intended for prediction rather than identification of physical parameters. However, both studies extended their models by including an increasing number of lagged input variables, while keeping the order of the output polynomial at one. As stated in Section 4.2.1, this means that the building in both cases was modelled with a single time constant. Furthermore, as the transfer function $H(B)$ in Equation (4.18) is improper, the systems in both studies are non-causal — future events influence the past [89].

Despite the non-causal systems just mentioned, other studies find similar tendencies on causal systems used for system identification of buildings. In [90] the order of the ARX output polynomial were found to be between 30 and 46, and in [91] the order of the output polynomial were found to be between 33 and 87.

Although some of the high-order models found in the literature are not causal, the conclusion is the same. ARX models seem to require higher order than what is physically sensible.

The reason for the high-order ARX models is most likely due to the fact that the stochastic process is more similar to an ARMAX process, rather than an ARX process. As invertible ARMAX models can be reformulated as infinite-order ARX models, it is not surprising that high-order ARX models are obtained if the underlying process is more similar to an ARMAX process. The invertible ARMAX model

$$\underbrace{\phi(B)Y_t = \omega(B)u_t + \theta(B)e_t}_{\text{ARMAX model}}\,, \tag{4.27}$$

can be described as

$$\underbrace{\theta^{-1}(B)\phi(B)Y_t = \theta^{-1}(B)\omega(B)u_t + e_t}_{\text{ARX model of infinite-order}}\,, \tag{4.28}$$

where $\theta^{-1}(B)$ is an infinite-order polynomial as per definition of invertible linear processes [72].

The question is therefore: Is it reasonable to believe that thermal dynamics are described by an ARMAX process rather than an ARX process?

The ARX Model with Observation Noise

In [72] (page 300-301) it is shown that the noise process of an observed random walk on state-space form is an MA(1) process. In the same manner, the ARX model with observation noise can be shown to be analogue to an ARMAX model.

First the ARX model with observation noise on state-space form is defined:

$$Y_t = \phi Y_{t-1} + \omega u_t + \eta_t\,, \tag{4.29}$$

$$Y_t^* = Y_t + \xi_t\,, \tag{4.30}$$

where Y_t is the state variable at time t, Y_t^* is the observation of Y_t, u_t is an input, ϕ and ω are the model parameters, and $\{\eta_t\}$ and $\{\xi_t\}$ is white noise with variance σ_η^2 and σ_ξ^2, respectively.

By substitution, Equation (4.29) and (4.30) can be formulated as

$$Y_t^* - \phi Y_{t-1}^* - \omega u_t = \eta_t + \xi_t - \phi \xi_{t-1} \,. \tag{4.31}$$

The left-hand side of Equation (4.31) is now expressed as a function of the system and observation noise. To determine which process it is, the auto-correlation function ρ can be calculated.

By definition the auto-correlation function of stationary processes is:

$$\rho(k) = \frac{\gamma(k)}{\gamma(0)} = \frac{\gamma(k)}{\sigma^2} \,, \tag{4.32}$$

where $\gamma(k)$ is the auto-covariance function of a stochastic process and its k times lagged values. Similarly, $\rho(k)$ is the auto-correlation for lag k [72].

Utilising the fact that the noise processes are white, and therefore uncorrelated in time, the covariance for lag $k = 0$ is calculated as:

$$\begin{aligned} \gamma(0) &= \mathrm{Cov}(\eta_t + \xi_t - \phi\xi_{t-1},\ \eta_t + \xi_t - \phi\xi_{t-1}) \\ &= \mathrm{Cov}(\eta_t,\ \eta_t) + \mathrm{Cov}(\xi_t, \xi_t) + \mathrm{Cov}(-\phi\xi_t, -\phi\xi_t) \\ &= \mathrm{Var}(\eta_t) + \mathrm{Var}(\xi_t) + \phi^2\,\mathrm{Var}(\xi_t) \\ &= \sigma_\eta^2 + \sigma_\xi^2(1+\phi^2) \,. \end{aligned} \tag{4.33}$$

In similar manner the covariance for $k = 1$ is calculated:

$$\begin{aligned} \gamma(1) &= \mathrm{Cov}(\eta_t + \xi_t - \phi\xi_{t-1},\ \eta_{t-1} + \xi_{t-1} - \phi\xi_{t-2}) \\ &= \mathrm{Cov}(-\phi\xi_{t-1},\ \xi_{t-1}) \\ &= -\phi\,\mathrm{Var}(\xi_{t-1}) \\ &= -\phi\,\sigma_\xi^2 \,. \end{aligned} \tag{4.34}$$

Finally, for $k > 1$ the auto-covariance function becomes zero. The auto-correlation function, $\rho(k) = \gamma(k)/\gamma(0)$, can therefore be written as

$$\rho(k) = \begin{cases} 1 & k = 0 \\ -\frac{\phi\,\sigma_\xi^2}{\sigma_\eta^2 + \sigma_\xi^2(1+\phi^2)} & |k| = 1 \\ 0 & |k| > 1 \,. \end{cases} \tag{4.35}$$

The auto-correlation function of the right-hand side of Equation (4.31) is equivalent to an MA(1) process [72]. Hence, the model in Equation (4.31) becomes

$$Y_t^* - \phi Y_{t-1}^* - \omega u_t = e_t + \theta e_{t-1} \,, \tag{4.36}$$

which clearly is an ARMAX model.

Doing the same for a state-space model of an n^{th}-order ARX model, one will see that the noise process can be formulated as an MA(n) process.

It can be concluded that the ARX model with observation noise on state-space corresponds to an ARMAX form, where the combination of state and observations noise results in an MA term.

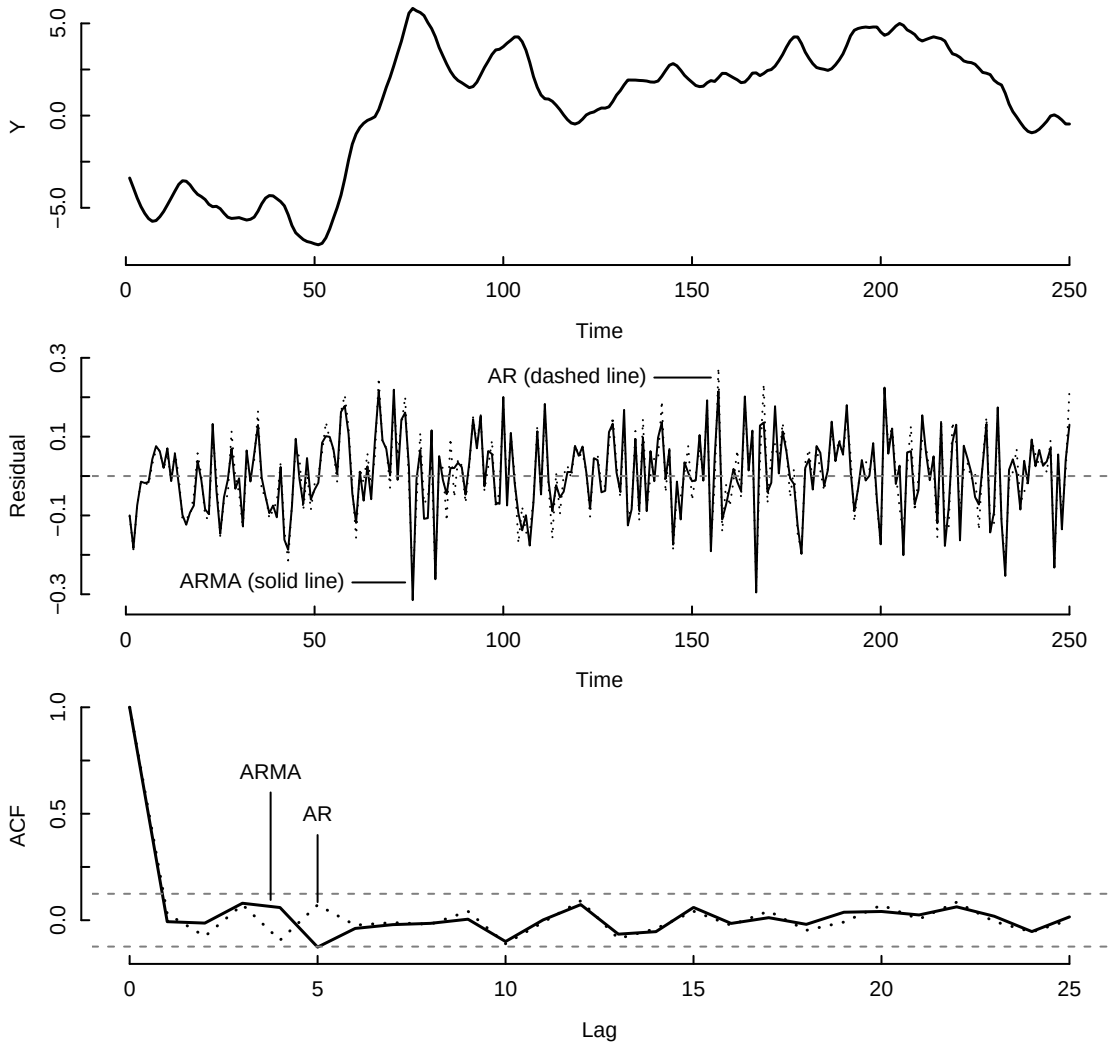

Figure 4.3: Realisation of the ARMA(2, 1) process defined in Equation (4.37) (first plot), the residuals and the auto-correlation functions of the estimated ARMA and AR models (second and third plot).

Estimation of ARX and ARMAX models on Simulation Data

To demonstrate that an ARMAX can be modelled as the high-order ARX model, a small simulation study has been made. For simplicity, the focus is here on auto-regressive models without exogenous input. I.e. AR and ARMA models.

First an ARMA(2, 1) process is defined as in Equation (4.37), and a simulated realisation with 250 time steps is made. The AR parameters are taken from one of the models in **Paper D**, and the MA parameter is selected such that the MA term is invertible. For MA(1) processes that is for $|\theta_1| < 1$, where θ_1 is the coefficient in the backshift polynomial found in Equation (4.16). The process is shown in Figure 4.3 (top).

$$(1 - 1.768B + 0.769B^2)Y_t = (1 + 0.9B)e_t \tag{4.37}$$

The best AR and ARMA model describing the process in Equation (4.37) is found by means of the Bayesian information criterion (BIC) and the Akaike information criterion (AIC) stated in Equation (4.41) and Equation (4.42). The model selection is done automatically with use of the *R* package *forecast* [74].

The best model fit were an ARMA(2, 1) model, with the estimated parameters and the standard error in the parenthesis: $\hat{\phi}_1 = 1.790\,(0.038)$, $\hat{\phi}_2 = -0.797\,(0.038)$, and $\hat{\theta}_1 = 0.905\,(0.033)$. The same

model were obtained when both the AIC and BIC selection criterion were used.

Using the same approach to find the best AR model which describes the ARMA process, a significantly higher number of parameters were needed. The best possible model found were an AR(9) model when the AIC was used for model selection, and an AR(6) model when the BIC was used.

Both the AIC and BIC were reduced by fitting an ARMA model instead of an AR model to the process in Equation (4.37) as shown in Table 4.1.

Table 4.1: Akaike and Bayesian information criterion of best fit of the model in Equation (4.37).

			Model order	
Model	AIC	BIC	p	q
AR	-416.5	-387.6	9 / 6	0
ARMA	-426.8	-412.7	2	1

The residuals and the auto-correlation functions of the residuals are shown for both the estimated ARMA and the AR model in Figure 4.3 (second and third plot). In both cases, there is no sign of auto-correlated residuals.

The demonstration shows that it is possible to model an ARMA process with a high-order AR model. In the same manner, ARMAX processes can be modelled as high-order ARX models.

Applying ARX models on building data may, therefore, result in more estimated time constants than anticipated and found in the literature on lumped RC models. Applying an ARMAX model will in contrast to this, limit the number of estimated time constants, and instead rely on the fact that the noise can be modelled with an MA term.

Estimation of ARX and ARMAX models on Building Data

Testing the same hypothesis that ARMAX models are capable of describing building dynamics by using fewer model parameters, can be tested on actual building data. In the following, three data sets from two different buildings are used for estimating of several different ARX and ARMAX models to validate the hypothesis further.

The general model which is tested, is

$$\phi(B)T_{\mathrm{i},t} = \omega(B)U_t + \theta(B)e_t\,, \tag{4.38}$$

where

$$U_t^\top = \begin{bmatrix} T_{\mathrm{e},t} & \Phi_{\mathrm{h},t} & I_{\mathrm{g},t} \end{bmatrix}\,, \tag{4.39}$$

$$\omega(B) = \begin{bmatrix} \omega_1(B) & 0 & 0 \\ 0 & \omega_2(B) & 0 \\ 0 & 0 & \omega_3(B) \end{bmatrix}\,. \tag{4.40}$$

The order of the polynomials $\omega_1(B)$, $\omega_2(B)$ and $\omega_3(B)$ is varied between 1 and 5 (both included), and the order of $\phi(B)$ and $\theta(B)$ is varies from 0 to 5. The ARX model is obtained for $\theta(B)$ of order zero such that $\theta(B)e_t$ becomes e_t.

Omitting the combinations where $\omega_1(B)$ to $\omega_3(B)$, and $\theta(B)$ is higher than the output polynomial $\phi(B)$, gives a total number of 1204 combinations.

The three data sets tested are from an occupied house in Gainsborough, England, and a test facility house with simulated occupants at the Fraunhofer Institute in Holzkirchen, Germany. Buildings and data descriptions can be found in [92, 93]. Two different data sets (i.e. two different periods) from the house in Gainsborough has been tested as well as one data set form the test house in Holzkirchen.

During any model selection process a certain measure of the model accuracy is used to determine if one model is better than another. A few examples are the likelihood ratio test described in Section 4.2.3, the Akaike information criterion (AIC), or Bayesian information criterion (BIC) used earlier. Common for all the methods is that they favour the model accuracy and penalise on the number of model parameters to avoid overfitting. For example, the AIC penalise two times the number of parameters, and the BIC $\log(n)$ times the number of parameters, where n is the number of observation used for model estimation.

$$\text{AIC} = 2k - 2\log(\mathcal{L})\,, \tag{4.41}$$

$$\text{BIC} = \log(n)k - 2\log(\mathcal{L})\,, \tag{4.42}$$

where k is the number of parameters, n is the number of observations, and $\mathcal{L}$ is the maximum likelihood of the model.

In a situation without penalisation on the number of parameters, the largest model would be preferred, as it will fit the training data better. However, the estimated model will be prone to overfitting. In a more general formulation of the information criteria of Equation (4.41) and (4.42), where $2k$ and $\log(n)k$ is generalised as $\text{PF} \cdot k$,

$$\text{IC} = \text{PF}\, k - 2\log(\mathcal{L})\,, \tag{4.43}$$

that would correspond to $\text{PF} = 0$.

In the first row of plots in Figure 4.4 the black line indicates the number of parameters included in the best possible ARX model with different values of the penalties factor PF in Equation (4.43). Without penalising on the number of parameters, the ARX model utilises the total number of possible parameters (20). Increasing the penalty factor, reduces the number of parameters. Eventually (but not shown in the figure) the number of parameters would reach 4, which is the minimum for the given model structure.

After the best ARX model was found for each level of PF, the smallest (in terms of the total number of parameters) ARMAX model which performed at least as good as the ARX model was found. This is indicated with the red line in the upper plots of Figure 4.4.

In the second row of plots, the corresponding information criteria calculated as in Equation (4.43) are shown. For reference, the dots on the lines indicates the Akaike information criterion (left) and the Bayesian information criterion (right).

The general trend in the upper plots is that the number of parameters can be significantly reduced by applying an ARMAX model instead of an ARX model when the penalty factor is low.

On the other hand, hard penalisation on the number of model parameters tends to make the ARX model preferable, if the goal is to keep the number of model parameters as small as possible. The potential dynamics in the model residuals are simply too costly to model with an MA term.

The plot shows for many cases, that the model can be reduced and thereby made more general by including an MA term to the ARX model. This means that what otherwise would have been described by several parameters in the ARX model, can be described by a simpler MA term. Provided a good model

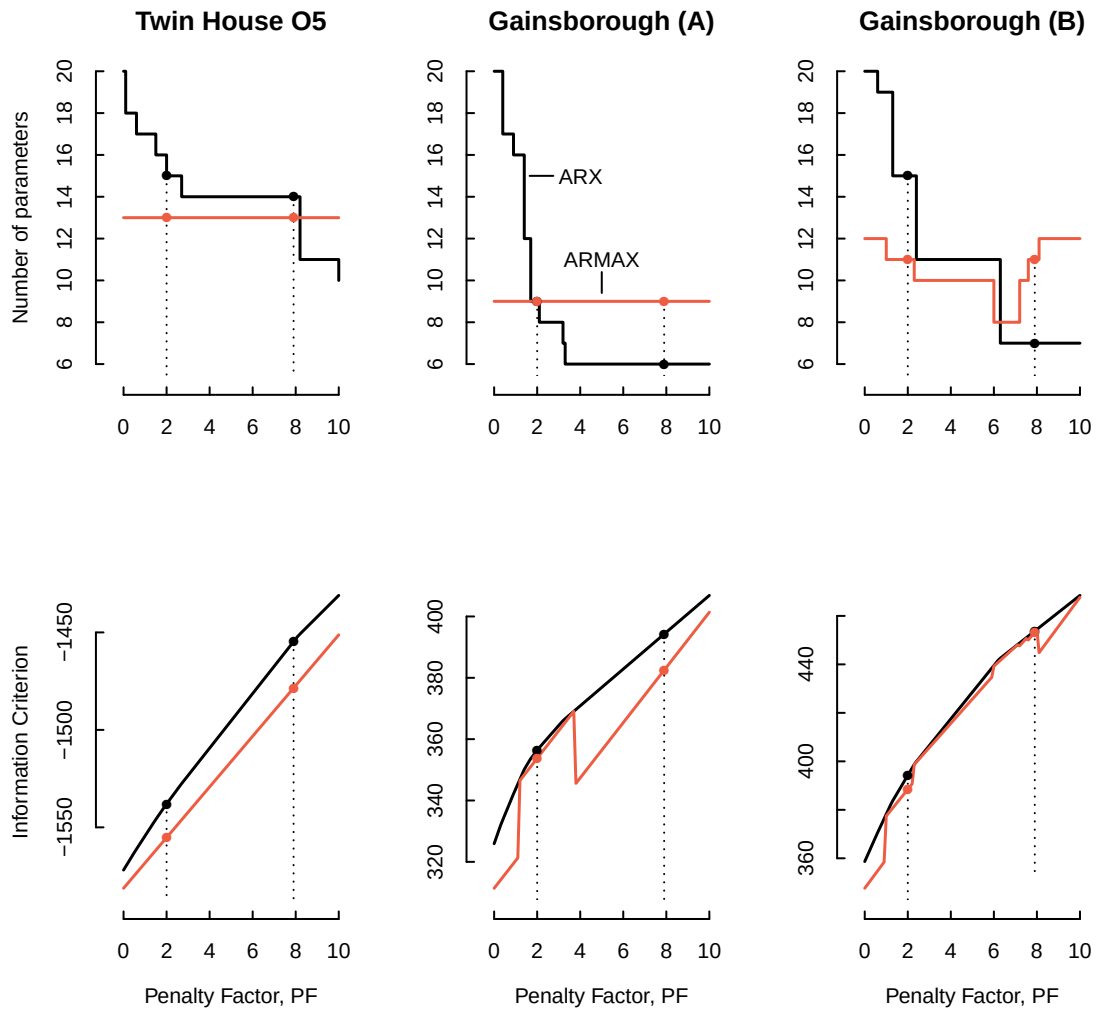

Figure 4.4: Comparison of the number of parameters (top) and the information criterion (bottom) for different levels of parameter penalisation when using ARX and ARMAX model for dynamical building modelling.

structure, the ARMAX model will make the AR term describe the systematic thermal dynamics, and the MA part describe the model and observation noise.

As the AIC penalise less on the number parameters (in practically any case) than the BIC, the selected ARX model is more likely to overfit. That means that it describes the noise in the data, which cannot be generalised to new observations.

On the other hand, by selecting the ARX model based on the BIC, one might end up with a model which describe the general building dynamics better. However, as the observation noise and potentially unmodelled effect will result in correlated errors as seen earlier, the ARX model which describes the true dynamics will show signs of auto-correlated residuals. Hence, it is might be difficult to validate the model by classical residual analysis methods.

One possible solution is, therefore, to use an ARMAX model instead of an ARX model, and select the best model based on cross-validation, such that a good balance between model bias (underfitting) and variance (overfitting) is obtained.

In Figure 4.5 the estimated heat loss coefficients obtained by the best ARX and ARMAX model are plotted as a function of the penalty factor PF. From the figure, there does not seems to be a difference in

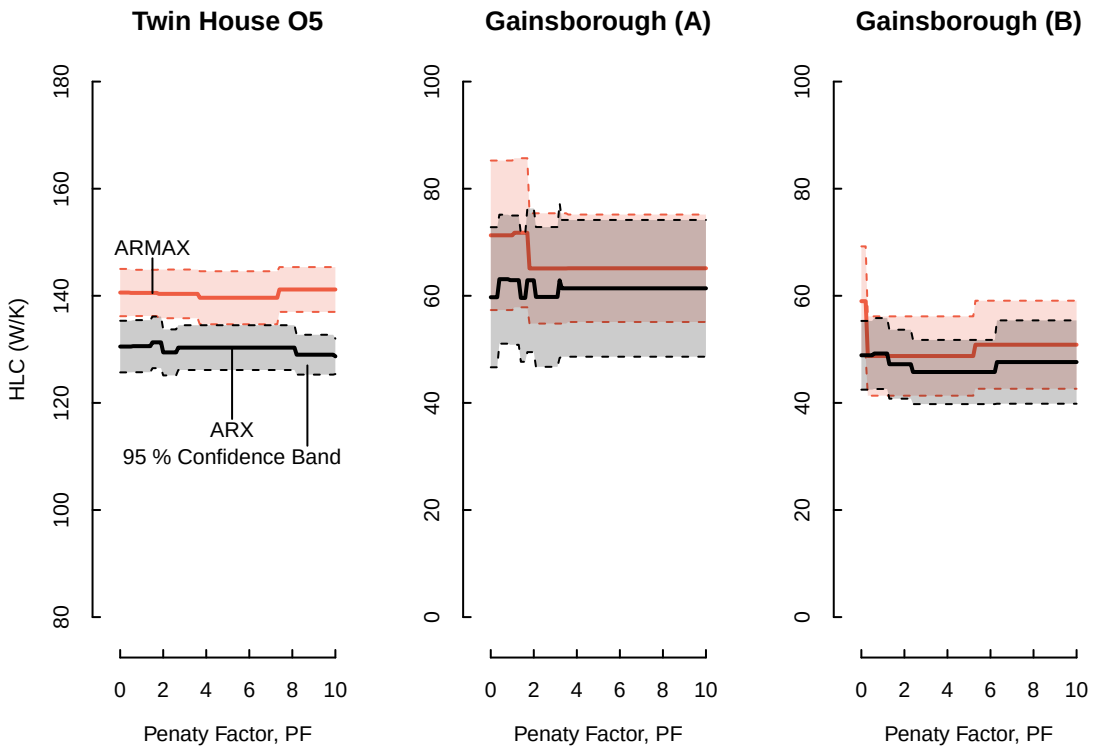

Figure 4.5: Estimated heat loss coefficients (HLC) from two different buildings when using ARX and ARMAX models.

the width of the 95 % confidence intervals for the individual estimated models. However, the estimated HLC from the ARMAX model (red line) is consistently higher than the estimated HLC obtained from the ARX model (black line).

As seen for the two right-most plots in Figure 4.5 the estimated HLC for the same house on two different periods gives similar results. However, it was expected that the match would be better by applying an ARMAX model rather than an ARX models, as the disturbances were expected to be handled better.

Other methods, such as omitting data with high levels of disturbances (e.g. occupied periods), might be useful to obtain more consistent estimates. This is further discussed in **Paper D** and in Section 4.4.

4.2.3 Continuous-Time State-Space Models

In the previously described ARX and ARMAX models, the parameters are dependent on the sampling time. Furthermore, the combined system and observation noise is assumed Gaussian and treated under a single term e. In the state-space models, the parameters can have direct physical meaning and they are invariant to the sampling time. Hence, the models can also be estimated on non-equidistant observations contrary to the ARX and ARMAX models. Furthermore, observation and system noise can be estimated separately.

The state-space models consist of one or more states which describe the main evolution of the system, and for the stochastic state-space models, the system and observation uncertainty is included as well.

The state equations in continuous time are often described by stochastic differential equations (SDEs), which will be explained in the following section. The observation equation is briefly described afterwards.

Stochastic Differential Equations

Stochastic differential equations are the natural extension of ordinary differential equations (ODEs). In general any SDE can be formulated as

$$\mathrm{d}X_t = \underbrace{f(X_t, U_t, t; \theta)\mathrm{d}t}_{\text{Drift}} + \underbrace{\sigma(X_t, U_t, t; \theta)\mathrm{d}W_t}_{\text{Diffusion}}, \tag{4.44}$$

where X_t is the state variable as function of time t with initial condition X_0. U_t is a vector of deterministic inputs, and θ is the model parameters. Finally, W_t is the standard Wiener process representing the system noise. A detailed introduction to stochastic differential equations and its applications can be found in for example [71, 94, 95].

The state variable X_t in Equation (4.44) can contain multiple states. The number of the states, is the order of the state-space model. One example of a second-order state-space model is given in Equation (4.20) to Equation (4.22).

Within the building modelling framework, the diffusion term in (4.44) is typically treated as independent of the stochastic state variables X_t. Furthermore, the dependence on the inputs U_t is rarely seen as well. It can, however, be utilised to introduce different level of system uncertainties by for example including information on estimated occupancy status as found in **Paper A**.

The evolution of the states of a dynamical system w.r.t. time is separated into two distinct terms, namely the drift and the diffusion term as shown in (4.44). Parametric, non-parametric or semi-parametric as well as linear or non-linear functions can be used to describe both the drift and diffusion term. This makes the SDEs capable of describing complex dynamical systems while handling measurement noise and process noise separately. The latter being model approximations and noise originating from unknown disturbances to the system [95]. The diffusion term might as well describe the noise in the otherwise deterministic inputs U_t, as long as it is approximately Gaussian.

Observation Equation

The observation equation related to the state-space model is in its general form written as

$$Y_k = g(X_{t_k}, U_{t_k}, t_k; \theta) + e_{t_k}\,, \tag{4.45}$$

where Y_k represents the discrete-time observations of the model output, which are linked with the continuous-time state equation through the linear or non-linear function $g(X_{t_k}, U_{t_k}, t_k; \theta)$. The subscript t_k with $k = 0, 1, \ldots, N$ represents the sampling instants and $e_{t_k} \sim \mathrm{N}(0, \sigma^2)$ represents the measurement noise. I.e. a zero mean white noise process. Generally, for all t and t_k, mutual independence is assumed amongst the stochastic entities X_t, W_t and e_{t_k}.

Maximum Likelihood Estimation

One approach to estimate the model parameters of stochastic differential equations is to use maximum likelihood estimation (MLE). The advantage of the MLE method over e.g. the least squares (LS) method is that this method allows for estimating the parameters related to the noise term as well. Here the MLE method is briefly outlined, but further details can be found in [96].

Given a sequence of measurements $\mathcal{Y}_N = \{Y_1, Y_2, \cdots, Y_N\}$, the likelihood function is the joint probability density of all the data but considered as a function of the unknown parameters. The likelihood function can therefore be written as the product of the one-step ahead conditional densities

$$\mathcal{L}(\theta|\mathcal{Y}_N, \mathcal{U}_N) = \prod_{k=1}^{N} p(Y_k|\theta, \mathcal{Y}_{k-1}, \mathcal{U}_k)\, p(X_0|\theta), \tag{4.46}$$

where θ is the set of parameters, $\mathcal{Y}_N$ and $\mathcal{U}_N$ are the sets of observations and inputs, and $p(Y_k|\theta, \mathcal{Y}_{k-1}, \mathcal{U}_k)$ is the probability of observing Y_k given the previous observations and inputs. This is the so-called exact likelihood function which contains a parametrisation of the density associated with the initial state X_0.

Since the systems are assumed driven by the Wiener process, which has Gaussian increments, the one-step ahead density for linear systems is also Gaussian. For most non-linear systems this is still a reasonable assumption, and can be checked – see e.g. [97].

In the Gaussian case the conditional density is completely characterised by the conditional mean (the prediction) and the conditional covariance. By introducing the one-step prediction error (also called the *innovation error* or *residuals*)

$$e_{k|k-1} = Y_k - \hat{Y}_{k|k-1}, \tag{4.47}$$

and the associated covariance, $R_{k|k-1} = \mathrm{Var}(Y_k|\mathcal{Y}_{k-1}, \theta)$ the likelihood function can be written as

$$\mathcal{L}(\theta|\mathcal{Y}_N, \mathcal{U}_N) = p(\mathcal{Y}_N|\mathcal{U}_N, \theta) \tag{4.48}$$

$$= \left(\prod_{k=1}^{N} \frac{\exp\left(-\frac{1}{2} e_k^\top R_{k|k-1}^{-1} e_k \right)}{\sqrt{\det\left(R_{k|k-1}\right)\left(\sqrt{2\pi}\right)^{\mathrm{L}}}} \right) p(X_0|\theta)\,, \tag{4.49}$$

where L is the dimension of the observation space.

Using logarithm we obtain the log-likelihood function

$$l(\theta|\mathcal{Y}_N, \mathcal{U}_N) = -\frac{1}{2} \sum_{k=1}^{N} \left(e_k^\top R_{k|k-1}^{-1} e_k + \log\left(\det\left(R_{k|k-1}\right) (2\pi)^{\frac{\mathrm{L}}{2}} \right) \right) + \log(p(X_0|\theta))\,.$$

The parameter estimates are found by maximising the log-likelihood function

$$\hat{\theta} = \arg\max_{\theta} \left\{ l(\theta|\mathcal{Y}_N, \mathcal{U}_N) \right\}. \tag{4.50}$$

The corresponding value of the log-likelihood is the observed maximum log-likelihood value given the available data set.

For linear models the conditional mean and covariance are calculated using an ordinary Kalman filter, while for nonlinear models an extended Kalman filter is used. See [96] for further details.

Model Selection with Likelihood Ratio Test

Given two nested models—i.e. two competing models where the smaller model is contained in the larger—the increased goodness of fit for the model extension can be tested with the likelihood ratio test (LRT).

The likelihood ratio is for a given set of observations $\mathcal{Y}_N$ and model inputs $\mathcal{U}_N$ defined as

$$\lambda(\mathcal{Y}_N, \mathcal{U}_N) = \frac{\sup_{\theta \in \Theta_0} \mathcal{L}(\theta; \mathcal{Y}_N, \mathcal{U}_N)}{\sup_{\theta \in \Theta} \mathcal{L}(\theta; \mathcal{Y}_N, \mathcal{U}_N)}\,, \tag{4.51}$$

where Θ_0 is the parameter space for the null model (i.e. the smaller model) and Θ is the parameter space for the alternative model (i.e. the larger model) [98].

For small values of λ the null hypothesis is rejected, hence the extended model is accepted. The evidence against the null model is measured by the p-value, which can be obtained from Wilk's likelihood ratio

test as two times the negative log-likelihood ratio converges to the chi-squared distribution with $k - m$ degrees-of-freedoms:

$$-2\log\lambda(\mathcal{Y}_N, \mathcal{U}_N) \to \chi^2(k-m)\,, \tag{4.52}$$

where $\chi^2(k-m)$ is the chi-squared distribution with $k-m$ degrees-of-freedoms, and k and m are the number of parameters in the extended and the null model, respectively [99].

For unnested models, other selection methods need to be applied. E.g. the Akaike information criterion (AIC) or the Bayesian information criterion (BIC) stated in Equation (4.41) and (4.42), respectively. For situations with plenty of data, cross-validation techniques can also be used.

State-space Models Used in Practice

The continuous-time state-space models have been used to characterise building dynamics for many years. In [60] a procedure for modelling and model selection is presented. In the study, which was performed on unoccupied buildings, it was found that a 4^{th}-order model was sufficient to describe the thermal dynamics. The estimated thermal resistances were, however, similar for all models, and the total effective heat capacity was of similar magnitude for 3rd to 5th-order models.

In [100] a grey-box model of 2^{nd}-order was found adequate to describe the thermal dynamics. The same article also lists several other studies (see [101–103]) where the order of the applied grey-box models varies from first to second-order models. All studies were conducted on unoccupied buildings or simulated data. Another study found that fourth to fifth-order models were optimal for describing the thermal dynamics of a building [104].

The variation in the number of states used to describe the thermal dynamics can be many. However, two, three or eventually four states seem to be sufficient for most cases.

As stated in [100], most studies found in the literature is carried out on either simulation data or unoccupied buildings. However, a recent study found in [105], utilise dynamical lumped thermal capacity models combined with Bayesian methods to identify thermal characteristics of occupied buildings. The models have been tested on two different occupied houses. A special focus in [105] been on modelling the solar gain by distinguishing between diffuse and direct solar irradiation, and using the irradiation in the plane of the building facades.

By training several models on subsets of the data, the best performing grey-box model was found. This model showed that the estimated heat loss coefficient varied as little as 15 % for the different sub data sets. This includes data sets of only 5 to 10 days duration in the summer. This is assumed to be possible only due to well modelled solar gains which are a main driving force for the thermal dynamics during a period with low temperature differences between inside and outside.

An alternative approach to dynamical solar gain modelling in buildings (and thermal energy systems in general) is given in **Paper B**. No information on the building is given. Instead, the daily variation of the solar transmittance is estimated directly from data by use of semi-parametric methods — i.e. B-splines.

4.3 Other Model Types

All methods mentioned until now have one thing in common. They are all used for system identification. That means, that the aim is to identify key parameters which describe the thermal building performance such as the heat loss coefficient, time constants, solar transmittance etc., and eventually use the model for prediction. Recently this machine learning practice has also been named *explainable artificial intelligence* (XAI) [106–109] or *physics enhanced artificial intelligence* (PEAI) [110].

Other machine learning techniques under the "classical" term artificial intelligence (AI) has also been applied on buildings with various goals. Common for most of them is, however, that they lack interpretability. That means that the models cannot be explained in a physical way and therefore categorised as black-box models. These methods are more often used for prediction, control and clustering. Consequently they are not relevant for quantification of thermal performance for the time being. A thorough review of black-box machine learning techniques can be found in [111].

4.4 Avoiding the Occupants – Selective Data Use

For the dynamical models especially, the data can contain significant amounts of dynamics which are not related to the actual building's thermal characteristics — but rather the occupants' behaviour and interaction with the building. For example, a temperature decay related to heat transmission through the building envelope, will not be noticeably different from a temperature decay related to a window opening. Both scenarios will result in some sort of decay, but with different decay rates. Estimating a rather simple model where the window openings are not included, the temperature decays due to window openings will affect the estimated time constants and the heat loss coefficient.

Fitting a model on data obtained from occupied buildings, will undoubtedly affect the estimated parameters. Furthermore, estimating the same model on the same house, but during different periods will most likely results in different results as it also was found in Section 4.2.2.

One way to reduce the occupants' effect on the estimated model, is to be selective about the data for model estimation.

A natural modelling approach to tackle the disturbances caused by the occupants would be to focus on measurements during night-time. For most dwellings, it would result in fewer disturbances as the occupants are asleep. Another benefit — if information about solar transmittance is not of interest — is that solar gains can be disregarded, which may be beneficial due to its complex nature.

A small investigation on the accuracy of the estimated heat loss coefficient has been made on an occupied house in England, Gainsborough, as part of the IEA-EBC Annex 71 [86].

The measurements were obtained between December 1 and December 10, 2012, from a two-story apartment of 67 m^2. Ten minutes samples of indoor and outdoor temperature, heat consumption, electricity consumption, and onsite photovoltaic (PV) production as a substitution for solar irradiation were used. The indoor temperature was calculated as the space volume-weighted mean temperature in each time step, based on the temperatures measured in the living room and the bedroom.

The measured heat consumption is a combination of heat consumption for space heating and domestic hot water (DHW) production. In this small study, several derived heat consumptions has been tested. That being, the combined space heating and hot water production Φ_{h_1}, the estimated space heating alone obtained by filtering out apparent DHW production Φ_{h_2}, and the estimated space heating and electricity consumption Φ_{h_3}. The filtering is outlined in the presentation by the author from the 3$^{\text{rd}}$ IEA-EBC Annex 71 Expert Meeting in Chambéry, France [112].

The tested model is

$$\phi(B)T_{\mathrm{i},t} = \omega(B)U_t + e_t\,, \tag{4.53}$$

where

$$U_t^\top = \begin{bmatrix} T_{\mathrm{e},t} & \Phi_{\mathrm{h},t} & Q_{\mathrm{pv},t} \end{bmatrix} , \tag{4.54}$$

$$\omega(B) = \begin{bmatrix} \omega_1(B) & 0 & 0 \\ 0 & \omega_2(B) & 0 \\ 0 & 0 & \omega_3(B) \end{bmatrix} , \tag{4.55}$$

with the order of the output polynomial being 4, and the order of the input polynomials $\omega_1(B)$, $\omega_2(B)$, and $\omega_3(B)$ equal to 0, 0, and 3, respectively. From Equation (4.13) it can be seen that order zero corresponds to a non-lagged input variable.

As mentioned in Section 4.2.1 the auto-regressive model relies on equidistant inputs and outputs. Consequently, it is not possible to omit the day-time data. Instead, the model can for example be estimated by means of weighted least squares. The day-time residuals are simply assigned with a weight of zero, and the night-time residuals with a weight of one.

Validating the models through the residuals' auto-correlation function, one needs to take the weightings into account. By using weights of zero, it essentially means that the corresponding data are omitted from the fitting process. The same data should, therefore, be omitted in the residual analyses. However, by just removing them and calculating the auto-correlation will be wrong. The reason is that the correlation between the first residuals in the night-time will be determined by the correlation between them, and the last residuals in the previous night-time. The missing values need therefore to be treated properly, as shown in e.g. [113].

The smallest model which fulfilled the requirements that the noise should be white with mean zero, when applied on both data sets was found.

In Table 4.2 the estimated heat loss coefficient (HLC) and the root mean squared error (RMSE) of the model residuals are shown. It can be seen that the HLC estimated from all the data varies by 12.8 W/K depending on the signal used for the heat input in the model. In contrast to that, the standard error of the HLC is significantly smaller when estimation is carried out on night-time data. That is despite the fact that the model is estimated on a smaller data set (one-third) due to the exclusion of the day-time values.

Table 4.2: Comparison of estimated heat loss coefficients (HLC), standard errors (σ), and root mean squared errors (RMSE) of the model fits when using all available data and night data, respectively.

	All data	Night data	Heat input
HLC (σ) [W/K]	69.8 (5.6)	55.7 (3.5)	Combined space heating and DHW
	57.9 (4.8)	54.3 (3.5)	Estimated space heating
	57.5 (4.8)	54.3 (3.5)	Estimated space heating and electricity use
RMSE [°C]	0.0438	0.0261	Combined space heating and DHW
	0.0432	0.0262	Estimated space heating
	0.0432	0.0262	Estimated space heating and electricity use

The model fit is also improved by using night-time data. By modelling the night-time data only, the RMSE was reduced by around 40 %.

In conclusion, the results show that the HLC estimate is far more consistent and precise when using night-time data. The model fit is better as well. This may indicate that day-time data consists of more disturbances than night-time data. This is most likely because the occupants interact with the building and therefore affect the thermal dynamics significantly more during day-time, than night-time. Additionally, the constant solar transmittance may not be sufficient to describe the solar gain as described in **Paper B**.

This technique is further applied to buildings with night-setback in **Paper D** to estimate the energy flexibility potential, and to cluster them accordingly.

As an alternative to omitting data entirely, **Paper A** presents a method for estimation of the presence of occupants in residential buildings, with the ultimate goal of modelling the system and/or the observation noise more carefully.

4.5 Inaccuracy Solar Gain Estimation – A Common Issue

In all of the previous presented models, the solar gain has either been neglected because night data were used, or it has been treated as a constant proportion of the solar irradiation. In this text the fraction of solar gain and solar irradiation is called solar transmittance. In the field of building engineering, the solar transmittance is solely a window property called the g value, or the gA value if window area is multiplied with it. The latter is expressed as

$$\mathrm{gA} = \frac{\Phi_{\mathrm{sol}}}{I}\,, \tag{4.56}$$

where Φ_{sol} is the solar gain measured in watts, and I is the solar irradiation measured in $\mathrm{W/m^2}$.

By using data-driven methods to estimate the solar transmittance, it does not only become a function of the window properties and window areas — but also a function of shading obstacles around the building, dirt on the windows, etc. It is therefore not directly comparable with the building physical term.

Solar transmittance is varying significantly during the day. The variation is dependent on things like the building geometry, the window properties, and the surroundings. So, it is dependent on factors which are not easily quantifiable from a data-driven modelling perspective. This is also why a simplification, such as treating the solar transmittance as constant is commonly used.

In the following, the variations in the daily solar transmittance is brought into focus.

The Fraunhofer data set [93] from the IEA-EBC Annex 71 project [86] used earlier, provides detailed measurements of solar irradiation, as well as indoor irradiation in the test buildings. This gives a great opportunity to investigate the actual solar gain in buildings. The data is obtained in December 2018 and January 2019.

The test building is a representation of a two-story single-family house of 165 $\mathrm{m^2}$, with windows towards the north (1.3 $\mathrm{m^2}$ glazing area), south (7.2 $\mathrm{m^2}$), east (1.3 $\mathrm{m^2}$) and west (2.6 $\mathrm{m^2}$). In one of each of the north, south, east and west windows the indoor and outdoor solar irradiation were measured in a parallel plane of the window. In Figure 4.6 the solar gain for each of the four orientations is shown. The solar gain is simply calculated as the product of the measured indoor irradiation and the corresponding glazing area.

From the south-oriented windows (7.2 $\mathrm{m^2}$ glazing area) it is seen that the solar gain can reach levels of up to 8000 W. This will undoubtedly affect the indoor temperature. A good solar gain model is therefore important to describe the thermal dynamics of the building.

It should be noted that the measurements in Figure 4.6 are obtained during a period with snow-covered ground. The number are, therefore, higher than one would expect due to increased ground reflection. The order of the effect is however unknown.

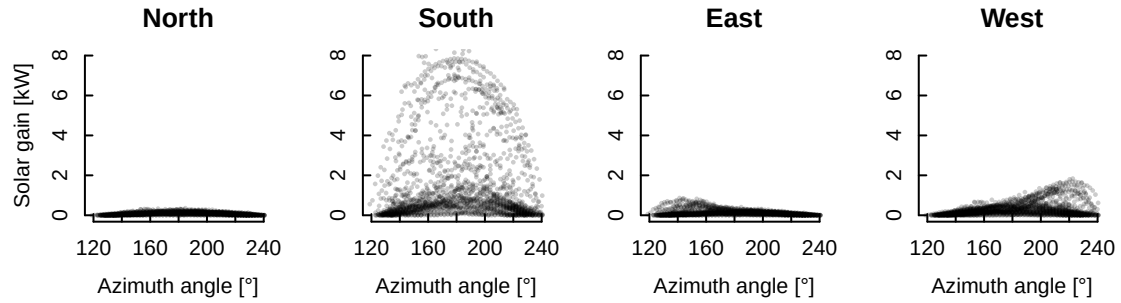

Figure 4.6: Solar gain obtained from measurements of outdoor and indoor measurements of total solar irradiation. The measurements are from a test building at the Fraunhofer Institute in Holzkirchen, Germany.

The typical modelling approach to estimate the solar transmittance gA (and consequently the solar gain Φ_{sol}) is

$$\Phi_{\text{sol}} = \text{gA}\, I_{\text{g}} + e, \tag{4.57}$$

where I_{g} is the global solar irradiation, and $e \sim \text{N}(0,\ \sigma^2)$ is the noise term.

The model in Equation (4.57) is fitted on the Fraunhofer data and the estimated transmittance and the residuals are shown in Figure 4.6.

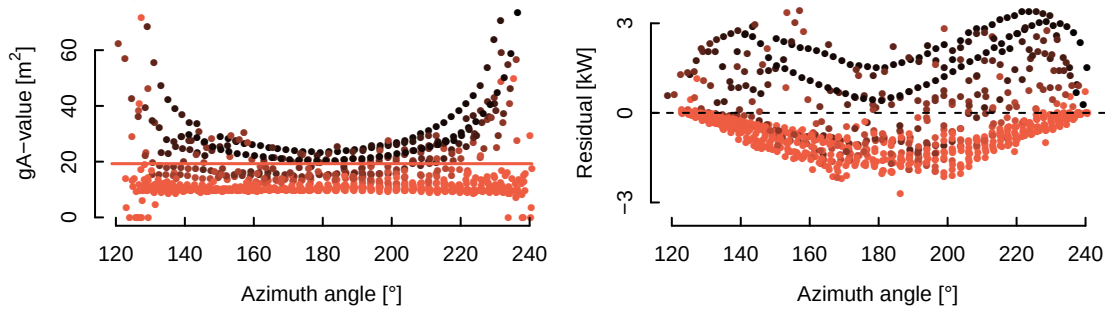

Figure 4.7: Solar gain estimated as a constant proportion of the global solar irradiation as shown in Equation (4.57). The red lines indicates the estimated solar transmittance and the bright red band (barely noticeable) indicates the 95 % confidence interval. The second column shows the solar gain residuals.

In the left plot in Figure 4.7 the solar transmittance obtained from the measurements of the indoor and outdoor total solar irradiation is shown (black and red dots). Two patterns dominate the picture: first, a dense point cloud of red dots with a constant mean of approximately 10 m^2 is seen, and secondly, a convex shape of black dots is seen in the upper region of the plot. The red dots indicate low levels of beam irradiation and the black dots indicate high levels of beam irradiation. It is clear that a constant solar transmittance is a poor model choice for such non-linear data. The red straight line and its barely noticeable 95 % confidence interval which minimises the squared errors of the predicted solar gain is an example of that. The estimated solar transmittance (gA) is obtained by Equation (4.57).

The right plot shows the errors of the predicted solar gain as a function of the azimuth angle, given the estimated constant solar transmittance. The residuals show, not only that the requirement of the model errors is violated, but also that rather large errors for a house with less than 13 m^2 of window glazing is obtained.

The residuals show clearly that there is a dependency on the azimuth angle, but it also shows two distinct patterns for overcast periods (red dots) and clear sky periods (black dots). To give a better description of the solar gain, a new sun position dependent semi-parametric method is proposed in **Paper B**.

4.6 Conclusion on Data-driven Methods

The method outlined in the previous sections shows examples of methods used in practice and methods used in research. In general, it can be said that practitioners tend to use quasi-stationery methods for documenting the thermal performance of buildings, while researchers tend to work and develop methods which can explain the thermal dynamics of the building.

Two central and related reasons for the dynamical models' high attention in the field of research, is, for the first, that dynamical models can be used for improved building control. This being for example model predictive control (MPC) which optimises the adjustments of the building systems according to e.g indoor climate criteria, energy price and/or weather forecasts in a proactive manner [114]. Second, the dynamical models naturally offer additional information about the thermal building performance that the steady-state model cannot provide. That being information on heat capacities and time constants of buildings. A recent publication suggested a simple method to characterise buildings' (and other systems') capability to act as energy storage [19] — a key element in the transition from a situation with a steady supply of energy from combustion or nuclear power plants, to fluctuating energy supply provided by renewable energy sources like wind and solar power. A demonstration of identifying energy flexibility is given in **Paper D**.

To achieve the best control strategy and get the best indication of the thermal building performance, robustness and reliability of the estimated models are important. The importance of accurate estimates are, however, even more important if it is used for building documentation, which potentially could have a financial impact on the various parties involved in the building design and construction. For prediction models — e.g. in MPC — the actual physical interpretability is less important as the focus is on prediction. That said, the models need to be physical meaningful in the sense that they are causal.

The current state-of-art in the field of parameter identification described earlier shows both progression and pitfalls. The pitfalls especially emerge when well functioning dynamical models used on experimental setups are applied to the occupied building as seen in e.g. [58]. In that case, special attention should be put on selecting data with the least amount of disturbances as done in **Paper D**, and/or describing the noise better by for example using ARMAX model rather than ARX models to identify thermal building dynamics.

In Chapter 5 the focus will be on the work carried out in as part of this thesis to tackle some of these issues.

5 Discussion of Contribution

In the following sections, the four articles contained in this PhD Thesis are presented and discussed.

The focus areas have been divided into two main areas: *modelling with disturbances in mind* and *obtaining reliable solar heat gains and dealing with unreliable observations*.

5.1 Modelling with Disturbances in Mind

In Section 4.4 it was briefly demonstrated how important it can be to treat different periods in the data differently.

In the following two sections, two papers contained in this thesis are discussed. **Paper D** shows how utilising only night-time data and be beneficial. The results of this are outlined in Section 5.1.1. Similarly, **Paper A** presents a method for estimating occupancy in dwellings, with the intent of describing the model noise in a more refined way. This paper is presented in Section 5.1.2.

5.1.1 Characterising Thermal Dynamics Based on Night-time Data

In **Paper D** the time constants — and from that, the energy flexibility potential as defined in [19] — of 39 Danish single-family houses were estimated based on measurements of indoor and outdoor temperatures only. The data used in this research consists of 10-minute samples of the indoor temperature, and hourly outdoor temperatures. The outdoor temperatures were upsampled to 10-minute values by linear interpolation, which was found reasonable during winter nights as the outdoor temperature varies slowly.

The assumption was as stated earlier: the least amount of disturbances in the thermal dynamics are found during the night. For houses with temperature night-setback, the time constants can then be estimated for the nightly temperature decay without any knowledge of the heat consumption. The temperature decay is described by the ARX model in Equation (5.1). Hence, the system is assumed to have two dominating time constants.

$$T_{\mathrm{i},t} = \phi_1 T_{\mathrm{i},t-1} + \phi_2 T_{\mathrm{i},t-2} + \omega T_{\mathrm{e},t} + e_t \,. \tag{5.1}$$

As for the previous notation, T_i and T_e are the the indoor and outdoor temperature, ϕ and ω are the model parameters, t is a time, and $e \sim \mathrm{N}(0, \sigma^2)$ is noise.

It is further shown to be equivalent to the set of stochastic differential equations in Equation (5.2) to (5.2) under certain assumptions. The main assumptions are that during the night, there is no heat contribution from the sun, and the heating is turned off. Therefore the heat input Φ_h and the solar gain $\mathrm{gA}I_\mathrm{g}$ can be neglected. Furthermore, it is assumed that there is no observation noise, which results in an ARX model rather than an ARMAX model as crystallised in Section 4.2.2.

$$\mathrm{d}T_\mathrm{i} = \frac{1}{C_\mathrm{i}} \left(\frac{1}{R_\mathrm{im}} (T_\mathrm{m} - T_\mathrm{i}) + \frac{1}{R_\mathrm{ie}} (T_\mathrm{e} - T_\mathrm{i}) + \Phi_\mathrm{h} + \mathrm{gA}I_\mathrm{g} \right) \mathrm{d}t + \sigma_\mathrm{i} \mathrm{d}W_\mathrm{i} \,, \tag{5.2}$$

$$\mathrm{d}T_\mathrm{m} = \frac{1}{R_\mathrm{im} C_\mathrm{m}} \left(T_\mathrm{i} - T_\mathrm{m} \right) \mathrm{d}t + \sigma_\mathrm{m} \mathrm{d}W_\mathrm{m} \,, \tag{5.3}$$

where C and R are the heat capacities and thermal resistances related to the two temperature states T_i and T_m, where the latter is the temperature of the the internal thermal mass. σ_m and σ_i are the scaling factors of the two Wiener processes W_m and W_i.

It was shown that the temperature differences ($T_{\mathrm{i},t} - T_{\mathrm{i},t-1}$) during the temperature decays were distributed distinctively different from the remaining temperature differences. This information were then used to pin-point the nightly temperature decays through a two state hidden Markov model (HMM). In [115] a similar method was used to detect occupants' activity levels based on CO_2 concentration measurements.

Besides that the model was tested on 39 occupied houses, the method was further tested on simulated data to show is capabilities of estimating the true time constants and thereby the energy flexibility potential of buildings.

The conclusion of the study was, that there is a clear relation between the estimated long time constant and the energy flexibility potential. The method therefore potentially serves as a valuable tool for large scale energy flexibility characterisation and clustering.

This is an utmost important capability in an energy market with variable prices, and for buildings with price-based heat control. The price signal can thereby be targeted specific end-user clusters to obtain the desired response. With large shares of renewable and fluctuating energy sources, the desired response would naturally be one that stabilises the energy grid.

In a market with CO_2 taxation on energy, the correct prices to achieve a desired end-user response (buy or wait) is directly related to the energy flexibility. Finally, to maximise the uptake of the produced renewable energy, reliable estimates of the flexibility are decisive, and by using night-time data for estimation, this can be achieved.

Additionally, the paper also highlights a possible pitfall regarding the reliability of the indoor temperature measurements. As a representative indoor temperature is hard or even impossible to measure as shown in Section 4.1.3, the model parameters describing the correlation between indoor and outdoor temperature are crucial.

For example, models with an insignificant model parameter ω in Equation (5.1) may indicate that the temperature decay is related to dynamics inside the house, rather than dynamics related to temperature loss to the outside. Such internal dynamics could be related to changing temperature stratification or heat loss to adjacent thermal zones, as the heating is turned off.

5.1.2 Estimating the Occupancy Status for Better Model Descriptions

As indicated in the study in Section 4.4 and as found in the literature in Section 3.1.1, the effect of the occupants is non-neglectable as they can cause the energy consumption to deviate significantly from what was anticipated. Therefore, their impact on the measurements used to characterise the thermal performance are important to take into account as well. Both the study on using night-time data in Section 4.4 and the work presented in **Paper D**, have dealt with this in a very strict manner — namely to disregard the day-time data entirely.

To utilise as much of the information in the data as possible while obtaining as accurate and precise performance estimates as possible, it seems natural to model the noise in a more sophisticated manner, instead of treating it as time-invariant or excluding certain data entirely.

The first problem at hand is therefore to gain knowledge about the occupancy status. As it is most unlikely to obtain data on the actual occupancy status, it needs to be estimated. One approach already mentioned, is by estimating different levels of occupancy activity based on CO_2 measurements [115]. Another approach with several similarities is to estimate the occupancy status by pattern recognition of the time variations in the CO_2 concentration. This methodology is described in **Paper A**.

The method builds on the tracer gas method commonly used for measuring ventilation rates in buildings. Typically, a tracer gas, like freon, is injected into a room, and the decay of the gas is monitored after the injection has stopped.

For tracer gases which are not present in the room under normal conditions the tracer gas mass balance can be written as

$$V\frac{\mathrm{d}c}{\mathrm{d}t} = -Qc\,, \tag{5.4}$$

where V is the space volume, c is the tracer gas concentration, Q is the ventilation rate, and t is the time.

The air change rate (i.e. the number of times the air volume is changed per unit of time) is defined as $N = Q/V$. Using that and solving Equation (5.4) the tracer gas concentration c can be modelled as

$$c(t) = c_0 \exp\left(-Nt\right) + c_\infty + e_t\,, \tag{5.5}$$

where c_0 is the initial tracer gas concentration after the cessation of the gas injection, and c_∞ is the steady-state tracer gas concentration [116].

Using the natural presence of CO_2 as a tracer gas, the air change rate N and the ultimate steady-state concentration c_∞ can be found and used as a proxy for the occupancy status. For example, is it reasonable to believe that the enclosed space which is investigated has been left unoccupied with windows and door to the outside closed, if the CO_2 concentration is decaying as described in Equation (5.5); the air change rate N is sufficiently slow (indicating that the air exchange occurs due to in- and exfiltration rather than ventilation); and the CO_2 concentration is approaching the outdoor concentration for $t \to \infty$.

As the CO_2 concentration of course is not decaying all the time, the decay periods need to be identified. The approach described in the article is based on non-parametric change point estimation, which tests for homogeneity in the distributions in pair-wise segments of time-ordered observations.

As the method is non-parametric, no prior knowledge of the distribution is needed. Furthermore, with the *E-divisive* change points detection algorithm used, both the locations and number of change points can be estimated [117].

Based on the detected change points of the CO_2 time series, the model in 5.5 can be fitted for the different segments, and evaluated in similar manners as described earlier. The full set of specification of the periods detected is listed in Table 5.1.

Table 5.1: Criteria for sleeping and unoccupied periods. All other periods not fulfilling the criteria are treated as occupied.

	Time [hh:mm – hh:mm]	N [h^{-1}]	c_∞ [ppm]	RMSE [ppm]
Sleeping	00:00 – 06:00	< 0.18	< 700	< 10
Unoccupied	—	< 0.18	< 460	< 10

Despite no proper model validation being possible, as the actual occupancy status were unknown, the results showed good agreement with other measures which typically also are related to the occupancy status — namely electricity and water use.

As the CO_2 concentration was only measured in the living room, there is a possibility that the method would cause false-positive errors. This is expected to occur in situations where the CO_2 concentration

decays due to air mixing with other rooms. E.g. if a door between a rooms with high and low concentrations suddenly is opened.

A few suggestions to tackle this problem could be to either install more sensors in the different rooms and monitor the CO_2 exchange between them, or potentially model the CO_2 concentration with a second-order model. That way a rapid first decay could indicate sudden exchange between to adjacent rooms, and the second slower decay could indicate the air exchange between inside and outside.

The result of the method reveals estimated periods with occupants, without occupants, and periods with sleeping occupants. This information can now be used as model inputs in a quasi-stationary or dynamic model as those outlines in Chapter 4, in order to treat the different periods in a certain manner. For instance, it might be beneficial to apply weighted error estimation techniques to maximise the information from unoccupied periods, while increasing the uncertainty of the data obtained form occupied periods. That way, no information is disregarded entirely, but instead partially down-weighted.

5.2 Reliable Heat Gains and Observations

As demonstrated in Chapter 4, the solar gain and the indoor temperature can result in significant errors if not treated properly, which is the focus of this section.

In **Paper D** only night-time data were used, and the problem with erroneous solar gain estimates were omitted. For day-time data the solar irradiation needs for most cases to be modelled. A novel method which describes the relationship between the sun position and the solar gain is given in **Paper B**, and presented in Section 5.2.1.

In Section 5.2.2 the content of **Paper C** is discussed. Here, the indoor temperature is disregarded entirely, and a base temperature is estimated instead, in order to overcome the issues of obtaining a representative indoor temperature.

5.2.1 Solar Gain Modelling

In Section 4.5 the effect of the solar irradiation was shown on a test house representing a single-family house. The total glazing area was approximately 13 m^2, where 7.2 m^2 face the south. By estimating the solar gain as a constant fraction of the solar irradiation, the model errors were found to be in the range from -2000 W to 3000 W.

In **Paper B** a new approach to model the solar gain has been proposed. The aim was to model the sun position dependent solar transmittance, and thereby the solar gain. To estimate an unknown function such as the solar transmittance, different methods can be applied. In **Paper B** the B-splines were chosen.

Splines, however, exist in many forms. Common for all of them is that they are characterised as piece-wise polynomials while being continuously differentiable in all points up to a certain order. The location where each piece connects with the next is called a knot.

Splines are often used for interpolation, smoothing, and function approximation of non-linear functions. They do not rely on any prior knowledge of the function one wants to estimate [118]. Furthermore, the non-linear operations are done before the model estimation by defining a series of knots and basis splines. A linear combination of the basis splines is then estimated in the model estimation process. Hence, the model can describe non-linear phenomenons but is kept linear.

In Figure 5.1 the estimated splines on the data from Section 4.5 is shown. In the upper-left plot, the spline is fitting to the global irradiation, and in the lower-left plot, the spline is fitted to the beam irradiation, and a constant solar transmittance is fitted on the diffuse solar irradiation.

Compared to the model in Section 4.5, the root mean squared error of the first model is reduced by 9 %, and by 50 % in the second case.

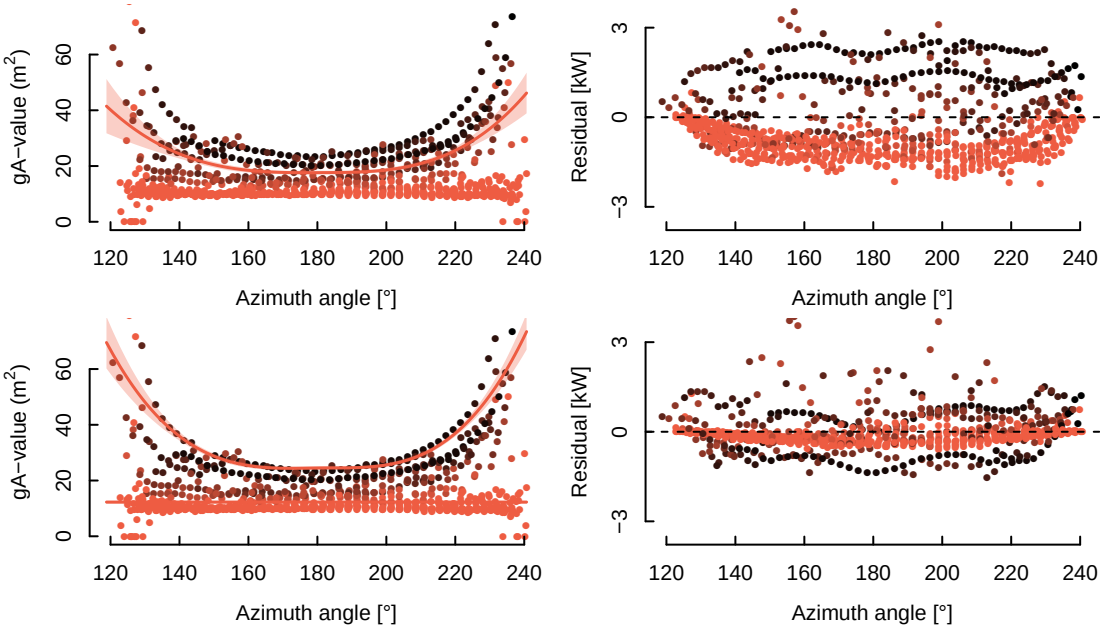

Figure 5.1: Solar gain estimated by splines. The upper-left plot shows the result of estimating the solar gain based on global irradiation only. The bottom-left plot shows the results of the solar gain estimated by a splines fitted to the beam irradiation, and a constant fitted to the diffuse irradiation. The fit and a 95 % confidence interval are indicated in the left plots. The plot to the right shows the solar gain residuals.

In **Paper B** the theory regarding basis spline construction and implementation in grey-box models are given. Additionally, the method was applied on two use cases — one for identification of thermal properties in an apartment, and one prediction and control focused use case for a solar collector field. Even though only the historic global irradiation data were available for the apartment case, the inclusion of splines improved the model significantly in terms of log-likelihood.

Regarding the solar collector field, the splines were able to capture the effect of a shading forest, which cast shadows on the collectors in the afternoon and hence reduced the return temperature.

The article showed a rather big potential across different fields where solar irradiation is a dominant factor of the thermal dynamics. However, there is still room for improvement as discussed in the remaining section.

Solar irradiation is most often measured in a horizontal plane — or at least a fixed plane — to limit maintenance of the sensors. This results in increased uncertainties as the incident angle between the sunbeams and the measurement plane increases. For global irradiation measurements, this is at sunrise and sunset. The result is that the solar transmittance is difficult to estimate in these regions.

From Figure 6 in **Paper B** an opposite pattern is however seen for the estimated spline in the morning. The reason is that the upper boundary of the left-most spline parameter was reached. A natural way of solving this issue would be to increase the boundary of the spline parameter. However, at the time it was believed that a solar transmittance of more than 25 m^2 (this was the upper bound for the parameter) were unreasonable for the apartment with approximately 11 m^2 of total window area.

With the Fraunhofer data shown in Figure 4.7 and Figure 5.1, it, however, became evident that the solar transmittance (measured in square meters) exceeded the actual window area by approximately a factor

five just after sunrise and before sunset. The total window area of the Fraunhofer test house is 12.4 m^2. However, the solar transmittance obtained from measurements is in some cases above 60 m^2. This is a direct implications of the vertical oriented windows and the horizontal solar irradiation measurement plane.

The parameter boundaries of the basis spline should therefore not be restricted too much in periods with large incident angles between the beam irradiation and the measurement plane.

Another consequence of using splines is that a knot sequence need to be defined before the basis splines can be constructed.

As the actual solar transmittance is unknown it can be troublesome to figure out where the spline knots should be located to increase the efficiency of the basis splines. Further research should ideally be put into this topic, or alternative "knot-free" methods such as Fourier series could be tested.

Finally, the physical interpretation of the estimated spline might in some cases be troublesome.

The straight forward interpretation of the estimated solar transmittance curve (i.e. the estimated spline) is that it is the fraction of solar irradiation which results in a solar gain at any given azimuth angle. There is, however, a few issues one need to be aware of before drawing too many conclusions.

Even though the use of splines may result in significantly better fits, the estimated function may not match the expectations. If, for example, a multi-room house is modelled as a single thermal zone, the estimated spline may depend on the rooms' heat capacities and how the indoor temperature is obtained. This seen in the following example.

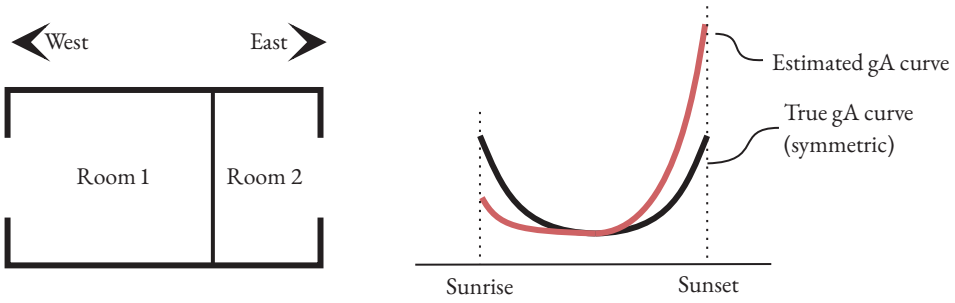

Figure 5.2: Conceptual illustration of estimated and true gA curve obtained for dynamical model of space volume-weighted indoor air temperature. The plan drawing to the left shows two rooms with same total heat capacity, and window size, but the space volume of Room 1 is two time the space volume of Room 2.

If the space volume-weighted average indoor temperature of the building in Figure 5.2 is modelled, certain unintended implications on the estimated solar spline may arise. In this example the total heat capacity and the window area is the same, however, the space volume of Room 1 is double the size of Room 2.

In that case, the volume-weighted average indoor temperature increment due to solar gain in Room 1, will be double the increment for the same level of solar gain in Room 2. This is in defiance of the fact that the actual window size is identical for Room 1 and Room 2.

The solar transmittance spline may, therefore, explain more than one anticipates. Consequently the model interpretation may be reduced, but the model accuracy is improved. A possible solution to increase the interpretability is to find a well-balanced sampling rate, which is short enough to contain the dynamics related to the solar gain, and long enough to make the effect of the solar gain kick through in all the rooms of the thermal zone.

5.2.2 Modelling Without Indoor Temperature Observations

In **Paper C** the focus has been on scalable models to estimate heat loss coefficients, solar transmittance, and indications of potential air leakage issues, etc. To do so, the traditional energy signature described in Section 4.1.3 has been reformulated such that the transition periods at which the building change from weather dependent to a weather independent thermal state is taken into account. Finally, the model errors are modelled separately to estimate the effect on the heat consumption caused by the occupants.

As the energy signature relies on quasi-stationary conditions, rather coarse time resolutions in the data need to be used. In this article, daily average values have been used.

As described in **Paper C** the energy signature is typically treated as a regime model, where the heat consumption is weather dependent in the first regime, and weather independent in the second.

For the 16 Danish dwellings investigated, no cooling or heat recovery systems were present. The weather independent regime is therefore treated as constant. The weather dependent periods, on the other hand, were modelled by five different model formulations, whereas the most general were

$$\Phi_{\mathrm{h}} = (\mathrm{UA}_0 + W_{\mathrm{s}}\,\mathrm{UA}_{\mathrm{W}})\,(T_{\mathrm{b}} - T_{\mathrm{e}}) - \mathrm{gA}\,I_{\mathrm{g}} + e\,, \tag{5.6}$$

where W_{s} is the wind speed, UA_0 is the heat loss coefficient for wind speeds equal to zero, and UA_{W} is the additional heat loss due to increments in the wind speed. Furthermore, gA is the solar transmittance, I_{g} is the global solar irradiation, T_{e} is the outdoor temperature, T_{b} is the base temperature, and $e \sim \mathrm{N}(0,\ \sigma^2)$ is the normally distributed noise with mean zero, and variance σ^2.

The base temperature T_{b} is the outdoor temperature at which the building is in thermal balance, which is

$$T_{\mathrm{b}} = T_{\mathrm{i}} - \frac{\Phi_{\mathrm{x}}}{\mathrm{UA}_0 + W_{\mathrm{s}}\,\mathrm{UA}_{\mathrm{W}}}\,, \tag{5.7}$$

where Φ_{x} is the unmodelled heat gains and losses. In the specific model used, the base temperature was, however, treated as constant such that

$$T_{\mathrm{b}} = T_{\mathrm{i}} - \frac{\Phi_{\mathrm{x}}}{\mathrm{UA}}\,. \tag{5.8}$$

The model suggested in this paper distinguish itself from the typical energy signature models found in the literature, by describing a smooth transition between weather dependent and weather independent periods. This is achieved by a more detailed description of the heat demand in the transitions period (i.e. including wind and solar irradiation), and secondly, by formulating the energy signature as the *smooth maximum function*, *LogSumExp*, typically used in neural networks.

The LogSumExp function used is

$$\mathrm{LSE}(f(x), g(x)) = \underbrace{\log\left[\exp(f(x)\,k) + \exp(g(x)\,k)\right] k^{-1}}_{\text{Smooth approximation of } \max\{f(x),\, g(x)\}}\,, \tag{5.9}$$

where $f(x)$ and $g(x)$ are substituted by Equation (5.6) and $\Phi_0 + e$, respectively. Φ_0 is the constant heat consumption during weather independent periods, and k is a hyperparameter describing the transition pace. The full model is

$$\Phi_{\mathrm{h}} = \log\left[\exp(((\mathrm{UA}_0 + W_{\mathrm{s}}\,\mathrm{UA}_{\mathrm{W}})\,(T_{\mathrm{b}} - T_{\mathrm{e}}) - \mathrm{gA}\,I_{\mathrm{g}})\,k) + \exp(\Phi_0\,k)\right] k^{-1} + e\,. \tag{5.10}$$

The results show that systematic errors (especially around the transition period) can be diminished, while the model accuracy is improved.

As the model treats the base temperature in Equation (5.8) as constant, it (in practice) means the that the indoor temperature and the unmodelled heat gains and losses are treated as constants as well. This is of course a crude assumption, which, as argued for in the article, also is the reason for the auto-correlated residuals.

Under the assumption that the thermal mass does not have any significant effect on the heat consumption when using day-to-day average values, the correlation is most likely due to occupants' time-correlated effects on the heat consumption. That means that the occupants' effect can be estimated as a function of time by non-parametric kernel estimation as used in [119] as well. Doing so, a corrected time-varying estimate of the unmodelled heat gains $\Phi_{\mathrm{x}}(t)$ can be obtained. The use of such estimate is further discussed in Section 5.3.

5.3 Quantifying Occupants' and Weather's Effect on the Energy Use

By estimating the occupants' related effect on the heat consumption as mentioned above and described in **Paper C**, the method in the paper offers a novel approach to separate the energy use caused by the occupants, as well as the weather conditions, and the building envelope.

To document the building performance and occupants' effect on the energy consumption, a few building design assumptions need to be known. That is the design weather data; the design indoor temperature; internal heat gains; and ventilation losses. From — at least —the Danish EPC calculation tool *Be18* these numbers can be extracted directly [46].

The documentation can be done in several steps to illuminate different reasons for a potential discrepancy between expected and realised energy use as described in **Paper C**.

A *Unintended occupants' related differences* in the energy consumption can be estimated as the difference between the estimated user related heat gain $\Phi_{\mathrm{x}}(t)$ and the user related heat gain, $\Phi_{\mathrm{x,design}}(t)$, assumed in the design phase.

   The user related heat gain $\Phi_{\mathrm{x,design}}(t)$, unaffected by the weather, can be estimated by

$$\Phi_{\mathrm{x,design}}(t) = \mathrm{UA}_0 \left(T_{\mathrm{i,design}} - T_{\mathrm{b}}(t)\right) + \Phi_{\mathrm{vent,design}} + \Phi_{\mathrm{int,design}} \,, \tag{5.11}$$

   where $T_{\mathrm{i,design}}$, $\Phi_{\mathrm{vent,design}}$ and $\Phi_{\mathrm{int,design}}$ is the anticipated design indoor temperature, design ventilation loss, and anticipated internal heat gain, respectively. UA_0 is the heat loss coefficient under wind-free conditions estimated by Equation (5.10), and $T_{\mathrm{b}}(t)$ is the time-varying estimate of the base temperature — see **Paper C** for details on this.

   The higher $\Phi_{\mathrm{x}}(t)$ is, the more occupants-related heat are required to bring the building in thermal balance, under the assumptions that the indoor temperature is equivalent to the actual indoor temperature, i.e. $T_{\mathrm{i,design}} = T_{\mathrm{i}}$.

   That means, if $\Phi_{\mathrm{x}}(t) > \Phi_{\mathrm{x,design}}(t)$ the internal heat gains are higher than expected in the design phase; the ventilation loss is lower than expected in the design phase; the indoor temperature is lower than the design temperature, or a combination.

   On the other hand, if $\Phi_{\mathrm{x}}(t) < \Phi_{\mathrm{x,design}}(t)$ the opposite is true.

B *Weather related differences* in the energy use can be estimated by comparing the predicted energy use with the actual weather conditions, and the predicted energy use with the outdoor tem-

perature, wind speed, and global solar irradiation used in the design phase. The model in Equation (5.10) is used for prediction.

C *Building envelope related differences* in the energy use can be estimated as the difference between the predicted energy use obtained using Equation (5.10) and the occupants and weather corrected energy use obtained from point A and B, above.

The concept is further illustrated in Figure 8 in **Paper C**.

The concept still needs to be validated on either simulated or actual building data, and the method for estimating the occupants' effect on the energy use may eventually be refined.

As the model is formulated as a fully differentiable model, contrary to the typical energy signature model, it opens up for more advanced estimation techniques. One natural model extension is to estimate the model in Equation (5.10) and the occupants' related heat gain $\Phi_{\mathrm{x}}(t)$, simultaneously. This can be done by formulating the model as a second-order state-space model, with the occupants' related heat gain $\Delta\Phi_{\mathrm{x}}(t)$ seen in Figure 5 in **Paper C**, as a mean-reverting hidden state.

Alternatively, the modelling approach presented in the paper can be estimated recursively, such that the estimate of $\Phi_{\mathrm{x}}(t)$ is fed back into the model in Equation (5.10) as an additional heat gain. A new realisation of $\Phi_{\mathrm{x}}(t)$ can then be obtained, and the routine can be repeated until convergence.

6 Perspectives and Conclusions

In the previous chapters, a summary of the work and some of the thoughts behind this PhD study have been presented. The focus has been on data-driven methods for reliable energy performance characterisation of buildings. The broad lines and trends concerning energy policies in the EU have been touched upon in Chapter 2, and issues regarding the widespread phenomenon of the energy performance gap were discussed in Chapter 3. From the review of the two topics, it is evident that better tools for monitoring the progression and alignment of visions and realities in the EU are needed, and so are tools for screening the building stock for high potential energy savings.

With increased data collection and improved data accessibility from the EU building stock, the market for data-driven methods for energy performance characterisation of buildings is expanding. The most widespread methods used in practice and found in the literature were outlined in Chapter 4, and in Chapter 5 some of the concerns and issues with the state-of-the-art methods are brought into focus. In the latter chapter mentioned, the main focus has been on issues which emerge as a consequence of the occupants' interaction with the building. That being increased disturbances of the thermal state of the building. Additionally, the importance of proper indoor temperature data and solar heat gain estimation were discussed.

Even though data-driven performance characterisation methods have been studied for years, it has never really gains traction within the field of civil engineering. Instead, energy performance is typically quantified by theoretical and deterministic models with assumptions that might not match reality.

Three reasons for the missing breakthrough are believed to be that 1) the general use of statistical methods in civil and building engineering practices is not common; 2) there is no "off-the-shelf" tools which can be used by the practitioners today and; 3) the reliability of the methods has been varying due to issues such as those outlines and tackled in this thesis.

Recently, an growing interest for data-driven performance characterisation tool has, however, emerged among building engineering consultancies and contractors. Likewise, has the focus of data and energy performance documentation within the EU intensified with the new Energy Performance of Buildings Directive (EPBD). A future with a simultaneous bottom-up and top-down willingness to implement data-driven performance characterisation tools, seems possible.

With the studies contained in this thesis, the data-driven performance characterisation methods are brought a big leap closer to practical use. This is done by providing a better understanding of how and why different methods should be used in order to overcome modelling issues related to occupants interactions with the building and unreliable data.

The concept of reducing the disturbances related to the occupants was tested on 39 occupied Danish single-family houses in **Paper D**. In this case, and as demonstrated in Section 4.4, the disturbances related to the occupants were reduced by modelling on night-time data only. The reasoning is that occupants most likely are asleep during the night, and consequently disturb the thermal dynamics less. Additionally, the complex nature of modelling the solar gain in the building can be disregarded.

Unreliable measurements of indoor temperatures have been brought into focus as well. A highly scalable method — which does not rely on indoor temperature measurements — for identifying key parameters related to the building's thermal performance and the occupants was presented in **Paper C**.

In **Paper A** the foundation for potentially more refined methods for handling the disturbances caused by the occupants was outlined. Here the occupancy status was estimated from measurements of CO_2 concentrations, which in the future can be used as model inputs in e.g. the diffusion term of a stochastic state-space model formulated by stochastic differential equations.

In most of the literature found on data-driven thermal building performance modelling, the focus is on the deterministic part of the model. However, as some significant heat gains (typically related to the occupants) cannot be quantified by feasible means, the deterministic part of the model formulation will inevitably be insufficient to provide independent and identically normal distributed errors as it typically is required

Future research on the topic of treating system and observation noise in physics-based models exposed to high levels of disturbances are therefore suggested.

Another source of significant errors is the simplified solar gain models. It has been shown, based on actual measurements, that solar gain can reach significant levels even for normal houses. Additionally, the solar gain is highly dependent on the building design, the window properties, and the surroundings, which for purely time series measurement-based models are unknown variables.

Contrary to the typical simplistic modelling approach found in the literature, namely that the solar transmittance is constant, a new and improved semi-parametric method for estimating the solar transmittance was proposed in **Paper B**.

In **Paper C** a methodology for estimating the effect of the occupants', the weather's, and the building envelope's contribution to the heat consumption is outlined. It is suggested that further research is carried out on this topic to fully understand and quantify the performance gap of buildings. With models of such simplicity in terms of required data, this opens op for large scale screening and documentation of the reasons for the performance gap.

Evidence-based quantification of the specific causes for the heat consumption may result in better building design and building construction practice. And, if presented in the right manner, it may even act as valuable end-user feedback with the end-goal of making them more educated and energy-aware building users.

In this thesis, the focus has to a large extend been on data-driven models applied on occupied buildings. The studies have revealed several pitfalls and challenges. To understand the data-driven models even better, it is suggested to step back and use simulated building data, and data obtained from controlled experiments, to verify the findings.

This PhD thesis is concluded by:

1. Disturbances and noisy data are both major sources of estimation errors. Proper handling of noise and disturbances (e.g. by including information on occupancy status as estimated in **Paper A**, or omitting particular noisy periods entirely as in **Paper D**) is therefore seen as important as the formulation of the deterministic part of the model. The deterministic and physics-based part of a data-driven building model brings the building performance estimates in the ballpark, whereas the description and handling of system disturbances and observation noise, increase the precision and consistency of the estimated models.

2. Often used methods for data-driven modelling of thermal building performance results in significant errors due to the simplified model formulations (such as the model formulation of solar gain),

and unreliable data (such as the indoor temperature). As presented in **Paper B** and **Paper C**, these obstacles can be overcome by applying appropriate modelling techniques.

3. The progression of reducing the performance gap issues in buildings sometimes seems to be stagnated. That is despite the fact that plenty of research suggests that the issue is evident. It is believed that one of the reasons is, that the performance discrepancies have been practically infeasible or even impossible to quantify. In **Paper C** a scalable method is, however, proposed. With further development and research, it is believed that a more clear picture of the phenomenon can be made in practice, and the relevant players can act accordingly to increase the reliability of the claimed energy performance. After all, a slightly modified quote from Jørgen Nørgaard found on page 3 is: *One unit of energy saved in your home, is better than any unit of energy saved in your engineers Excel sheet*.

Bibliography

[1] *Consumption of Energy*. 2016. URL: https://ec.europa.eu/eurostat/statistics-explained/index.php?title=Main_Page/Consumption_of_energy (visited on 05/26/2017).

[2] Energispareråd et. *Anbefalinger fra Energispareråd et til den Langsigtede Bygningsrenoveringsstrategi 2019*. Sept. 2018.

[3] *Directive 2010/31/EU of the European Parliament and of the Council on the Energy Performance of Buildings (Recast)*. May 2010. URL: http://data.europa.eu/eli/dir/2010/31/oj (visited on 04/12/2020).

[4] *Directive (EU) 2018/844 of the European Parliament and of the Council – Amending Directive 2010/31/EU on the Energy Performance of Buildings and Directive 2012/27/EU on Energy Efficiency*. May 2018. URL: http://data.europa.eu/eli/dir/2018/844/oj (visited on 04/12/2020).

[5] Maarten De Groote et al. *Smart Buildings in a Decarbonised Energy System, 10 Principles To Deliver Real Benefits For Europe's Citizens*. Buildings Performance Institute Europe (BPIE), June 2016.

[6] *BetterHome*. URL: https://www.betterhome.today (visited on 05/26/2020).

[7] *EU Buildings Factsheets*. URL: https://ec.europa.eu/energy/eu-buildings-factsheets_en (visited on 04/14/2020).

[8] *Status for Energimærkningsordning for Bygninger*. Energistyrelsen (The Danish Energy Agency), 2018. URL: %7Bhttps://ens.dk/sites/ens.dk/files/Energimaerke/status_for_energimaerkningsordningen_for_bygninger.pdf%7D.

[9] *REBUS – Renovating Buildings Sustainably*. URL: http://rebus.nu (visited on 05/31/2020).

[10] *Nearly Zero-Energy Building Strategy 2020 (ZEBRA2020)*. URL: http://bpie.eu/wp-content/uploads/2017/12/State-of-the-building-stock-briefing_Dic6.pdf (visited on 04/14/2020).

[11] *Directive 2012/27/EU of the European Parliament and of the Council on Energy Efficiency*. Oct. 2012. URL: http://data.europa.eu/eli/dir/2012/27/oj (visited on 04/12/2020).

[12] *Nearly Zero-Energy Building Strategy 2020 (ZEBRA2020)*. URL: https://zebra2020.eu/ (visited on 04/14/2020).

[13] Ea Energianalyse. *Samfundsøkonomisk Værdi af Varmebesparelser, Optimum Mellem Forsyningsomkostninger og Varmebesparelser i Eksisterende Bygninger*. Mar. 2018.

[14] *Factsheet: Sweden, Current Use of EPCs and Potential Links to iBRoad*. Individual Building Renovation Roadmaps (iBRoad), 2017.

[15] *Nyt Energiatlas Vil Samle Data om Bygninger og Deres Energiforbrug (New Energy Atlas to Collect Building Data and the Energy Consumption)*. May 2020. URL: https://www.danskindustri.dk/brancher/di-energi/nyhedsarkiv/nyheder/2020/5/nyt-energiatlas-skal-pa-sigt-samle-data-om-bygninger-og-deres-energiforbrug/ (visited on 05/27/2020).

[16] *Communication From the Commission to the European Parliament, The Council, the European Economic and Social Committee, the Committee of the Regions and the European Investment Bank – A Framework Strategy for a Resilient Energy Union with a Forward-Looking Climate Change Policy*. Feb. 2015. URL: https://eur-lex.europa.eu/legal-content/EN/ALL/?uri=COM:2015:80:FIN (visited on 04/15/2020).

[17] Directorate-General for Energy (European Commission). *Clean Energy for All Europeans*. European Commission, May 2019.

[18] Frances Bean et al. *Future-Proof Buildings for All Europeans, A Guide To Implement The Energy Performance Of Buildings Directive (2018/844)*. Buildings Performance Institute Europe (BPIE), May 2019.

[19] Rune Grønborg Junker et al. "Characterizing the Energy Flexibility of Buildings and Districts". In: *Applied energy* 225 (2018), pp. 175–182.

[20] *A Guide to: The Implementation of the Amended Energy Performance Of Buildings Directive (EPBD) 2018*. The European Alliance of Companies for Energy Efficiency in Buildings (EuroACE), 2019.

[21] J Wingfield, D Miles-Shenton, and M Bell. "Comparison of Measured Versus Predicted Heat Loss for New Build UK Dwellings". In: *Unpublished Data, Leeds Metropolitan University, Leeds, UK* (2011).

[22] Jason Palmer et al. *Building Performance Evaluation Programme: Findings from Domestic Projects – Making Reality Match Design*. Innovate UK, Jan. 2016.

[23] Davide Calì et al. "Energy Performance Gap in Refurbished German Dwellings: Lesson Learned From a Field Test". In: *Energy and buildings* 127 (2016), pp. 1146–1158.

[24] Chris Van Dronkelaar et al. "A Review of the Energy Performance Gap and its Underlying Causes in Non-domestic Buildings". In: *Frontiers in Mechanical Engineering* 1 (2016), p. 17.

[25] H Bell, R Milagre, and C Sanchez. "Achieving the Green Dream: Predicted vs. Actual-Greenhouse Gas Performance in Green Star-certified Office Buildings". In: *Green Building Council of Australia* (2013).

[26] Xing Shi et al. "Magnitude, Causes, and Solutions of the Performance Gap of Buildings: A Review". In: *Sustainability* 11.3 (2019), p. 937.

[27] Alfonso Pablo Ramallo-González. *Modelling, Simulation and Optimisation of Low-energy Buildings*. 2013.

[28] Henrik Brohus et al. "Influence of Occupants' Behaviour on the Energy Consumption of Domestic Buildings". In: *Aalborg University, Denmark* (2010).

[29] Frédéric Haldi and Darren Robinson. "The Impact of Occupants' Behaviour on Building Energy Demand". In: *Journal of Building Performance Simulation* 4.4 (2011), pp. 323–338.

[30] Zachary M. Gill et al. "Low-energy Dwellings: The Contribution of Behaviours to Actual Performance". In: *Building Research & Information* 38.5 (2010), pp. 491–508. DOI: 10.1080/09613218.2010.505371.

[31] Yixing Chen, Tianzhen Hong, and Xuan Luo. "An Agent-based Stochastic Occupancy Simulator". In: *Building Simulation*. Vol. 11. 1. Springer. 2018, pp. 37–49.

[32] *Occupancy Simulator*. URL: http://occupancysimulator.lbl.gov (visited on 04/17/2020).

[33] *ProccS - An Occupancy Simulation Tool for Private Households*. 2020. URL: https://www.proccs.org (visited on 05/27/2020).

[34] Sebastian Wolf et al. "Room-level Occupancy Simulation Model for Private Households". In: *Journal of Physics: Conference Series*. Vol. 1343. 1. IOP Publishing. 2019, p. 012126.

[35] Christoffer Rasmussen et al. "Method for Scalable and Automatised Thermal Building Performance Documentation and Screening". In: *Energies* (2020).

[36] Christoffer Rasmussen, Rishi Relan, and Henrik Madsen. "Identification of Occupancy Status by Statistical Change Point Detection of CO_2 Concentration". In: *2018 IEEE Conference on Control Technology and Applications (CCTA)*. IEEE. 2018, pp. 1761–1766.

[37] Manuel Herrera et al. "A Review of Current and Future Weather Data for Building Simulation". In: *Building Services Engineering Research and Technology* 38.5 (2017), pp. 602–627.
[38] Stephen Wilcox and William Marion. "Users Manual for TMY3 Data Sets". In: (2008).
[39] Silvia Erba, Francesco Causone, and Roberto Armani. "The Effect of Weather Datasets on Building Energy Simulation Outputs". In: *Energy Procedia* 134 (2017), pp. 545–554.
[40] Tianzhen Hong, Wen-Kuei Chang, and Hung-Wen Lin. "A Fresh Look at Weather Impact on Peak Electricity Demand and Energy Use of Buildings Using 30-year Actual Weather Data". In: *Applied energy* 111 (2013), pp. 333–350.
[41] *ANSI/ASHRAE/IES Standard 90.1-2010 – Energy Standard for Buildings Except Low-Rise Residential Buildings*. American Society of Heating and Air-Conditioning Engineers (ASHRAE), 2010.
[42] Steffen Petersen. *BeREAL – Beregnet vs. Faktisk Energiforbrug, Nyt Værktøj til Beregning af Bygningers Energiforbrug*. Nov. 2017. URL: https://vimeo.com/240810111 (visited on 04/20/2020).
[43] Christoffer Rasmussen et al. "Semi-parametric Modelling of Sun Position Dependent Solar Gain Using B-splines in Grey-box Models". In: *Solar Energy* 195 (2020), pp. 249–258.
[44] Hugo Hens et al. "Brick Cavity Walls: A Performance Analysis Based on Measurements and Simulations". In: *Journal of Building Physics* 31.2 (2007), pp. 95–124.
[45] *BeREAL, Guide*. URL: http://be15real.dk (visited on 04/20/2020).
[46] *Be18*. URL: https://sbi.dk/beregningsprogrammet/Pages/Start.aspx (visited on 04/21/2020).
[47] Donald G Malcolm et al. "Application of a Technique for Research and Development Program Evaluation". In: *Operations research* 7.5 (1959), pp. 646–669.
[48] Salah Imam, David A Coley, and Ian Walker. "The Building Performance Gap: Are Modellers Literate?" In: *Building Services Engineering Research and Technology* 38.3 (2017), pp. 351–375.
[49] Tor Nørretranders. *Verden Vokser: Tilfældighedens Historie*. Art People, 2019.
[50] *ISO 9869-1:2014 - Thermal Insulation – Building Elements – In-situ Measurement of Thermal Resistance and Thermal Transmittance — Part 1: Heat Flow Meter Method*. International Organization for Standardization, 2014.
[51] An-Heleen Deconinck and Staf Roels. "Comparison of Characterisation Methods Determining the Thermal Resistance of Building Components From Onsite Measurements". In: *Energy and Buildings* 130 (2016), pp. 309–320.
[52] RC Sonderegger and MP Modera. "Electric Co-heating: A Method for Evaluating Seasonal Heating Efficiencies and Heat Loss Rates in Dwellings". In: *Proceedings of the Second International CIB Symposium, Energy Conservation in the Built Environment, Copenhagen*. 1979.
[53] Robert C Sonderegger, Paul E Condon, and Mark P Modera. *In-situ Measurements of Residential Energy Performance Using Electric Co-heating*. Tech. rep. California Univ., Berkeley (USA). Lawrence Berkeley Lab., 1980.
[54] Geert Bauwens and Staf Roels. "Co-heating Test: A State-of-the-art". In: *Energy and Buildings* 82 (2014), pp. 163–172.
[55] Eric Mangematin, Guillaume Pandraud, and Didier Roux. "Quick Measurements of Energy Efficiency of Buildings". In: *Comptes Rendus Physique* 13.4 (2012), pp. 383–390.
[56] Johann Meulemans et al. "QUB/e: A Novel Transient Experimental Method for In Situ Measurements of the Thermal Performance of Building Fabrics". In: *Building Information Modelling, Building Performance, Design and Smart Construction*. Springer, 2017, pp. 115–127.

[57] G Pandraud et al. "QUB: A New Rapid Building Energy Diagnosis Method". In: *Proceedings of CLIMA*. 2013.

[58] Marieline Senave et al. "Mapping the Pitfalls in the Characterisation of the Heat Loss Coefficient From On-board Monitoring Data Using ARX Models". In: *Energy and Buildings* 197 (2019), pp. 214–228.

[59] Henrik Madsen et al. "IEA-EBC Annex 58 – Reliable Building Energy Performance Characterisation Based on Full Scale Dynamic Measurements. Report of Subtask 3, Part 2: Thermal Performance Characterisation Using Time Series Data – Statistical Guidelines". In: (2016).

[60] Peder Bacher and Henrik Madsen. "Identifying Suitable Models for the Heat Dynamics of Buildings". In: *Energy and Buildings* 43.7 (2011), pp. 1511–1522.

[61] Henrik Madsen and JM Schultz. "Short Time Determination of the Heat Dynamics of Buildings". In: *Thermal Insulation Laboratory, Report No. 243*. Technical University of Denmark, 1993.

[62] Margaret F. Fels. "PRISM: An Introduction". In: *Energy and Buildings* 9.1 (1986), pp. 5–18. ISSN: 0378-7788. DOI: https://doi.org/10.1016/0378-7788(86)90003-4. URL: http://www.sciencedirect.com/science/article/pii/0378778886900034.

[63] Stig Hammarsten. "A Critical Appraisal of Energy-signature Models". In: *Applied Energy* 26.2 (1987), pp. 97–110. ISSN: 0306-2619. DOI: https://doi.org/10.1016/0306-2619(87)90012-2. URL: http://www.sciencedirect.com/science/article/pii/0306261987900122.

[64] Stig Hammarsten. *Estimation of Energy Balances for Houses*. National Swedish inst. for building research, 1984.

[65] Gustav Nordström, Helena Johnsson, and Sofia Lidelöw. "Using the Energy Signature Method to Estimate the Effective U-value of Buildings". In: *Sustainability in Energy and Buildings*. Springer, 2013, pp. 35–44.

[66] Jimmy Vesterberg, Staffan Andersson, and Thomas Olofsson. "Robustness of a Regression Approach, Aimed for Calibration of Whole Building Energy Simulation Tools". In: *Energy and Buildings* 81 (2014), pp. 430–434.

[67] Andrea Acquaviva et al. "Energy Signature Analysis: Knowledge at Your Fingertips". In: *2015 IEEE International Congress on Big Data*. IEEE. 2015, pp. 543–550.

[68] Lorenza Pistore et al. "From Energy Signature to Cluster Analysis: An Integrated Approach". In: Purdue University, 2016.

[69] Martin Eriksson, Jan Akander, and Bahram Moshfegh. "Development and Validation of Energy Signature Method, Case Study on a Multi-family Building in Sweden Before and After Deep Renovation". In: *Energy and Buildings* (2020), p. 109756.

[70] ASHRAE. *ASHRAE Guideline 14-2002 – Measurement of Energy and Demand Savings*. American Society of Heating, Refrigerating and Air-Conditioning Engineers (ASHRAE), 2002.

[71] Henrik Madsen, Jan Holst, and Erik Lindström. "Modelling Non-linear and Non-stationary Time Series". In: *Lecture Notes, Technical University of Denmark, Dpt. of Informatics and Mathematical Modeling, Kgs. Lyngby, Denmark* (2000).

[72] Henrik Madsen. *Time Series Analysis*. CRC Press, 2007.

[73] R Core Team. *R: A Language and Environment for Statistical Computing*. R Foundation for Statistical Computing. Vienna, Austria, 2018. URL: https://www.R-project.org/.

[74] Rob Hyndman et al. *forecast – Forecasting Functions for Time Series and Linear Models. R package version 8.5*. 2019. URL: http://pkg.robjhyndman.com/forecast (visited on 04/29/2020).

[75] Henrik Spliid. "Multivariate Time Series Estimation using marima". In: *38. Symposium i Anvendt Statistik 2016*. Danmarks Statistik. 2016, pp. 108–123.

[76] *TSA (Time Series Analysis) version 1.2.1*. June 2018. URL: https://www.rdocumentation.org/packages/TSA (visited on 05/05/2020).

[77] *MATLAB version 9.8.0.1359463 (R2020a) Update 1*. The Mathworks, Inc. Natick, Massachusetts, 2020.

[78] Inc. The MathWorks. *System Identification Toolbox*. Natick, Massachusetts, United State, 2020. URL: https://se.mathworks.com/help/ident/.

[79] Henrik Madsen and Jan Holst. "Estimation of Continuous-time Models for the Heat Dynamics of a Building". In: *Energy and buildings* 22.1 (1995), pp. 67–79.

[80] MJ Jiménez, Henrik Madsen, and Klaus Kaae Andersen. "Identification of the Main Thermal Characteristics of Building Components Using MATLAB". In: *Building and Environment* 43.2 (2008), pp. 170–180.

[81] Jaume Palmer Real et al. "Characterization of Energy Dynamics of Residential Buildings with Scarce Data". In: *Energy and Buildings* (2020).

[82] MJ Jiménez and MR Heras. "Application of Multi-output ARX Models for Estimation of the U and g values of Building Components in Outdoor Testing". In: *Solar Energy* 79.3 (2005), pp. 302–310.

[83] I Naveros et al. "Physical Parameters Identification of Walls Using ARX Models Obtained by Deduction". In: *Energy and Buildings* 108 (2015), pp. 317–329.

[84] *IEA-EBC Annex 58: Reliable Building Energy Performance Characterisation Based on Full Scale Dynamic Measurement*. URL: https://bwk.kuleuven.be/bwf/projects/annex58/index.htm (visited on 04/28/2020).

[85] Peder Bacher and Philip Hvidthøft Delff Andersen. "IEA Common Exercise 4: ARX, ARMAX and Grey-box Models for Thermal Performance Characterization of the Test Box". In: (2014).

[86] *IEA-EBC Annex 71: Building Energy Performance Assessment Based on In-Situ Measurements*. URL: https://bwk.kuleuven.be/bwf/projects/annex71/index.htm (visited on 04/28/2020).

[87] Eric M Burger and Scott J Moura. "ARX Model of a Residential Heating System With Backpropagation Parameter Estimation Algorithm". In: *ASME 2017 Dynamic Systems and Control Conference*. American Society of Mechanical Engineers Digital Collection. 2017.

[88] Lin Chen, Biswajit Basu, and David McCabe. "Fractional Order Models for System Identification of Thermal Dynamics of Buildings". In: *Energy and Buildings* 133 (2016), pp. 381–388.

[89] *Lecture Note: State Space Systems Analysis, Relative Degree and Zeros of State Space Systems (Continued)*. URL: http://www.uta.edu/utari/acs/ee4314/lectures/Lecture%5C%203.pdf (visited on 04/28/2020).

[90] Marieline Senave et al. "Assessment of Data Analysis Methods to Identify the Heat Loss Coefficient From On-board Monitoring Data". In: *Energy and Buildings* 209 (2020), p. 109706.

[91] Marieline Senave et al. "Towards the Characterization of the Heat Loss Coefficient Via On-board Monitoring: Physical Interpretation of ARX Model Coefficients". In: *Energy and Buildings* 195 (2019), pp. 180–194.

[92] *Common Exercise 1bis - Instruction Document*. IEA-EBC Annex 71, Jan. 2018.

[93] Matthias Kersken and Paul Strachan. *Empirical Whole Model Validation Modelling Specification – Twin House Experiment, IEA-EBC Annex 71 Validation of Building Energy Simulation Tools*. IEA-EBC Annex 71, Oct. 2019.

[94] Uffe Thygesen. *Lecture Notes on Diffusion and Stochastic Differential Equations*. Polyteknisk boghandel, Aug. 2016.

[95] B. Øksendal. *Stochastic Differential Equations: An Introduction with Applications*. Springer, 2010. ISBN: 9783642143946.

[96] Niels Rode Kristensen, Henrik Madsen, and Sten Bay Jørgensen. "Parameter Estimation in Stochastic Grey-box Models". In: *Automatica* 40.2 (2004), pp. 225–237. ISSN: 0005-1098.

[97] Jakob Bak et al. "Goodness of fit of stochastic differential equations". English. In: *21. Symposium i anvendt statistik*. null ; Conference date: 01-01-1999. 1999.

[98] Henrik Madsen and Poul Thyregod. *Introduction to General and Generalized Linear Models*. CRC Press, 2010.

[99] Samuel S Wilks. "The Large-sample Distribution of the Likelihood Ratio for Testing Composite Hypotheses". In: *The Annals of Mathematical Statistics* 9.1 (1938), pp. 60–62.

[100] Hassan Harb et al. "Development and Validation of Grey-box Models for Forecasting the Thermal Response of Occupied Buildings". In: *Energy and Buildings* 117 (2016), pp. 199–207.

[101] Samuel F Fux et al. "EKF Based Self-adaptive Thermal Model for a Passive House". In: *Energy and Buildings* 68 (2014), pp. 811–817.

[102] Thomas Berthou et al. "Development and Validation of a Gray-box Model to Predict Thermal Behavior of Occupied Office Buildings". In: *Energy and Buildings* 74 (2014), pp. 91–100.

[103] Elena Palomo Del Barrio et al. "Using Model Size Reduction Techniques for Thermal Control Applications in Buildings". In: *Energy and Buildings* 33.1 (2000), pp. 1–14.

[104] Glenn Reynders, Jan Diriken, and Dirk Saelens. "Quality of Grey-box Models and Identified Parameters as Function of the Accuracy of Input and Observation Signals". In: *Energy and Buildings* 82 (2014), pp. 263–274.

[105] Frances P Hollick, Virginia Gori, and Clifford A Elwell. "Thermal Performance of Occupied Homes: A Dynamic Grey-box Method Accounting for Solar Gains". In: *Energy and Buildings* 208 (2020), p. 109669.

[106] Amina Adadi and Mohammed Berrada. "Peeking Inside the Black-box: A survey on Explainable Artificial Intelligence (XAI)". In: *IEEE Access* 6 (2018), pp. 52138–52160.

[107] Sina Mohseni, Niloofar Zarei, and Eric D Ragan. "A Survey of Evaluation Methods and Measures for Interpretable Machine Learning". In: *arXiv preprint arXiv:1811.11839* (2018).

[108] Filip Karlo Došilović, Mario Brčić, and Nikica Hlupić. "Explainable Artificial Intelligence: A Survey". In: *2018 41st International convention on information and communication technology, electronics and microelectronics (MIPRO)*. IEEE. 2018, pp. 0210–0215.

[109] Or Biran and Courtenay Cotton. "Explanation and Justification in Machine Learning: A Survey". In: *IJCAI-17 workshop on explainable AI (XAI)*. Vol. 8. 1. 2017.

[110] Patrick O'Driscoll, Jaehoon Lee, and Bo Fu. "Physics Enhanced Artificial Intelligence". In: *arXiv preprint arXiv:1903.04442* (2019).

[111] Saleh Seyedzadeh et al. "Machine learning for Estimation of Building Energy Consumption and Performance: A Review". In: *Visualization in Engineering* 6.1 (2018), p. 5.

[112] Christoffer Rasmussen, Peder Bacher, and Henrik Madsen. *ARX Models for Building Energy Performance Assessment Based on In-situ Measurements*. Oct. 2017. URL: https://www.slideshare.net/ChristofferRasmussen/arx-models-for-building-energy-performance-assessment-based-on-insitu-measurements (visited on 05/12/2020).

[113] Henrik Madsen. *Statistically Determined Dynamical Models for Climate Processes – IMSOR Thesis No. 45*. Technical University of Denmark, 1985.

[114] James B Rawlings. "Tutorial Overview of Model Predictive Control". In: *IEEE control systems magazine* 20.3 (2000), pp. 38–52.

[115] S. Wolf et al. “A Markov-Switching Model for Building Occupant Activity Estimation”. In: *Energy and Buildings* 183 (2019), pp. 672–681.

[116] Hazim Awbi. *Ventilation of Buildings*. 2nd Editio. Spon Press, 2005. ISBN: 0419252800.

[117] David S Matteson and Nicholas A James. “A Nonparametric Approach for Multiple Change Point Analysis of Multivariate Data”. In: *Journal of the American Statistical Association* 109.505 (2014), pp. 334–345.

[118] Carl de Boor. “Spline Basics”. In: *Handbook of Computer Aided Geometric Design*. Elsevier, June 2007, pp. 141–163. DOI: 10.1016/b978-044451104-1/50007-1.

[119] Henrik Aalborg Nielsen et al. “Analysis of Energy Consumption in Single Family Houses”. In: *DYNASTEE International Workshop on Dynamic Methods for Building Energy Assessment*. 2010.

Part II

Publications

Preprint submitted to 2018 IEEE Conference on Control Technology and Applications (CCTA)

Identification of Occupancy Status by Statistical Change Point Detection of CO_2 Concentration

Christoffer Rasmussen*, Rishi Relan*, Henrik Madsen*

***Abstract*— There is an increasing focus on energy savings in buildings but still there exist a gap between the calculated and the realised energy performance. A statistical analysis performed on in situ measurements of occupied buildings is one way to reveal if the occupants' behaviour, the build quality, or the building design is the underlying reasons for this performance gap. A critical issue when carrying out the statistical analysis of the measurements from occupied buildings is to handle the measurement disturbances caused by the occupants' interaction with the building. In this paper, an offline method combining ventilation theory of buildings with change point detection of time series measurements of indoor CO_2 concentrations is proposed to detect vacant and sleeping periods in dwellings. The proposed method is tested using the CO_2 measurements obtained from a single apartment. The method developed has classified 19 % of a 14-days period as a vacant or sleeping period with an 81 % accuracy based on indirect measures.**

I. Introduction

Within the European Union, households account for 25 % of the total energy consumption of which 65 % is used for space heating [1]. Consequently, a significant amount of the greenhouse gas emission is directly related to the operation of the building stock. On the other hand, buildings offer great possibilities for considerable energy savings as well as aid in the reduction of greenhouse gases through energy renovation. To reach the European goal of reducing greenhouse gas emission by 80-95 % by 2050, as compared to 1990 [2], reducing the greenhouse gas emission from the building stock is necessary.

Often, the energy consumption for buildings is underestimated. One study shows that the difference between the estimated and the actual energy consumption can exceed 100 % [3]. In another study, a difference of 300 % has been observed between identical buildings [4]. This discrepancy between the estimated and the realised energy consumption can be related to oversimplified assumptions of, e.g. the occupants' behaviour, general mistakes in the design, as well as unmethodical workmanship during the construction phase. Contrary to this, the common misconception of this discrepancy is substantiated by the "faulty" behaviour of the occupants. However, it is difficult to ascertain whether the energy performance gap, in fact, is related to the occupants or the design and build quality of the building.

The authors would like to acknowledge the financial support obtained from the project Renovating Buildings Sustainably (REBUS), and the International Energy Agency's Energy in Buildings and Communities Programme (IEA EBC) Annex 71 for providing data and technical support.

*Department of Applied Mathematics and Computer Science, Technical University of Denmark, 2800 Kgs. Lyngby, Denmark. chrras@dtu.dk, risre@dtu.dk, hmad@dtu.dk

Today, there is no operational method or tool available that can identify, quantify and analyse the reasons for the discrepancies between expected and realised energy performance. Often, energy labelling system relies on assumptions similar to those in the design phase of a building which enhances the probability of unreliable results. Alternative methods for identifying the total heat loss coefficient like the co-heating or the quick U-value of buildings (QUB/e) method [5], requires that the building of interest is vacant during the measurements. In addition to this, these methods are labour intensive and cannot selectively analyse the thermal performance of specific building parts. Hence, the development of reliable tools for in situ characterisation of the actual energy performance is of utmost importance. Such tools can help map potential renovation focus areas of the building, ensure substantial energy savings, improve thermal comfort and eventually raise the build quality.

Data-driven methods—especially the grey-box models—present great potential in solving some of the issues discussed above because the dynamics of the system under consideration can be learned directly from data without the need to describe the full complexity of the building physics. Most of the current research on data-driven methods for the determination of energy performance of buildings deal with unoccupied buildings [6]–[8]. Consequently, they disregard the stochastic and fluctuating dynamics, such as ventilation, infiltration and hot water draws caused by the occupants.

Due to ease of prediction of heat load from people and the limited interaction of occupants with office buildings, a method for identifying the energy performance of occupied office buildings was proposed in [9]. These assumptions might not be valid for the dwellings, as the occupants are free to interact with the building, and therefore, strongly affect the indoor environment, the energy consumption, and ultimately the complexity of models that can describe the building dynamics. Grey-box models of the building dynamics of occupied dwellings was proposed in [10]. These models did not account for the presence of occupants and the occupants' interaction with the building which led to inconsistent results.

One way to account for occupants, is to track their presence, and include that information in the modelling procedure. However, this is in many cases inexpedient. Detection of occupancy status from other measures such as CO_2 is therefore important. Time series segmentation of CO_2 and pattern recognition techniques for detecting different predefined occupancy profiles were presented in [11], and several other approaches for occupancy detection with different levels of complexity exist in the literature [12].

As mentioned, the energy consumption is related to the status (presence, absence, sleeping, etc.) of the occupants of the building. It is therefore of interest to identify the status of the occupants to develop accurate models of the thermal dynamics. The gained information on the occupancy status can be used in conjunction with systems identification techniques. This enables us to quantify not only the performance of the dwelling itself but also the occupants' influence on the energy consumption and the thermal environment of the building. The direct use of such information is relevant for e.g. energy labelling of buildings and policy-making regarding energy renovation investments.

In this paper we propose to combine a statistical non-parametric approach to change point detection (CPD) and the physics-based ventilation theory of buildings to detect periods with the least interaction between occupants and the building. This support a robust estimate of occupied dwelling's thermal performance. The periods of interest is specifically the vacant and sleeping periods.

The remaining paper is structured as follows: Section II-A discusses how the ventilation theory of buildings can be applied to identify the CO_2 signature during the vacant and sleeping periods. In Section II-B, a method to detect change points in CO_2 time series measurements is explained. Finally, experimental results are discussed in Section III, and conclusions and plans for the future work are described in Section IV.

II. Method

In this section, we first describe how the ventilation theory of buildings can be used to identify the CO_2 signature of the occupancy status of interest through time series measurement. After that, we describe how a statistical change point method can be used to detect potential time segments of vacant and sleeping periods using time series measurements of indoor CO_2 concentration.

A. CO_2 Signature: A Ventilation Theory Approach

By using the ventilation theory for buildings, the air change rate of an enclosed space can be determined by the concentration decay method [13]. In practice, this is done by injecting a tracer gas—e.g. CO_2—into the enclosed space and tracking the concentration decay for a period of time after the injection has stopped. The air change rate can then be calculated by utilising the tracer gas mass balance. If the potential outdoor tracer gas concentration is neglected, the tracer gas mass balance equation is given by (1) [13].

$$V\frac{\mathrm{d}c}{\mathrm{d}t} = -Qc \tag{1}$$

where V is the space volume, c is the CO_2 concentration, Q is the ventilation rate and t is time. By introducing the air change rate, $N = Q/V$, and reformulating (1), the dynamics of the CO_2 concentration can be described as in (2).

$$c(t) = c_0 \exp(-Nt) + c_\infty \tag{2}$$

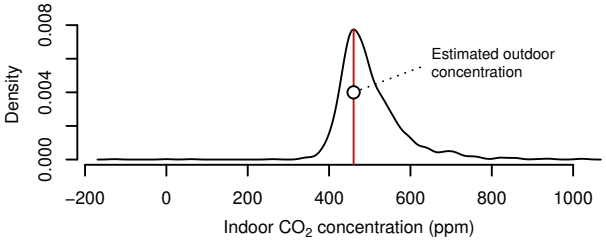

Fig. 1. Histogram of registered daily minimum indoor CO_2 concentrations. The outdoor concentration is assumed to be represented by the most frequent observed daily minimum concentration (460 ppm), and is used as vacancy criteria for c_∞ in (2).

where c_0 is the initial tracer gas concentration after the cessation of the gas injection. Notice the added constant, c_∞, which is the steady-state tracer gas concentration.

In this case, the injected gas is the CO_2 emitted by the occupants and the enclosed space is the apartment. If the CO_2 concentration follows (2) and decays sufficiently slow towards the outdoor concentration, it can be assumed that the apartment is vacant. Limiting the decay rate ensures that the air exchange is caused by infiltration rather than ventilation. In addition, sleeping periods can be detected by allowing a higher steady-state concentration during nighttime. To observe a CO_2 decay, however, measurements should be obtained from rooms without sleeping people.

1) Steady-state CO_2 Concentration: In Figure 1 the histogram of the daily minimum CO_2 concentration measured is shown. In this study, the most frequently observed concentration is assumed to represent the estimate of the true outdoor concentration, which is used as baseline for the further analyses. From the data described in Section III-A, the estimated outdoor concentration is found to be 460 ppm. During the night, which is defined from 0:00 to 6:00, the maximum steady-state CO_2 concentration of 700 ppm is accepted, as the occupants produce some CO_2 during sleep but do not interact with the building.

2) Air Change Rate: A reasonable estimate of a sufficiently slow air change rate for vacant and sleeping periods is the infiltration rate. The infiltration rate is the unintentional air exchange between inside and outside the building. The measured air permeability, q_{50}, of the apartment is 3.65 cubic meter air per hour per square meter building envelope (see Section III-A for details on the data). Whereas the air permeability is a static measure of the air change rate obtained under a pressure difference of 50 Pa between the inside and outside environment, the infiltration rate is dependent on the wind conditions, topology of the building and its surroundings, and the temperature. The average infiltration rate per square meter of the heated floor can be approximated by $0.06 \cdot w_{50}$ for vacant periods [14], where w_{50} is the air permeability. Notice, that w_{50} and q_{50} is based on the floor area and the envelope area, respectively. The infiltration rate, N_i, can now be determined from (3).

$$N_i = \frac{0.06 \cdot q_{50} \cdot A_e}{V} = 0.18\ \mathrm{h}^{-1} \tag{3}$$

where A_e is the area of the envelope (161 m^2) and V is the air volume enclosed by the building envelope (193 m^3).

If the steady-state CO_2 concentration, c_∞, in (2) is below the outdoor concentration of 460 ppm, the apartment is assumed to be either vacant or heavily ventilated. However, if $N < N_i = 0.18$ h^{-1}, no ventilation is assumed to occur, and the CO_2 decay is a result of pure infiltration with no additional CO_2 production inside the apartment. Hence, the apartment is assumed to be vacant.

B. Nonparametric CPD of CO_2 Time Series

In practice, the observed CO_2 concentration is highly fluctuating and does not decay exponentially most of the time. Therefore, the time segments with the characteristic exponential decay need to be identified. To achieve this, in this paper, we employ the *E-divisive* algorithm proposed in [15]. It is a nonparametric approach to multiple change point analysis of a multivariate time series.

In general, both parametric and nonparametric approached can be used for change point detection. The advantage of the nonparametric approaches is, however, that no assumptions about the underlying distribution family is needed. Furthermore, the *E-divisive* algorithm is capable of estimating both the number of change points and their locations [15], unlike other nonparametric methods [16]–[18]. Finally, the *E-divisive* algorithm is based on the Euclidean distance between sample observations, hence no explicit estimation of the multivariate density function is needed. Below we give a very brief introduction to the CPD methodology in general and the *E-divisive* algorithm.

For instance, let $Z_1, Z_2, \cdots, Z_T \in \mathbb{R}^d$ be an independent sequence of time ordered observations (in this case CO_2 time series). For simplicity let us assume that there is only one change point location τ such that, $Z_1, Z_2, \cdots, Z_\tau \overset{i.i.d}{\sim} P_1$ and $Z_{\tau+1}, Z_{\tau+2}, \cdots, Z_T \overset{i.i.d}{\sim} P_2$, where P_1 and P_2 are unknown probability distributions. The basic methodology behind CPD is to test the homogeneity in distribution, $H_0 : P_1 = P_2$ against $H_A : P_1 \neq P_2$. In case, if H_0 is rejected then it can be concluded that there exist a change point at τ. This methodology can be further modified to test the existence of unknown number and the location of the change points using different methods [15].

The *E-divisive* method employed in this case study is a combination of the bisection method [19] and the multivariate divergence method proposed by [20]. To elaborate, let us consider a case with two random variables $X, Y \in \mathbb{R}^d$ and let $X_n = X_i : i = 1, \cdots, n$ and $Y_m = Y_j : j = 1, \cdots, m$ be i.i.d samples from the distribution of $X, Y \in \mathbb{R}^d$, respectively, such that $\mathrm{E}|X|^\alpha, \mathrm{E}|Y|^\alpha < \infty$ for some $\alpha \in (0, 2]$. Then, the scaled sampled measure of the divergence between their distributions can be written as follows:

$$\widehat{\mathbb{Q}}(X_n, Y_m; \alpha) = \frac{mn}{m+n} \widehat{\mathscr{E}}(X_n, Y_m; \alpha) \tag{4}$$

where $\widehat{\mathscr{E}}(X_n, Y_m; \alpha)$ is the empirical divergence measure [15].

Now, for estimating the location of the change point using the divergence measure in (4) for a time series, let us consider $Z_1, Z_2, \cdots, Z_T \in \mathbb{R}^d$ to be an independent sequence of time ordered observations as described above and let $1 \leq \tau < \kappa \leq T$ be constants. We can now define the following two sets, $X_\tau = \{Z_1, Z_2, \cdots, Z_\tau\}$ and $Y_\tau(\kappa) = \{Z_{\tau+1}, Z_{\tau+2}, \cdots, Z_\kappa\}$. Then, a change point location $\hat{\tau}$ can be estimated by solving the following optimisation problem [15]:

$$(\hat{\tau}, \hat{\kappa}) = \underset{(\tau,\kappa)}{\arg\max}\, \widehat{\mathbb{Q}}(X_\tau, Y_\tau(\kappa); \alpha) \tag{5}$$

To estimate multiple change points, the above discussed method is then applied iteratively. For instance, let us suppose that $k-1$ change points have been estimated at locations $0 < \hat{\tau}_1, < \cdots < \hat{\tau}_{k-1} \leq T$, such that the observations are clustered into k clusters $\widehat{C}_1, \widehat{C}_2, \cdots, \widehat{C}_k$ where $\widehat{C}_i = \{Z_{\widehat{\tau}_{i-1}}, \cdots, Z_{\widehat{\tau}_i}\}$ and $\widehat{\tau}_0 = 0$ and $\widehat{\tau}_k = T$. Once these clusters have been found the next step is to find a single change point to the observations within each of the k clusters.

Therefore, by denoting a proposed change point location as $\widehat{\tau}(i)$ and its associated constant $\widehat{\kappa}(i)$ for the i^{th} cluster $\widehat{C}_i$ as defined by (5), now let

$$i^* = \underset{i \in \{1, \cdots, k\}}{\arg\max}\, \widehat{\mathbb{Q}}(X_{\widehat{\tau}(i)}, Y_{\widehat{\tau}(i)}(\widehat{\kappa}(i)); \alpha), \tag{6}$$

in which $X_{\widehat{\tau}(i)}$ and $Y_{\widehat{\tau}(i)}(\widehat{\kappa}(i))$ are defined with respect to $\widehat{C}_i$ with following test statistic

$$\widehat{q}_k = \widehat{\mathbb{Q}}(X_{\widehat{\tau}_k}, Y_{\widehat{\tau}_k}(\widehat{\kappa}_k); \alpha), \tag{7}$$

where $\widehat{\tau}_k = \widehat{\tau}(i^*)$ corresponds to the k^{th} estimated change point, located within the cluster $\widehat{C}_{i^*}$ and $\widehat{\kappa}_k = \widehat{\kappa}(i^*)$ the corresponding constant. To segment the time series of the CO_2 concentration with $\alpha = 2$, the *R* implementation is used [21], [22]. The detected change points now serves as start and end points for the fitting procedure for the exponential decay function shown in (2).

C. Fitting and Classifying

At this point, the functional behaviour of the CO_2 concentration is known, namely the exponential decay function in (2), and the structural change points can be determined. It can now be tested if there is no interaction between occupants and the building, i.e. if the building is under vacant conditions or when occupants are sleeping, by fitting the exponential decay function to segregated CO_2 data.

The fitted exponential functions are evaluated by the mean square error (MSE). As baseline, MSE < 100 is used as criterion. The exponential decay function is repetitively fitted to each of the identified segments. If the fit of (2) fulfils the criteria $N < 0.18$ h^{-1}, MSE < 100, and furthermore, $c_\infty < 460$ ppm for daytime or $c_\infty < 700$ ppm for nighttime, the period is classified as a vacant or a sleeping period, respectively. If multiple sequential segments fulfils the above criteria, one fit is made for the combined segments.

III. Experimental Validation

A. Data

For this case study, the building data from IEA EBC Annex 71 [23] is used to validate the performance of the

developed method. The building is located in an urban area in England, and consists of four apartments with two floors. The measurements come from the southern apartment, which has a floor area of 67 m^2 equally distributed on the ground and the first floor. The ground floor consists of living room, kitchen, bathroom and hallway with access to the first floor. The data consist of measurements from October 2012 to November 2015. The period from October 2012 to January 2013 was occupied by two adults and one child whereas the second period from March 2013 to November 2015 was occupied by one adult and two children. In the remaining period the apartment was vacant and unheated. The apartment is equipped with a monitored mechanical ventilation unit.

The data consists of the measurements of energy consumption, indoor environmental parameters of the apartment, as well as the weather data from a weather station nearby. The data from the house has a time resolution of 5 minutes and the weather data has a time resolution of 1 hour. The data does not contain information on occupation. The only CO_2 sensor installed is located in the living room on the ground floor of the apartment. All three bedrooms are located on the first floor. The technical specifications of the CO_2 sensor are not known.

B. Results and Discussion

The theoretical response functions of the CO_2 concentration is exponential for both decay and built-up given constant CO_2 supply and ventilation rate [13]. Hence, the time series of the CO_2 concentration is assumed to be a combination of these exponential functions. A natural detection signal is thus the percentage rate of change (ROC) as shown in the top plot of Figure 2.

In Figure 2 the identification of vacant and sleeping periods throughout the 24-hours period from January 22 to January 23, 2014, is shown. From the top, the plots shows the detection signal, the measured CO_2 concentration, the water consumption, and the electricity consumption.

In the second plot, the detected vacant, sleeping and occupied period is shown. One sleeping period is detected form 01:05 to 06:15 in the morning and a vacant period is detected between 13:05 and 14:55. Both periods are indicated with a red fitted curve on top of the CO_2 concentration signal. The grey fitted curve from 09:20 to 11:30 indicates a period with an exponential decay, but with a steady-state CO_2 concentration that exceeds the limit of 460 ppm. Furthermore, the segment immediately before 09:20 seems to be part of the exponential decay but was not detected. In the beginning of the sleeping period some water consumption is observed, which in general is assumed to be related to the presence of awake occupants.

Due to unavailability of any data on the actual presence of occupants in the apartment, the validity of the classification performance could not be tested directly. However, an indication of the performance can be established by comparing the detected sleeping and vacant periods with the water consumption.

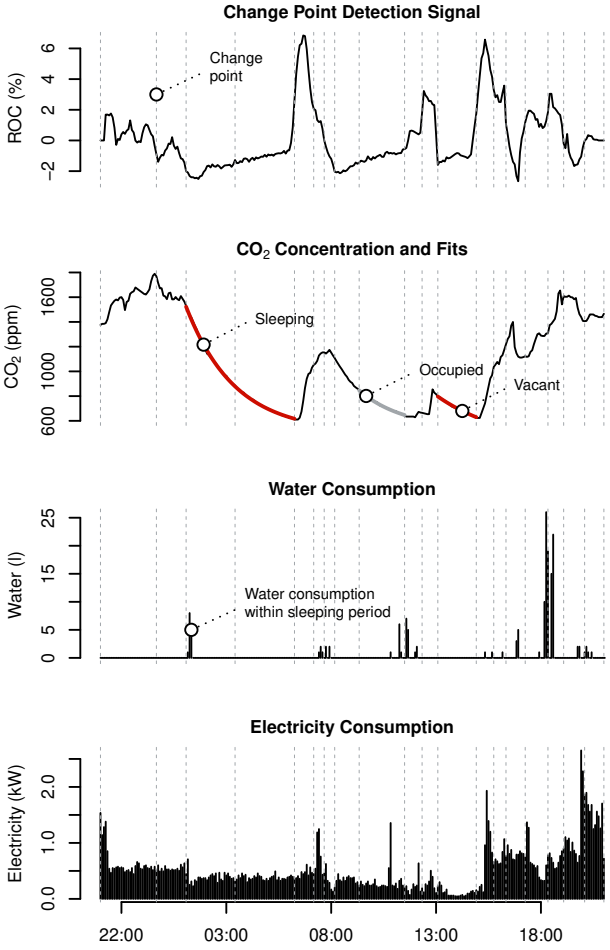

Fig. 2. Identification of vacant and sleeping periods for a 24-hours period during January 22-23, 2014. The first plot shows the signal used in the *E-divisive* algorithm. The signal is defined as the moving average smoothed percentage rate of change (ROC). The second plot shows the CO_2 concentration along side with the detected change points. The red and grey curves on top of the CO_2 curve shows the fitted CO_2 decays. The grey curve shows an identified exponential CO_2 decay, which does not fulfil the steady-state CO_2 criterion as $c_\infty = 536$ ppm $\not< 460$ ppm. The third plot shows the water consumption, which are use for indirect validation. It is expected that the water consumption is lower for sleeping and vacant periods than for occupied periods. The fourth plot illustrates the electricity consumption. Simultaneous electricity use and water consumption can indicate a running dishwasher or washing machine, which may run in vacant and sleeping periods. For the sudden water consumption during the nighttime in this figure, no electricity peak is observed. Hence, it is not reasonable to believe that the the water consumption is automated.

The majority of the water consumption is assumed to be directly related to a physical interaction with the water system—either by means of water draws from taps, showers or toilet flushes. In addition to this, a minor part of the water consumption throughout the day can be automated and timed by washing machines and dishwashers. Based on this, it is expected that the water consumption is significantly lower for estimated vacant and sleeping periods.

For a 14-days period from January 15 to January 29, 2014, the water consumption during the entire period, and the vacant and sleeping periods is shown in Table I. The

TABLE I

WATER USE IN ESTIMATED VACANT AND SEEPING PERIODS

	All periods		Vacant / Sleeping	
	Mean	Median	Mean	Median
Flow (l/h)	13.9	8.9	14.5	0.0
Draws (h^{-1})	1.6	1.6	0.7	0.0
Draws (h^{-1}) [a]	0.8	0.6	0.3	0.0

[a] Water draws with simultaneous electricity use of less than 500 W.

table shows the flow rate and the numbers of water draws. In addition, we distinguish between any water draws and water draws with simultaneous electricity consumption of less than 500 W. In this way, it can be indicated if the water consumption is related to water-consuming white goods running during vacant or sleeping periods.

Contrary to the expectation, the mean flow for the vacant and sleeping periods in Table I, is higher than for the entire 14-days period, and the mean number of water draws is only reduced by approximately 50 %. The results does not reflect the results shown in Figure 2. Inspecting the medians instead tells us that only a few water draws are affecting the means, and potentially that only a few time segments are incorrectly classified.

In addition to that, it seems reasonable to assume that a significant share of the water consumption is related to water consuming white goods running while the occupants are either not present or sleeping. This can be seen by the decrease in mean from 0.7 to 0.3 water draws per hour for the vacant and sleeping periods in Table I.

1) Performance Evaluation: From the 14-days period investigated, 20 % of the time is estimated to be vacant or sleeping periods with the baseline criteria. However, only 1 % of this is estimated to be vacant periods. In comparison, 13 % of the time is classified as occupied, meaning that the steady-state CO_2 concentration, air change rate or mean squared error criterion is violated. Without occupation data, it is not possible to tell if the apartment actually is vacant for only 1 % of the time. However, a higher percentage was expected, and it is suspected that some vacant periods are incorrectly classified as occupied. The validity of the detection criteria is therefore tested and shown in Figure 3. The *detection power* is the estimated vacant and sleeping periods without any water consumption, and the *detected hours* is the share of hours classified as vacant or sleeping period.

From the first plot in Figure 3 the share of detected hours and detection power stay constant from roughly 640 ppm and above. Increasing the nighttime steady-state CO_2 criteria does therefore not affect the results. On the other hand, for all the periods estimated as occupied, the daytime steady-state CO_2 concentration of 460 ppm was exceeded. It could be argued that a higher daytime steady-state concentration should be used due to low sensor precision or higher outdoor CO_2 concentration than assumed. Hence the number of detected vacant hours would increase. The second plot in Figure 3

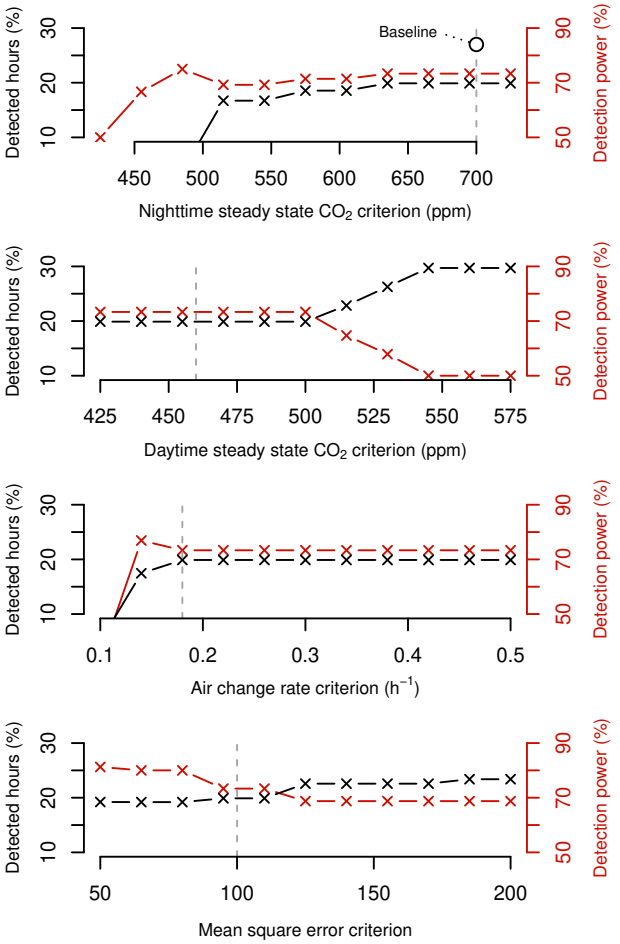

Fig. 3. Indicative performance for various detection criteria. Detected hours tells the percentage of hours that have been estimated to be either vacant or sleeping periods for the 14-days period in January 2014. The detection power tells the percentage of periods that have been detected as either vacant or sleeping periods without any water consumption.

reveals that an increment of the daytime CO_2 criterion up till 500 ppm has no effect, provided that the remaining criteria remain fixed. Increasing the criterion above 500 ppm, the number of detected hours increase, but at the expense of the detection power, as other criteria is violated.

The threshold for the air change rate is determined solely on the information in the air tightness of the building. As the apartment is equipped with a mechanical ventilation system, it is natural to conclude that the threshold is too low for periods with the ventilation system running. However, the maximum air change rate of 0.18 h^{-1} was never reached for any of the periods classified as occupied, as illustrated in the third plot of Figure 3.

Finally, by decreasing the maximum allowable mean squared error of the fits, as illustrated in the fourth plot of Figure 3, the detection power goes up and the share of hours detected barely goes down. Based on this analysis, it is preferable to decrease the the MSE to at least 50. Doing this, the percentage of detected hours drops from 19.9 to 19.2 % and the detection power increase from 73.3 to 81.3 %.

In summary, we see a direct trade-off between detection power and hours detected for both the daytime steady-state CO_2 concentration and the MSE criterion. Increasing these two criteria only gives rise to a higher number of false-positive classifications of vacant periods.

For the the air change rate, we do not see any increment of detected hours as the criterion is loosened (i.e. increased). This is counter-intuitive as the apartment is equipped with a mechanical ventilation system that would increase the air change rate to a level above the infiltration rate—which is used as criterion in this case study. Without any detected effect of the mechanical ventilation system, the experiment is considered natural ventilated.

Conclusively, we observe either; decreasing detection power as the share of detected hours increase, or unaffected detection power and share of detected hours as the detection criteria in loosened. This indicates that the house actually was occupied for most of the 14-days period investigated, as detected.

IV. Conclusions and Future Work

Energy performance measurements of a building during occupied periods can be profoundly affected by the occupants' interaction with it. In this paper, we proposed an algorithm for identifying the vacant and the sleeping periods in a dwelling using the concentration decay method from the ventilation theory and statistical change point detection of the CO_2 time series data. This algorithm seeks to ensure that the occupancy periods can be treated separately while determining the thermal performance of the building. In future, this information about the vacant and the sleeping periods will be used in conjunction with grey-box modelling methods in revealing the thermal performance of dwellings.

Even though the CO_2 concentration data were obtained from only one sensor located in the living room of the two-story apartment, promising results were obtained during the investigation. Based on indirect measures of occupancy status, 19 % of a 14-days period was classified as vacant or sleeping periods with an accuracy of 81 %. However, a direct validation based on data with the information on occupancy status is therefore preferable.

The algorithm shows good results, but the performance can easily be enhanced by employing data from more measurement locations. In addition, a proper selection of the sensor location, tuning of the hyper-parameter α in the detection algorithm is also important for an optimal occupancy detection. Furthermore, the apartment was considered to be naturally ventilated. Hence, further work is needed to make the algorithm applicable for mechanically ventilated dwellings.

References

[1] Eurostat, "Consumption of Energy," 2016. [Online]. Available: http://ec.europa.eu/eurostat/statistics-explained/index.php/Consumption_of_energy

[2] European Commission, "2050 Energy Strategy," 2017. [Online]. Available: https://ec.europa.eu/energy/en/topics/energy-strategy-and-energy-union/2050-energy-strategy

[3] H. Brohus, P. K. Heiselberg, A. Simonsen, and K. C. Sørensen, "Influence of Occupants Behaviour on the Energy Consumption of Domestic Buildings," in *Clima 2010: 10th Rehva World Congress*, 2010.

[4] R. H. Socolow, "The Twin Rivers Program on Energy Conservation in Housing: Highlights and Conclusions*," *Energy and Buildings*, vol. 1, no. 3, pp. 207–242, 1977.

[5] J. Meulemans, F. Alzetto, D. Farmer, and C. Gorse, "QUB/e A Novel Transient Experimental Method for In Situ Measurements of the Thermal Performance of Building Fabrics," in *International SEEDS Conference 2016: Sustainable Ecological Engineering Design for Society*, 2016, pp. 14–15.

[6] K. K. Andersen, H. Madsen, and L. H. Hansen, "Modelling the Heat Dynamics of a Building Using Stochastic Differential Equations," *Energy and Buildings*, vol. 31, no. 1, pp. 13–24, 2000.

[7] P. Bacher and H. Madsen, "Identifying Suitable Models for the Heat Dynamics of Buildings," *Energy and Buildings*, vol. 43, no. 7, pp. 1511–1522, 2011.

[8] H. Madsen, P. Bacher, G. Bauwens, A.-H. Deconinck, G. Reynders, S. Roels, E. Himpe, and G. Lethé, "EBC Annex 58 Reliable building Energy Performance Characterisation Based on Full Scale Measurements," The International Energy Agency, Belgium, Tech. Rep., 2016.

[9] O. Mejri, E. P. Del Barrio, and N. Ghrab-Morcos, "Energy Performance Assessment of Occupied Buildings Using Model Identification Techniques," *Energy and Buildings*, vol. 43, no. 2, pp. 285–299, 2011.

[10] H. Harb, N. Boyanov, L. Hernandez, R. Streblow, and D. Müller, "Development and Validation of Grey-box Models for Forecasting the Thermal Response of Occupied Buildings," *Energy and Buildings*, vol. 117, pp. 199–207, 2016.

[11] A. Szczurek, M. Maciejewska, A. Wyłomańska, R. Zimroz, G. Żak, and A. Dolega, "Detection of Occupancy Profile Based on Carbon Dioxide Concentration Pattern Matching," *Measurement*, vol. 93, pp. 265–271, 2016.

[12] W. Shen and G. Newsham, "Implicit Occupancy Detection for Energy Conservation in Commercial Buildings: A Review," in *Computer Supported Cooperative Work in Design (CSCWD), 2016 IEEE 20th International Conference on*. IEEE, 2016, pp. 625–631.

[13] H. Awbi, *Ventilation of Buildings*, 2nd ed. Spon Press, 2005.

[14] S. Aggerholm and K. Grau, "SBi-anvisning 213 – Bygningers Energibehov, PC-program og Beregningsvejledning," 2005.

[15] D. S. Matteson and N. A. James, "A Nonparametric Approach for Multiple Change Point Analysis of Multivariate Data," *Journal of the American Statistical Association*, vol. 109, no. 505, pp. 334–345, 2014.

[16] D. M. Hawkins, "Fitting Multiple Change-point Models to Data," *Computational Statistics & Data Analysis*, vol. 37, no. 3, pp. 323–341, 2001.

[17] M. Lavielle and G. Teyssiere, "Detection of Multiple Change-points in Multivariate Time Series," *Lithuanian Mathematical Journal*, vol. 46, no. 3, pp. 287–306, 2006.

[18] A. Lung-Yut-Fong, C. Lévy-Leduc, and O. Cappé, "Homogeneity and Change-point Detection Tests for Multivariate Data Using Rank Statistics," *arXiv preprint arXiv:1107.1971*, 2011.

[19] L. Vostrikova, "Detection of the Disorder in Multidimensional Random-processes," *Doklady Akademii Nauk SSSR*, vol. 259, no. 2, pp. 270–274, 1981.

[20] G. J. Szekely and M. L. Rizzo, "Hierarchical Clustering via Joint Between-within Distances: Extending Ward's Minimum Variance Method," *Journal of classification*, vol. 22, no. 2, pp. 151–183, 2005.

[21] N. A. James and D. S. Matteson, "ecp: An R Package for Nonparametric Multiple Change Point Analysis of Multivariate Data," *arXiv preprint arXiv:1309.3295*, 2013.

[22] R Core Team, *R: A Language and Environment for Statistical Computing*, R Foundation for Statistical Computing, Vienna, Austria, 2017. [Online]. Available: https://www.R-project.org/

[23] The International Energy Agency, "EBC ANNEX 71 Building Energy Performance Assessment Based on In-situ Measurements," 2017. [Online]. Available: http://www.ecbcs.org/projects/project?AnnexID=71

Semi-parametric Modelling of Sun Position Dependent Solar Gain Using B-splines in Grey-box Models

Christoffer Rasmussen[a,*], Linde Frölke[a,*], Peder Bacher[a], Henrik Madsen[a], Carsten Rode[b]

[a]*Department of Applied Mathematics and Computer Science*
[b]*Department of Civil Engineering*
Technical University of Denmark
2800 Kgs. Lyngby, Denmark

Abstract

Modelling the effects of solar irradiation plays an important role in various applications. This paper describes a semi-parametric (combined grey-box and spline-based), data-driven technique that can be used to model systems in which the solar gain depends on the sun position. The *solar gain factor* is introduced, i.e. the absorbed fraction of measured solar irradiation, and estimated as a continuous non-parametric function of the sun position. The implementation of the spline-based solar gain factor in a grey-box model framework is described. The method is tested in two case studies—in a model of the internal temperature of a dwelling in Aalborg, Denmark, and a model of the return temperature of a solar collector field in Solrød, Denmark. It is shown that the solar gain factor as a function of sun position is able to account for structural variations in solar gain that may occur due to factors such as shading obstacles and window or absorber orientation. In both test cases, the spline-based solar gain function improved the model accuracy significantly, and largely reduced structural errors in prediction residuals. In addition, the shape of the estimated function provided insight into the dynamics of the system and the local solar input characteristics. Accurate representation of such site characteristics was not possible with any data-driven method found in the literature. Besides the grey-box models used in this study, the solar gain factor can be used in a variety of data-driven models, for example in linear regression models.

Keywords: Solar gain modelling, Grey-box modelling, Splines, Thermal dynamics, Building energy, Solar heat collectors

1. Introduction

Solar irradiation is a crucial factor in the field of building engineering, renewable energy generation, and many other applications. In many cases, measurements or predictions of the solar irradiation are available, and the effect of solar irradiation needs to be captured in a model. However, the relation between solar gain and measured solar irradiation is typically non-linear and dependent on the position of the sun and site characteristics. This paper, presents and implements a data-driven model for dynamical thermal systems, that include a sun position dependent solar gain. The model is tested in two thermal systems: a building and a solar collector field.

In both systems, the heat dynamics related to solar irradiation are modelled for various reasons. For buildings, models are used to document the energy performance and identify a potential energy performance gap (Roels et al., 2017; Johnston et al., 2016; Haldi and Robinson, 2011; Brohus et al., 2010; Socolow, 1977). For instance, this has been done using data-driven thermal dynamic building models such as grey-box models (Roels et al., 2017; Bacher and Madsen, 2011; Madsen and Holst, 1995). As solar heat gain can significantly affect estimated thermal building properties, the model used for solar heat gain needs to be accurate. This is especially true for well-insulated buildings with low thermal mass and large window areas.

Similarly, for solar collector fields, forecasting models need to describe solar irradiation effects accurately to improve heat output forecasts and system control. The control must respond to rapid fluctuations in solar irradiation to prevent the collector fluid from boiling, and to ensure a high and stable outlet temperature. As solar irradiation is the dominating effect on the outlet temperature, an accurate model of the absorbed solar energy can improve predictions and hence operation of solar heat systems.

The following two sections present a literature review on typical implementations of data-driven solar heat gain in thermal building and solar heat plant models.

1.1. Solar Gain in Thermal Building Models

The solar gain factor of an enclosed space (often called solar aperture, effective window area, or gA-value) can be seen as the equivalent area of a perfectly transparent surface that transmits the same amount of solar energy as the actual windows of the space.

For inverse problem solving, the location of windows and shading obstacles are often unknown. Even if the location of the shading obstacles is known, it can still be cumbersome to

*These authors contributed equally to this work.
Email addresses: chrras@dtu.dk (Christoffer Rasmussen), linfr@dtu.dk (Linde Frölke), pbac@dtu.dk (Peder Bacher), hmad@dtu.dk (Henrik Madsen), car@byg.dtu.dk (Carsten Rode)

Nomenclature

Abbreviations

HVAC	Heating, ventilation, and air conditioning
IAM	Incidence angle modifier
RC	Resistance-capacity
SDE	Stochastic differential equation
SDHP	Solar district heat plant
SHP	Solar heat plant

Mathematical Notation

$B_{i,m}$	The i$^{\text{th}}$ B-spline of order m
S	Spline function
ϕ_i	Control point of the i$^{\text{th}}$ B-spline
ω	Wiener process
σ	Standard deviation of Wiener process
ϵ	Measurement error

Physical Parameters

t	Time	s
T	Temperature	°C
T^*	Measured temperature	°C
α	Elevation angle of the sun	°
γ	Azimuth angle of the sun	°
θ	Solar incidence angle	°
I	Solar irradiation	W/m^2
η	Solar gain factor	m^2 *or* unitless[a]
Φ	Heat input	W
c	Specific heat capacity	J/(kg K)
C	Heat capacity	J/K
$(mC)_{\text{e}}$	Heat capacity of collector	J/(m^2 K)
Q	Mass flow per collector area	kg/s/m^2
R	Thermal resistance	K/W
U	Heat loss coefficient	W/(m^2 K)
K	IAM function	unitless
b_0	IAM parameter	unitless
κ	Ambrosetti IAM parameter	unitless

Subscripts

a	Ambient air
i	Internal air
m	Internal thermal mass
w	Building envelope
f	Collector fluid
s, r	Supply and return
fa	Interaction between f and a
mi	Interaction between m and i
wa	Interaction between w and a
wi	Interaction between w and i
g, t, b, d	Global, total, beam, and diffuse irradiation
heat	Space heating
sol	Solar gain
t	Time
k	Discrete time step

[a] For the dynamical building models the unit of η is square meter (m^2). In the solar heat production forecasting setting η is unitless.

estimate their thermal effects, just as it is difficult to estimate the effects of other factors such as reflections or dirt on the windows.

Some data-driven thermal dynamic building models disregard the solar gain (Zeifman and Roth, 2016; Coley and Penman, 1992) and consequently treat solar gain as model uncertainty and observation noise. In other models, solar gain is considered a constant fraction of the global solar irradiation (Rabl, 1988; Bauwens and Roels, 2013; Madsen and Holst, 1995; Bacher and Madsen, 2011; Jimenez and Madsen, 2008), for example

$$\Phi_{\text{sol}} = \eta I_{\text{g}}\,, \tag{1}$$

where Φ_{sol} is the solar gain, I_{g} is the global radiation, and η is the solar gain factor. The solar gain factor can then be estimated from data.

When assessing the energy performance of buildings, Mejri et al. (2011) describe the solar gain in buildings as a hidden forcing function. They propose a method in which the solar irradiation striking each building facade, I_i, is estimated separately as

$$I_i = k_i I_{\text{g}}\,, \tag{2}$$

where i is the facade number and k_i is a constant for the i^{th} facade. Letting the constant, k_i, account for the properties of the windowpane—e.g. the solar energy transmittance (g-value) and the area—this method could be used to calculate the solar gain coming through the windows in a manner analogous to Eq. (1). However, there is no evidence that this method would improve model accuracy compared to the simpler approach in Eq. (1).

Both of the above approaches assume that the solar gain is independent of the sun position. While these approaches may be sufficient for buildings with limited window area (and therefore limited solar gain), they may fall short for buildings with higher sensitivity to solar irradiation. As suggested by Bacher and Andersen (2014) and Madsen et al. (2016), parametric grey-box models could be used in conjunction with non-parametric models of solar gain, such as splines. Hence, rather than assuming a constant solar gain factor for the entire enclosed space or the facade of interest, the factor can be described as a function of the sun position. The present paper details the specific procedure for achieving this.

1.2. Solar Gain in Solar Heat Plant Models

Solar irradiation is the main factor that determines the heat production of a solar heat plant (SHP), so it is crucial to include the effects of solar radiation in detail when modelling the return temperature (also called outlet temperature) of a solar heat

field. The solar incidence angle on the panel largely influences the share of reflected irradiation, and thereby the solar gain. Furthermore, the position of the sun affects the solar gain due to possible shading objects around the collectors. It is common for the collector rows to cast shade on one another at some point in the afternoon as well. Finally, dirt or snow on the panels may affect the solar gain.

The most recent standard for performance testing of solar heat collectors by the International Organization for Standardization (ISO) is described in ISO 9806:2017 (European Committee for Standardization (CEN) Technical Committee, 2017). The method is considered to be the state-of-the-art for solar collector modelling (Kicsiny, 2014). The solar gain is included in the ISO dynamic model as

$$\Phi_{\mathrm{sol}} = \eta\, K(\theta)\, I_{\mathrm{t}}\,, \tag{3}$$

where I_{t} is the total radiation in the collector plane. The parameter η (usually named $F'(\tau\alpha)_{\mathrm{en}}$ in this application) represents the fraction of solar irradiation that is absorbed by the panels at an incidence angle equal to zero, whereas the incidence angle modifier (IAM) $K(\theta)$ accounts for incidence angle dependence of the solar gain. The incidence angle θ is defined as the angle between the sunbeam and the normal of the collector plane. When beam and diffuse irradiation are measured separately and an incidence angle modifier is used, the solar gain is modelled as

$$\Phi_{\mathrm{sol}} = \eta\left(K_{\mathrm{b}}(\theta)\, I_{\mathrm{b}} + K_{\mathrm{d}}\, I_{\mathrm{d}}\right), \tag{4}$$

where the diffuse IAM K_{d} is a constant, as it is independent of the incidence angle.

The standard incidence angle modifier (IAM) used in the ISO performance test is

$$K_{\mathrm{b}}(\theta) = 1 - b_0\left(\frac{1}{\cos(\theta)} - 1\right). \tag{5}$$

Depending on the applied model type, the parameter b_0 that determines the slope of the curve is manually tuned or fitted to data using statistical techniques. For most flat plate collectors, this equation is considered sufficiently accurate for describing incidence angle effects (Perers, 1997).

Another IAM given in ISO 9806:2017 is the *Ambrosetti* function

$$K_{\mathrm{b}}(\theta) = 1 - \tan^{\kappa}\left(\frac{\theta}{2}\right). \tag{6}$$

In this case, the dimensionless parameter κ determines the slope of the function.

Almost all models intended for control of SHPs present in the scientific literature combine (partial) differential equations with parameters estimated from data, see for example Pasamontes et al. (2013) and de Andrade et al. (2015). The incidence angle dependence is either neglected, or modelled using IAM functions such as in Eq. (5) and (6). The vast majority of existing models for SHP control do not take shadowing effects into account (Bava, 2017; Bava and Furbo, 2018).

Although these IAM functions may suffice for performance testing and simulation, they may not be accurate enough for control purposes. The functions used currently are tuned by a single parameter and therefore only a limited amount of function shapes are possible. Furthermore, the functions do not allow for asymmetric diurnal variations of efficiency, which may exist due to shading of the collectors.

1.3. Motivation

This paper aims to formulate and test a novel non-parametric method to estimate the solar heat gain in thermal dynamical systems such as buildings and solar collector fields. To the best of our knowledge, and as seen in the literature review, only simple data-driven methods for modelling solar gain in buildings exist, i.e. models in which the solar gain is independent of the sun position. For solar collectors, parametric incident angle modifiers (IAM) have been widely applied in the literature, in both steady-state and dynamic models. However, these IAMs are not able to account for potential shading patterns on the collectors.

As the relationship between solar gain and measured solar irradiation is sun position dependent and site-specific, it is often not feasible to choose a parametric representation of this relationship. In addition, the solar gain factor, i.e. the share of measured solar irradiation that is absorbed in the system, depends on the sun position non-linearly.

Spline functions address both of these issues. A key benefit of this non-parametric modelling technique is that no model structure needs to be specified. Furthermore, the splines can model non-linear phenomena, but the nonlinear operations in the construction of basis splines are performed before the model fitting process. Hence, only linear operations on the constructed basis splines are carried out in the model fitting procedure, as will be demonstrated later.

This study implements and tests the spline-based solar gain factor in a grey-box model setting. Grey-box models are a class of parametric physics-based statistical models, which in form lie between the deterministic white-box models known from simulation tools such as TRNSYS, and entirely data-driven black-box models such as simple linear regression and neural networks. Grey-box models are often relatively simple and computationally lightweight, they have excellent forecasting properties, and parameters that are directly related to physical properties.

In Section 2 the proposed method is discussed, including the mathematics behind the applied B-spline functions (Section 2.1), the applied grey-box model (Section 2.2), and the actual implementation of splines in state-space models (Section 2.3). In Section 3 the approach is applied to two use cases: modelling the effect of solar irradiation on the internal temperature of a dwelling in Aalborg, Denmark (Section 3.1), and forecasting the heat production from a solar collector field in the municipality of Solrød, Denmark (Section 3.2). Lastly, in Section 4, the approach is discussed and closing conclusions are drawn in Section 5.

2. Method

This section presents the used modelling procedure, which is also outlined in Figure 1. First, Section 2.1 introduces spline functions and the construction and usage of a B-spline basis for data fitting, corresponding to the first step in Figure 1. Next, Section 2.2 presents the resistance-capacity grey-box models and model selection procedure used in this article, which span all remaining steps in Figure 1. Finally, Section 2.3 discusses in detail how the spline functions are implemented in the grey-box model setting in particular.

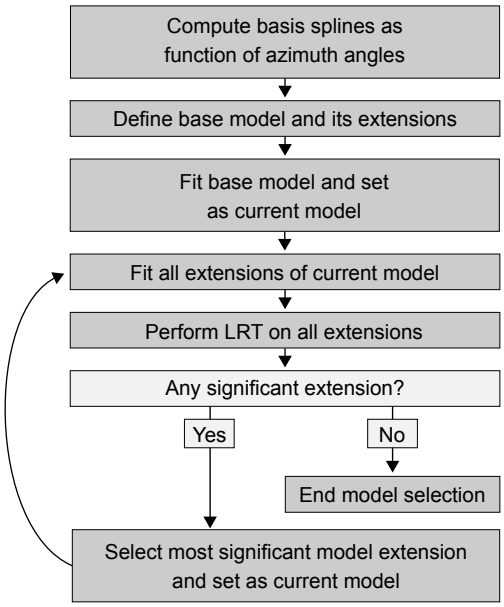

Figure 1: Modelling procedure.

2.1. Splines

Splines are piece-wise polynomials that are continuously differentiable up to a certain order. The points at which these piece-wise polynomials connect are called knots. Splines are in practice used for interpolation, smoothing, and function approximation (de Boor, 2007). This paper concerns the latter challenge, and aims to estimate the solar gain factor from data as a smooth function.

Splines are attractive for function approximation due to several properties. The functions are smooth up to a certain order, have compact support, and their formulas are explicit and rather simple (Prautzsch et al., 2002; Christensen, 2010).

The proposed method is based on a specific type of spline function: the B-spline. Given a knot sequence, one can construct a set of B-splines that form a basis for all splines with this same knot sequence (de Boor, 2007; Prautzsch et al., 2002). The construction of the cardinal B-spline basis will be discussed in Section 2.1.1, and in Section 2.1.2 a more general construction of B-splines is shown.

2.1.1. Cardinal B-splines

The B-spline $B_m(x)$ is a piece-wise polynomial of order m, meaning that the spline consists of m polynomials of degree $m-1$. A transition point from one polynomial to the next is called a knot. If the knot sequence is uniformly spaced, it is called a *cardinal* B-spline or a cardinal basis spline.

The cardinal B-spline can be defined and constructed in various ways. A compact definition is the recursive convolution relation, first shown by Schoenberg (1946),

$$B_{m+1}(x) = (B_m * B_1)(x), \quad x \in \mathbb{R}, \tag{7}$$

where $*$ is the convolution operator $m \in \mathbb{N}$ and B_1 is defined by the characteristic function

$$B_1(x) = \begin{cases} 1 & \text{if } 0 \le x < 1 \\ 0 & \text{otherwise.} \end{cases} \tag{8}$$

The B-spline has a number of desirable properties, one of which is continuity of the 0^{th} to $(m-2)^{\text{th}}$ derivatives in the knots, i.e. $B_m \in \mathbb{C}^{m-2}$ (Sauer, 2006). For example, the B-spline of order $m = 4$ is a piece-wise polynomial, each of these polynomials is of third degree, and the function value, slope and curvature are continuous in each knot.

Another property is that infinitely many cardinal B-splines point-wise add up to unity, when evenly distributed along the x-axis with a distance corresponding to the distance between two neighbouring knots (Christensen, 2010).

As demonstrated later, the B-splines are suitable for estimating the solar gain factor as a smooth function of sun position. The estimated function is obtained by summing the scaled B-splines. In many use cases, one is only interested in a series of B-splines that covers a finite range of the x-axis. However, the sum of a finite set of cardinal B-splines will go to zero at the boundary regions as seen in Figure 2A. Therefore, the cardinal B-splines near the boundaries need to be modified to add up to unity for the entire finite domain. The following section illustrates this modification of the B-splines.

2.1.2. B-splines in a Finite Domain

For a strictly increasing series of knots $x_1, x_2, x_3, \ldots$, it is possible to define the i^{th} B-spline of order m, $B_{i,m}(x)$, in Eq. (7) by the alternative Cox-de Boor recursion formula,

$$B_{i,m}(x) = \frac{x - x_i}{x_{i+m} - x_i} B_{i,m-1}(x) + \frac{x_{i+m+1} - x}{x_{i+m+1} - x_{i+1}} B_{i+1,m-1}(x). \tag{9}$$

The Cox-de Boor recursion formula can be used to define B-splines with non-uniform knot distances and to shift the B-spline along the x-axis. The above criterion is relaxed from *strictly increasing* to *non-decreasing* knots, so that knots may be positioned at equal locations. In order to still use Eq. (9) in this generalised case, division by zero is considered as zero.

If the first m knots of the knot sequence $x_1, x_2, x_3, \ldots$ are equal, i.e. $x_1 = x_2 = \cdots = x_m$, and the same holds for the last m knots of the knot sequence, then the B-splines as defined in Eq. (9) will add up to unity on the finite domain. The leftmost B-spline will have have m coinciding knots, the second leftmost

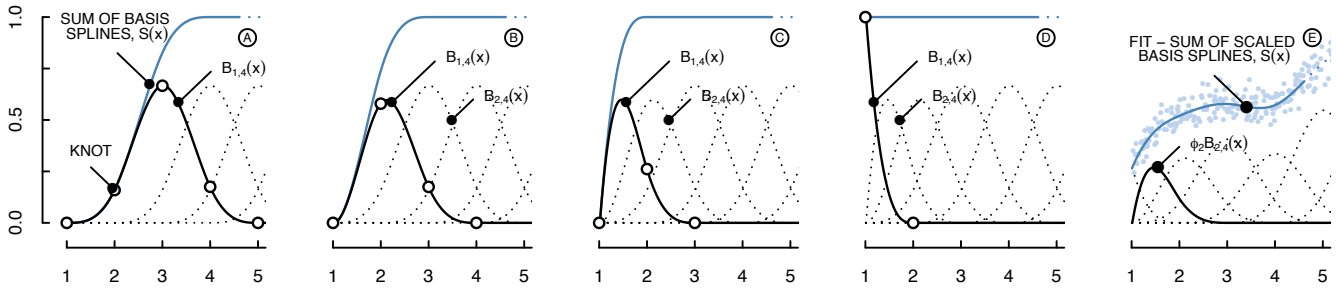

Figure 2: Positioning of B-splines on a finite domain, and a spline function fitted to data. In (A) a series of cardinal basis splines and their sum is shown. In each of the proceeding figures one new basis spline is added on the left, so that knots accumulate at knot position 1. The knots of the leftmost basis spline, $B_{1,4}(x)$, in (B) are $x = \{1, 1, 2, 3, 4\}$, and finally in (D) the knots are $x = \{1, 1, 1, 1, 2\}$. In (E) the basis splines are scaled such that the resulting cubic spline fits a given set of data.

B-spline will have $m-1$ coinciding knots, etc. The resulting set of B-splines has the same properties as the cardinal B-splines, except that continuity is reduced in the coinciding knots to $\mathbb{C}^{m-n}$, where n is the number of coinciding knots.

Figures 2A-D illustrate how the basis splines change shape as more knots are coinciding and eventually how the resulting spline $S(x)$ adds up to unity on the finite domain.

2.1.3. Data Fitting with Splines

The property that the B-spline series sums up to unity for the entire range of interest is especially useful for data fitting. By scaling and summing the individual B-splines as in Eq. (10), the spline function $S(x)$ is obtained:

$$S(x) = \sum_{i=1}^{q} \phi_i B_{i,m}(x)\,, \tag{10}$$

where ϕ_i is the scaling factor (and model parameter) of the i^{th} B-spline. Typically linear ($m = 2$), quadratic ($m = 3$), or cubic ($m = 4$) splines are used.

Figure 2E illustrates how it is possible to fit a spline to a certain data set by scaling the individual basis splines. By utilising the modified boundary basis spline as described in the previous section, it is possible to estimate a nonzero value at the left and right side of the spline domain. Section 2.3 will further discuss the implementation of the spline function $S(x)$ in a grey-box setting.

2.2. Grey-box Models

Grey-box models are mathematical representations of a physical system that is described by a number of inputs, outputs and state variables. The state variables are described by first order differential or difference equations for continuous and discrete time, respectively. This paper focuses on grey-box models with states in continuous time and observations in discrete time.

In a grey-box model, a noise term is added to the—otherwise deterministic—white-box model. The stochastic nature of these models furthermore allows for the application of statistical methods for structural model identification, such as the likelihood ratio test.

A grey-box model consists of a series of stochastic differential equations (the system equations) and one or more observation equations. The grey-box model in the form used in this article, namely the state-space form, is written

$$\mathrm{d}\boldsymbol{x}_t = \boldsymbol{A}\boldsymbol{x}_t\mathrm{d}t + \boldsymbol{B}\boldsymbol{u}_t\mathrm{d}t + \boldsymbol{\sigma}\mathrm{d}\boldsymbol{\omega}_t \tag{11}$$

$$\boldsymbol{y}_{t_k} = \boldsymbol{C}\boldsymbol{x}_{t_k} + \boldsymbol{\epsilon}_{t_k}\,. \tag{12}$$

In the above equations $\boldsymbol{x}_t$ is the state vector, $\boldsymbol{y}_{t_k}$ is the observed output vector, $\boldsymbol{A}$ is the transition matrix, $\boldsymbol{B}$ is the input matrix, $\boldsymbol{C}$ is the output matrix, $\boldsymbol{u}_t$ is the input vector, t is the time, k is the number of the discrete time step, $\boldsymbol{\epsilon}$ is the measurement noise, and finally $\boldsymbol{\omega}_t$ is a vector of Wiener processes. The measurement error vector $\boldsymbol{\epsilon}_{t_k} \sim N(0, \boldsymbol{\sigma}_{\text{obs}})$ is assumed to be i.i.d., and $\boldsymbol{\omega}_t$ and $\boldsymbol{\epsilon}_{t_k}$ are assumed independent.

Further theory on stochastic differentiation and integration can be found in for example (Kloeden et al., 1994) and (Zastawniak and Brzezniak, 1998). For the purposes of this paper, a basic knowledge of random variables suffices.

2.2.1. Model Selection Procedure

In order to choose the optimal number of B-splines to approximate a functional relationship present in the data, several possibilities are implemented and compared. For cubic splines with intercept, the minimum number of splines is 4. The maximum is kept at 12, which typically is sufficient for the specific modelling purposes.

Forward model selection is used, in which a simple model is iteratively extended. The procedure is visualised in Figure 1. In each iteration, the most significant model extension is selected using the likelihood ratio test (LRT), a statistical test providing a p-value that expresses the significance of the extension (Madsen and Thyregod, 2010). The model selection ends when no extension is significant. A significance level of 0.05 is used throughout the model selection. The likelihood ratio test is also used to determine the optimal number of B-splines in each model extension.

2.3. Implementing Splines in State-space Models

Figure 2E visualised how a set of basis splines is scaled such that the resulting spline fits a certain data set. For the case of

modelling the solar gain in a given energy system, the exact same approach can be used.

The position of the sun is uniquely defined by the solar azimuth angle, γ, and the sun elevation, α, which can be determined from latitude, longitude and time. This paper deals with the solar gain factor as a function of the azimuth angle only. This is a valid assumption for sufficiently short time periods during which the sun elevation corresponding to each azimuth angle is approximately constant over the days included in the data.

In the following, the spline-based approach is described for modelling solar gain in a resistance-capacity (RC) grey-box model. Only cubic B-splines with equidistant knots are used here. When the data set covers all times between sunset and sunrise, the boundary knots are placed at these two moments. Otherwise the boundary knots are placed at the extremes of the azimuth angle present in the data.

The solar heat gain Φ_{sol} in an RC model can be expressed by multiplying the solar gain factor and the outdoor solar irradiation measured in a certain plane as shown in Eq. (1), (3), and (4). To include azimuth angle dependence of the solar gain, the solar gain factor is substituted with the spline,

$$\Phi_{\text{sol}} = \begin{cases} \eta(\gamma)\, I = \sum_{i=1}^{q} \phi_i B_{i,m}(\gamma)\, I & \text{for } \alpha > 0° \\ 0 & \text{for } \alpha \leq 0°\,. \end{cases} \tag{13}$$

One needs to specify a sequence of knots in any sub-interval of $\gamma \in [0°,\ 360°)$, where γ is the azimuth angle of the sun. This sub-interval will typically include the azimuth angles between sunrise and sunset. Thereby the functional representation of the solar gain Φ_{sol} is obtained as in Eq. (13), where α is the sun elevation, and I is the solar irradiation. The knots are defined as described in Section 2.1.2 to ensure that the spline curve can take any value for the entire chosen sub-interval. Depending on the complexity of the shadow pattern over the day, the number of base splines can be adjusted.

The basis splines $B_{i,m}(\gamma)$ are uniquely defined by the knot sequence and the azimuth angle time series. Therefore, the basis splines can be constructed before model fitting, as seen in the first step of Figure 1.

Assuming that the solar radiation only affects the first state, the stochastic differential equations on state-space form in Eq. (11) can be written as:

$$\mathrm{d}\boldsymbol{x}_t = \boldsymbol{A}\boldsymbol{x}_t\mathrm{d}t + \underbrace{\boldsymbol{B}\boldsymbol{u}_t\mathrm{d}t}_{\boldsymbol{B_1}\boldsymbol{u}_{\boldsymbol{1},t} + \boldsymbol{B_2}\boldsymbol{u}_{\boldsymbol{2},t}} + \boldsymbol{\sigma}\mathrm{d}\omega_t\,, \text{ where}$$

$$\boldsymbol{B_1} = \frac{1}{C}\begin{bmatrix} \phi_1 & \phi_2 & \cdots & \phi_q \\ 0 & 0 & \cdots & 0 \\ \vdots & \vdots & \ddots & \vdots \\ 0 & 0 & \cdots & 0 \end{bmatrix}_{p\times q} \qquad \boldsymbol{u}_{\boldsymbol{1},t} = \begin{bmatrix} B_{1,m}(\gamma_t)\, I_t \\ B_{2,m}(\gamma_t)\, I_t \\ \vdots \\ B_{q,m}(\gamma_t)\, I_t \end{bmatrix}_q \tag{14}$$

$\boldsymbol{B_2}\boldsymbol{u}_{\boldsymbol{2},t}$: Second input matrix, $\boldsymbol{B_2} \in \mathbb{R}^{p\times r}$, and its associated input vector, $\boldsymbol{u}_{\boldsymbol{2},t} \in \mathbb{R}^r$, excluding solar gains.

In Eq. (14), p is the number of states, q is the number of basis splines used to model the solar gain, r is the number of inputs excluding solar irradiation, ϕ_i is the scaling factor of the i^{th} basis spline, $B_{i,m}(\gamma_t)$, C is the heat capacity of the temperature node to which the solar gain is assigned, and I_t is a time series of the measured outdoor solar irradiation. Finally, $\boldsymbol{A} \in \mathbb{R}^{p\times p}$, is the transition matrix and $\boldsymbol{x} \in \mathbb{R}^p$ is the state vector.

Note that the matrix $\boldsymbol{B_1}$ can be modified to make the solar gain affect more than one state, however, for simplicity of the formulations this is not done here.

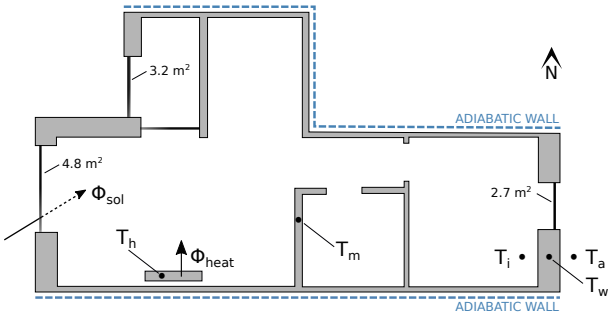

Figure 3: Floor plan of the modelled apartment including temperature nodes, modelled heat gains, window areas and orientation.

3. Case Study

This Section describes the implementation of the spline-based approach for solar gain modelling of two dynamical thermal systems. In the first case (Section 3.1), the splines are included in a model of the heat dynamics of a single apartment. In the second case (Section 3.2), splines are applied to model the solar gain in a solar collector field.

In the following sections the used data and applied models are described for each case, along with results of the model selection procedure.

All models are formulated and fitted with use of the package *ctsmr* (Continuous Time Stochastic Modelling for R, version 0.6.17) (Juhl, 2013), which uses a Kalman filter and maximum likelihood methods for parameter estimation. The B-spline basis functions are generated with use of the R-core package *splines* (version 3.5.1) (R Core Team, 2017).

3.1. Modelling the Thermal Dynamics of a Building

In this case study, the physical parameters of a building, such as heat loss coefficients, heat capacities, and time constants, were estimated. The following sections show how the models improve when the solar gain is modelled with splines. This semi-parametric model allows the estimation of the azimuth-dependent solar gain factor and the resulting solar gain.

3.1.1. Data

During the period from February 13 to April 1, 2018, measurements were obtained from a two-room apartment in Aalborg, Denmark. The apartment consists of an open kitchen and living room, a bedroom, a bathroom, a small corridor, and a heated weather porch. The apartment has a gross floor area of 67 m^2 and a total window area of 10.7 m^2. Similar heated

apartments are located on the north side, south side, and above the apartment. An unconditioned basement is located below the apartment. The floor plan of the apartment is shown in Figure 3, including window sizes and the physical parameters used for modelling.

The total space heating of the apartment was measured every 15 minutes, and the air temperature in eight locations in the apartment was measured every 5 minutes. The internal temperature used in the model was the arithmetic mean temperature of all eight sensors in each time step.

In addition to the heating power Φ_{heat} (kW) and the internal temperature T_{i} (°C), the outdoor ambient temperature T_{a} (°C) and the global solar irradiation I_{g} (kW/m^2), were measured every minute at Aalborg University, 2.6 km away. All measurements were re-sampled to hourly values by averaging. A subset of the data is plotted in Figure 4.

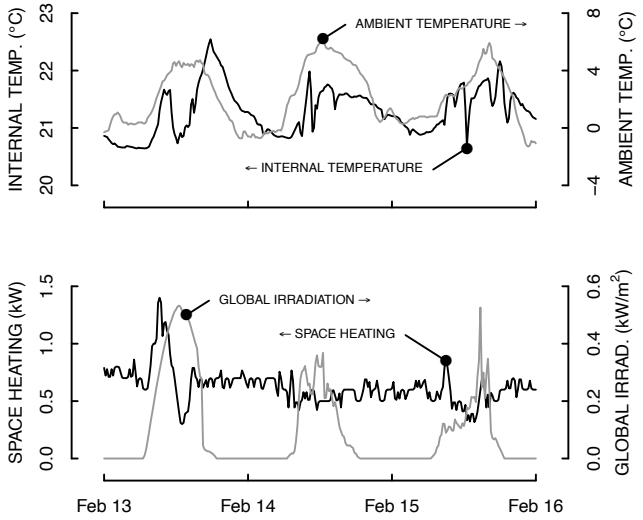

Figure 4: Three out of 47 days of measurements (February 13 to April 1, 2018) for dynamical building model estimation: ambient temperature, space heating, global solar irradiation, and internal temperature.

3.1.2. Models

The model that all the other models originate from is the single-state model T_{i} as given by

$$\text{T}_{\text{i}} \begin{cases} \mathrm{d}T_{\text{i}} = \frac{1}{C_{\text{i}}}\left(\frac{T_{\text{a}}-T_{\text{i}}}{R_{\text{w}}} + \Phi_{\text{heat}} + \eta I_{\text{g}}\right)\mathrm{d}t + \sigma_{\text{i}}\mathrm{d}\omega_{\text{i}} \\ T_{\text{i}}^{*} = T_{\text{i}} + \epsilon\,. \end{cases} \tag{15}$$

Note that the time indices shown in e.g. Eq. (11) and (12) are omitted for simplicity.

In the model above, the only state is the internal temperature T_{i}, as indicated by the model name. The C_{i}, R_{w}, η, σ_i and the variance of ϵ are model parameters which are to be estimated. T_{a}, Φ_{heat} and I_{g} are model inputs, and T_{i}^{*} is the observed internal temperature. For further specification, see the Nomenclature.

All models include the state variables in their names. The temperature of an internal thermal mass, the heating system, and the exterior wall/building envelope are represented by T_{m}, T_{h}, and T_{w}, respectively. Finally, the postfix S_{q} indicates that the solar gain is modelled by a cubic spline with q basis spline.

For illustrative purposes Eq. (16) presents a model with two states: the internal temperature T_{i}, and the hidden state temperature of the building envelope T_{w}. The inputs of model $\text{T}_{\text{i}}\text{T}_{\text{w}}$ are the ambient temperature T_{a}, space heating Φ_{heat}, and global irradiation I_{g}.

$$\text{T}_{\text{i}}\text{T}_{\text{w}} \begin{cases} \mathrm{d}T_{\text{i}} = \frac{1}{C_{\text{i}}}\left(\frac{T_{\text{w}}-T_{\text{i}}}{R_{\text{wi}}} + \Phi_{\text{heat}} + \eta I_{\text{g}}\right)\mathrm{d}t + \sigma_{\text{i}}\mathrm{d}\omega_{\text{i}} \\ \mathrm{d}T_{\text{w}} = \frac{1}{C_{\text{w}}}\left(\frac{T_{\text{i}}-T_{\text{w}}}{R_{\text{wi}}} + \frac{T_{\text{a}}-T_{\text{w}}}{R_{\text{wa}}}\right)\mathrm{d}t + \sigma_{\text{w}}\mathrm{d}\omega_{\text{w}} \\ T_{\text{i}}^{*} = T_{\text{i}} + \epsilon \end{cases} \tag{16}$$

To convert a model with constant solar gain factor, η, to a model with azimuth-dependent solar gain factor, $\eta(\gamma)$,the spline function in Eq. (10) is substituted by

$$\eta = \eta(\gamma) = \sum_{i=1}^{q} \phi_i B_{i,m}(\gamma) \tag{17}$$

The solar gain $\left(\Phi_{\text{sol}} = \eta I_{\text{g}}\right)$ is assigned to a single state, namely the internal temperature node T_{i}, for all fitted models.

3.1.3. Results

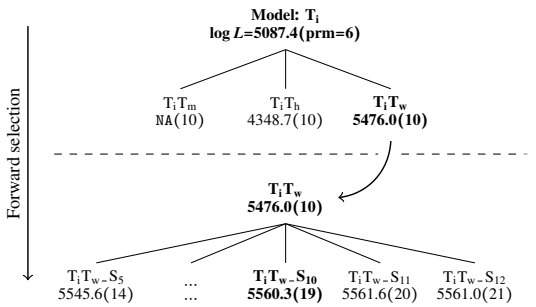

Figure 5: Forward model selection framework for dynamical building modelling. For each model the log-likelihood ($\log L$) and the number of parameters (prm) are shown. One model did not converge, indicated by the log-likelihood of `NA`.

Figure 5 shows the model selection framework and the result of the model selection. The diagram shows that the simplest model T_{i} is first extended with a hidden state without use of solar splines (row 2). In this case, the model $\text{T}_{\text{i}}\text{T}_{\text{w}}$ was found to be the best model. No more than one hidden state has been tested, to avoid potential structural identifiability issues. After the model was fitted, it was extended further by introducing splines to estimate the azimuth-dependent solar gain factor. This is shown in the lower part of the figure.

All the spline models with five or more basis splines (except the models with eight and nine, which did not converge) outperform the null model $\text{T}_{\text{i}}\text{T}_{\text{w}}$. However, no statistically significant improvement was found when more than ten basis splines were used for this particular data set.

The likelihood ratio test between the null model $\text{T}_{\text{i}}\text{T}_{\text{w}}$ and the alternative model $\text{T}_{\text{i}}\text{T}_{\text{w}}\text{-S}_{10}$ reveals a p-value of less than $2.2e\cdot$

10^{-16}, which clearly shows a significant improvement obtained by the alternative model. The best model was therefore found to be the two-state model $\mathrm{T_iT_{w\_}S_{10}}$, with a cubic spline describing the solar gain based on ten basis splines.

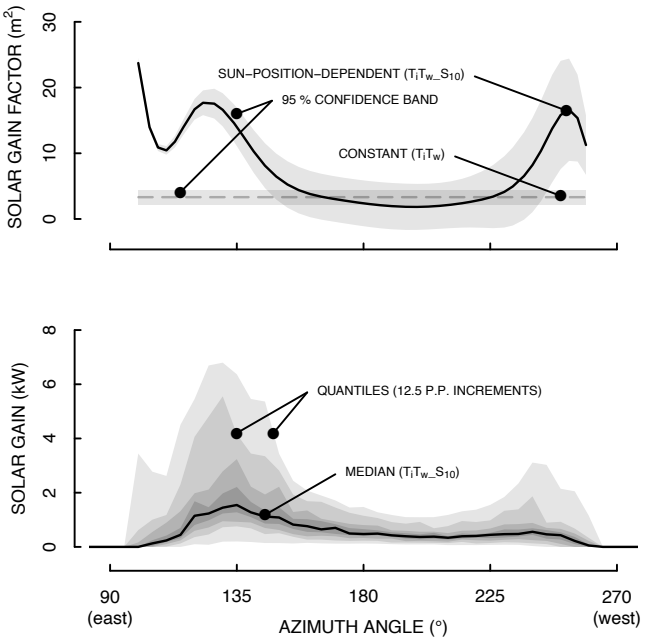

Figure 6: The top figure compares the constant solar gain factor from model $\mathrm{T_iT_w}$ and the sun position dependent solar gain factor from model $\mathrm{T_iT_{w\_}S_{10}}$. The bottom figure shows the resulting median and quantiles of the solar gain for model $\mathrm{T_iT_{w\_}S_{10}}$ with 12.5 percentage point increments (0.0, 12.5, 25.0, 37.5, 62.5, 75.0, 87.5, 100.0 %).

Figure 6 shows the estimated solar gain factor of model $\mathrm{T_iT_w}$ and $\mathrm{T_iT_{w\_}S_{10}}$. In the azimuth interval from 110° to 260°, two distinct peaks in the solar gain factor from model $\mathrm{T_iT_{w\_}S_{10}}$ and a flat insignificant section in-between can be seen. This is in agreement with the apartment layout as it has windows towards the east and west, as seen in Figure 3.

It is noted that solar gain factor for the morning hours (azimuth angle from 100° to 110°) is rather high and oscillates. As the solar irradiation intensity is low in this period of the day it is expected that the scaling factor of the basis spline is difficult to estimate. Furthermore, the confidence band is underestimated, as the scaling factor in this region is reaching the upper parameter search boundary. However, due to the low irradiation intensity, the effect on the model states is limited as well. This is seen in the general low solar gain levels in the interval from 100° to 110°, in the lower plot in Figure 6.

3.2. Forecasting Solar Heat Generation

In the second use case, the aim was to predict the return (outlet) temperature of a solar heat field. As the solar irradiation has a dominant influence on this variable, it can be expected that accurate modelling of shading patterns improves the model performance significantly.

3.2.1. Data

Measurements were collected at the Aalborg CSP Solar Heat Plant in Solrød Municipality between May 23, 2017 and May 31, 2017. The total panel area is 2569 $\mathrm{m^2}$, which yields around 1300 MWh annually with a peak power of 1.9 MW, serving a community of 350 households. A schematic overview of the site and measurements are shown in Figure 7. The following measured inputs were used: total solar irradiation in collector plane I_t, fluid flow per panel surface area Q_f, fluid supply and return temperature T_s and T_r, and ambient temperature T_a. The solar azimuth angle was computed from the longitude, latitude, and time. In Figure 7, note the trees located west of the collectors, which shade (part of) the field in the afternoon.

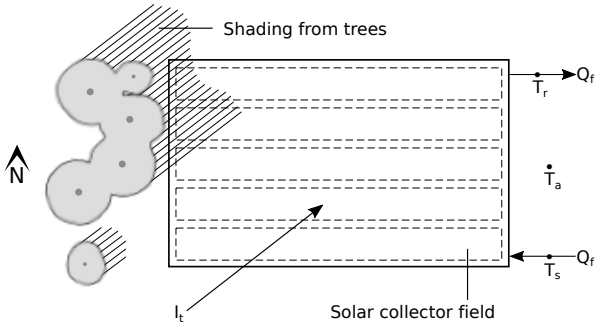

Figure 7: Schematic setup of solar collector field and surrounding trees, including used measurements.

A subset of the measurements is depicted in Figure 8. The values were 1 minute averages of measurements taken every second. A control of the return temperature had already been implemented at the time of data collection, which limited the variation in measured return temperature, T_r.

A subset of the data was selected for parameter estimation. Periods of low or zero flow were excluded, as well as data points with large incidence angle θ, such that $\cos(\theta) < 0.2$ (i.e. $\theta > 78.5°$). Finally, some periods in which the plant switches back and forth from preheating to operating were removed. This results in a data set with gaps and a varying number of measurements per day, including days with clear sky and days with intermittent cloud cover. This is, however, not a problem in the grey-box model setup.

3.2.2. Models

An initial stochastic state-space model was taken from Bacher et al. (2011), whose model in turn derives from Perers (1997). An extended form of the heat balance proposed by the latter is used in the current ISO standard for quasi-dynamic testing (European Committee for Standardization (CEN) Technical Committee, 2017). The resulting state-space formulation for the base model $\mathrm{T_r}$ is

$$\mathrm{T_r}\begin{cases} \mathrm{d}T_\mathrm{r} = \frac{U_\mathrm{fa}(T_\mathrm{a}-T_\mathrm{f})+\eta I_\mathrm{t}+c_\mathrm{f}Q_\mathrm{f}(T_\mathrm{s}-T_\mathrm{r})}{(mC)_\mathrm{e}}\,\mathrm{d}t + \sigma_\mathrm{r}\mathrm{d}\omega_\mathrm{r} \\ T_\mathrm{r}^* = T_\mathrm{r} + \epsilon\,. \end{cases} \tag{18}$$

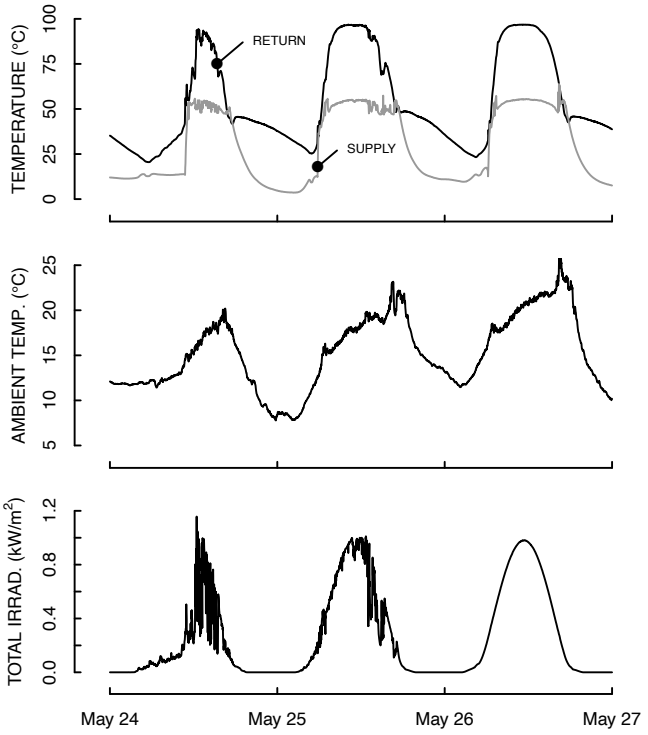

Figure 8: Three out of nine days of measurements (May 24–26, 2017) used for fitting the solar collector field model: supply and return temperature (top), ambient temperature (middle), and total irradiation (bottom).

The modelled quantity is the return temperature T_r. The measured inputs are T_a, Q_f, T_s, and I_t. The variable T_f is the average of supply and return temperature. The factor c_f is a given constant, whereas $(mC)_\mathrm{e}$, U_fa, η, σ_f and σ_obs are parameters to be estimated. The exact specification of the variables can be seen in the nomenclature.

Four extensions of the base model $\mathrm{T_r}$ were considered, which all add detail to modelling the effect of solar irradiation. One extension was the splined solar gain factor, which is indicated by $\mathrm{S_q}$ in the model name, where q is the number of splines. In addition, two different IAM functions were implemented. The model name includes IAM for the standard function as given in Eq. (5), and $\mathrm{IAM_a}$ for the Ambrosetti IAM from Eq. (6). Finally, the total irradiation was split into direct and diffuse components, using the method proposed by Ruiz-Arias et al. (2010). Models including this irradiation split contain $\mathrm{I_{split}}$ in their names. All applied models lump the field into a single compartment with one corresponding state variable, the return temperature T_r.

All extensions were applied to the base model in an iterative manner that is visualised in Figure 9. In each iteration, the model was extended in several ways, one extended model for each of the remaining extensions. The extension with the lowest p-value were selected, and the procedure was repeated until no extensions were significant or all extensions were implemented.

Note that in cases of the split radiation being combined with the splined solar gain factor $\eta(\gamma)$, the solar gain was modelled differently to Eq. (4) to ensure identifiability. Instead, it was given by

$$\Phi_\mathrm{sol} = \eta(\gamma)\, K_\mathrm{b}(\theta)\, I_\mathrm{b} + K_\mathrm{d}\, I_\mathrm{d}\,, \tag{19}$$

where $K_\mathrm{b}(\theta) = 1$ in case where the model did not include an IAM.

3.2.3. Results

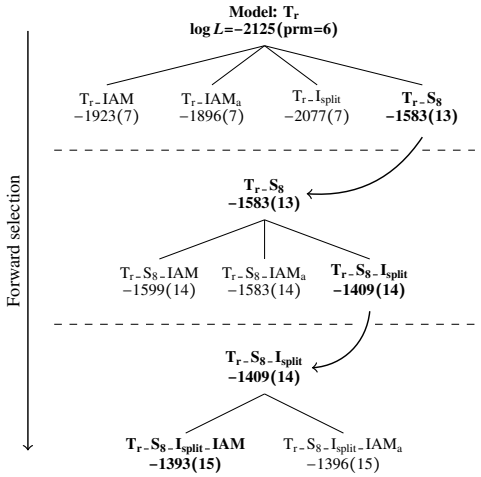

Figure 9: Forward selection framework for solar heat field model. For each model the log-likelihood ($\log L$) and the number of parameters (prm) are shown. Among the spline models ($\mathrm{T_r\text{-}S_8}$, $\mathrm{T_r\text{-}S_8\text{-}I_{split}}$, etc.), only the best model is shown in the diagram, however, models with four to eight basis splines were tested.

In the first model extension, the spline was the most significant improvement to the model, in particular $\mathrm{T_r\text{-}S_8}$. The next selection round included the radiation split to the model, where again the version with eight basis splines was most significant. Finally, the model was extended with one of the IAM functions, again with eight basis splines. The model selection ended here, as all extensions considered were accepted. Note that the final model includes both a state-of-the-art Amrbrosetti incidence angle modifier and spline functions, which together model the sun-position dependence of the solar gain factor. This result shows that several solar gain modelling components can be combined and in this way complement each other.

The combined effect of the IAM, split radiation, and spline functions on the estimated solar gain factor for the (estimated) direct radiation is shown as a function of azimuth angle in Figure 10. The models have different estimated heat capacities $(mC)_\mathrm{e}$, which scale the functions to different maximum values. In order to compare the possible function shapes of the solar gain factor function that the different models provide, for this plot the functions were scaled to a common maximum value of 1. The spline-based solar gain factor decreases faster in the afternoon (azimuth angle from 225° to 280°), which indicates that the effect of the shading forest is captured in these models, but not in the state-of-the-art model.

Model performance was compared using prediction with perfect forecasts of the inputs, that is, using the actual measurements as inputs. Figure 11 shows how the model predictions

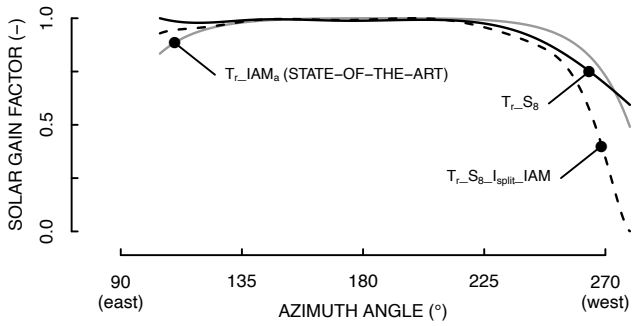

Figure 10: Solar gain factor for the modelled solar heat plant for three different models: the state-of-the-art IAM model $T_r\_IAM_a$, the model $T_r\_S_8$ with splines only, and the final model $T_r\_S_8\_I_{split}\_IAM$ that combines the Ambrosetti IAM with the spline functions. For comparison, all functions are scaled to a maximum value of 1.

improved due to the added solar gain function. Note that all models, including the final model, overestimate the return temperature at the end of the day due to a measurement error in the ambient temperature. The measurement error occurs due to exposure of the sensor to direct sunlight. This could be accounted for in future improvements of the model, but is outside the scope of this article.

Figure 11A compares the residuals of two of the base model extensions, T_r_IAM and the selected $T_r\_S_8$. It is clear that the spline-based model is able to account for shading, and thereby reduces structural prediction errors that were present when modelling incidence angle effects with an IAM only. Figure 11B shows improvements in the residuals after the final model extension from $T_r\_S_8\_I_{split}$ to $T_r\_S_8\_I_{split}\_IAM$. The improvement was less pronounced than in 11A, but it can be seen that the residuals in the late afternoon were slightly improved by including the IAM. The remaining error in the late afternoon is explained by the ambient temperature measurement error.

With each model extension, the time of day from which the model starts overestimating the return temperature is postponed. As one might expect, the improvements are less pronounced on cloudy days than on sunny days as plotted here, but still present.

4. Discussion

First of all, it is noted that although the splined solar gain factor was applied in grey-box models here, the used of the method is not limited to this model type. The B-splines can also be used in other models in which the parameters are fitted from data, such as linear regressions.

In the present article, the splined solar gain factor only affected a single state in the state-space models. It is however a simple adaptation to assign the solar gain to the system in more complex ways, e.g. by assigning it to more than one state.

While only equidistant spline knot sequences are used in this article, the location of the knots can perhaps be optimised by concentrating more knots around azimuth angles for which fast changes in the shading pattern occur. One should in this case be aware of potential overfitting when spline knots are placed too closely together, as the individual basis splines would be fitted to fewer data points.

When using longer periods of measurements covering several months, there will be a larger range of sun elevations associated with a single azimuth angle. As the elevation also affects shading patterns and the incidence angle, one may need to account for this as well. This can be solved in several ways. First, an additional spline curve can be introduced to account for the sun elevation variation of the solar gain factor. The downside of this approach is that it requires significant amounts of data to estimate the splines and adds parameters to the model. This will increase the computation time and may even result in an unidentifiable model.

A more convenient approach than introducing a second spline curve is to apply an adaptive model in which parameters are allowed to change over time. One example of adaptive time-varying parameters estimation is presented by Joensen et al. (2000). In that way the scaling factors of the B-splines will be specific to shorter time periods of data, so that the azimuth angle again largely determines the shading pattern within this time period.

An important note regarding the estimated spline curve is that its physical interpretation is not always straightforward. The splines may account for other effects than solar irradiation such as systematic use patterns (heat gain from people, computers etc.) or systematic measurement errors. These concerns are mostly relevant for climates or measurement periods with low daily variation in solar irradiation, i.e. climates and periods with mainly clear sky conditions.

Finally, it should be noted that it can be difficult to estimate the scaling factors for periods with low solar irradiation, e.g. close to sunrise and sunset. This may be prevented by placing the boundary knots closer towards the south, and fitting a constant or linear solar gain factor to the periods outside these bounds.

5. Conclusion

Modelling solar gain is of crucial importance for energy system models. This paper shows that the approaches for solar gain modelling in the literature can be improved significantly by taking the position of the sun into account when modelling the thermal dynamics of an apartment and a solar collector field.

This paper has proposed B-splines as a non-parametric method to estimate the relation between measured solar irradiation and the solar gain. In two case studies, this method was implemented and tested in grey-box models that included the solar gain as a function of the azimuth angle. This function is estimated using coefficients on a B-spline basis. The splines have been used on the global, total, and beam irradiation in different model versions.

A two-state model of an apartment was improved significantly by estimating the solar gain factor with use of a diurnal spline factor instead of the commonly used constant solar gain factor. The estimated solar gain curve showed good agreement with the authors expectations for the specific apartment with

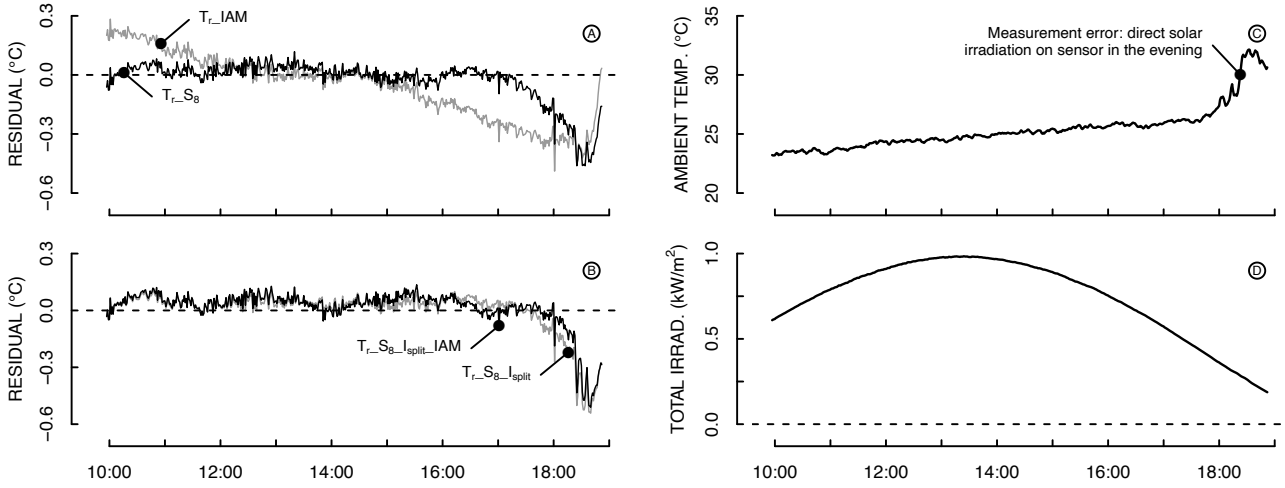

Figure 11: One-step prediction residuals of the return temperature on a sunny day. Panel (A) shows a comparison between two extensions of the base model: spline-based model ($T_r\_S_8$) and current state-of-the-art model (T_r_IAM). In (B) we compare residuals of a more complex model that applies splines only $T_r\_S_8\_I_{split}$ to its extension $T_r_S_8_I_{split}$_IAM), which combines the splines and the Ambrosetti IAM. Panel (C) and (D) show measured ambient temperature and measured total irradiation in the plane of the collectors, respectively.

east- and west-facing windows, as the peak in solar gain occurred during morning and evening.

For a return temperature model of a solar collector field, it has been shown that the splines account for local shading patterns caused by the panels themselves and trees next to the field, while also accounting for incidence angle effects. The key difference compared to the methods from ISO 9806:2017 and most models in the literature is that the spline-based solar gain factor has a higher degree of freedom than frequently used single-parameter incidence angle modifier (IAM) functions. This makes it capable of accounting for site-specific shading patterns, which largely reduced structural prediction errors. In addition, the splines can be combined with standard IAM functions to achieve even better results.

Acknowledgements

This work was supported by the project Renovating Buildings Sustainably (REBUS) [5151-00002B]; the Danish Innovation Fund [DSF1305-00027B–CITIES]; and by EUDP: Danish Participation in IEA EBC Annex 71 [64017-05139].

The authors would furthermore like to thank Aalborg CSP for the use of their data set and providing further information.

References

Bacher, P., Andersen, P., 2014. IEA Common Exercise 4: ARX, ARMAX and grey-box models for thermal performance characterization of the test box. Tech. rep., DTU Compute.

Bacher, P., Madsen, H., 2011. Identifying suitable models for the heat dynamics of buildings. Energy and Buildings 43 (7), 1511–1522.

Bacher, P., Madsen, H., Perers, B., 2011. Models of the heat dynamics of solar collectors for performance testing. Proceedings of ISES Solar World Conference 2011.

Bauwens, G., Roels, S., 2013. Characterizing thermal performance of buildings using dynamic model identification. In: Thermal Performance of the Exterior Envelopes of Whole Buildings XII International Conference. ASHRAE, pp. 72–86.

Bava, F., 2017. Modeling of solar collector fields for solar heating plants in district heating systems. Ph.D. thesis, DTU.

Bava, F., Furbo, S., 2018. Impact of different improvement measures on the thermal performance of a solar collector field for district heating. Energy 144, 816–825.
URL `https://doi.org/10.1016/j.energy.2017.12.025`

Brohus, H., Heiselberg, P., Simonsen, A., Sørensen, K. C., 2010. Influence of occupants behaviour on the energy consumption of domestic buildings. Aalborg University, Denmark.

Christensen, O., 2010. Functions, spaces, and expansions: mathematical tools in physics and engineering. Springer Science & Business Media.

Coley, D., Penman, J., 1992. Second order system identification in the thermal response of real buildings. paper ii: recursive formulation for on-line building energy management and control. Building and Environment 27 (3), 269–277.

de Andrade, G. A., Álvarez, J. D., Pagano, D. J., Berenguel, M., 2015. Nonlinear controllers for solar thermal plants: A comparative study. Control Engineering Practice 43, 12–20.
URL `http://dx.doi.org/10.1016/j.conengprac.2015.06.002`

de Boor, C., jun 2007. Spline Basics. In: Handbook of Computer Aided Geometric Design. Elsevier, pp. 141–163.

European Committee for Standardization (CEN) Technical Committee, 2017. ISO 9806:2017: Solar energy Solar thermal collectors Test methods. Tech. rep., International Organization for Standardization, Geneva, Switzerland.

Haldi, F., Robinson, D., 2011. The impact of occupants' behaviour on building energy demand. Journal of Building Performance Simulation 4 (4), 323–338.

Jimenez, M. J., Madsen, H., 2008. Models for describing the thermal characteristics of building components. Building and Environment 43 (2), 152–162.

Joensen, A., Madsen, H., Nielsen, H. A., Nielsen, T. S., 2000. Tracking time-varying parameters with local regression. Automatica 36 (8), 1199–1204.

Johnston, D., Farmer, D., Brooke-Peat, M., Miles-Shenton, D., 2016. Bridging the domestic building fabric performance gap. Building Research & Information 44 (2), 147–159.

Juhl, R., 2013. ctsmr: CTSM for R. R package version 0.6.7.

Kicsiny, R., 2014. Multiple linear regression based model for solar collectors. Solar Energy 110, 496–506.

Kloeden, P. E., Platen, E., Schurz, H., 1994. Numerical solution of SDE through computer experiments. Springer.

Madsen, H., Bacher, P., Bauwens, G., Deconinck, A.-H., Reynders, G., Roels, S., Himpe, E., Lethé, G., 2016. EBC Annex 58 Reliable building Energy Performance Characterisation Based on Full Scale Measurements. Tech. rep., The International Energy Agency, Belgium.

Madsen, H., Holst, J., 1995. Estimation of continuous-time models for the heat

dynamics of a building. Energy and buildings 22 (1), 67–79.
Madsen, H., Thyregod, P., 2010. Introduction to general and generalized linear models. CRC Press.
Mejri, O., Del Barrio, E. P., Ghrab-Morcos, N., 2011. Energy performance assessment of occupied buildings using model identification techniques. Energy and Buildings 43 (2-3), 285–299.
Pasamontes, M., Àlvarez, J. D., Guzman, J. L., Berenguel, M., Camacho, E. F., 2013. Hybrid modeling of a solar-thermal heating facility. Solar Energy 97, 577–590.
Perers, B., 1997. An improved dynamic solar collector test method for determination of non-linear optical and thermal characteristics with multiple regression. Solar Energy 59 (4-6 -6 pt 4), 163–178.
Prautzsch, H., Boehm, W., Paluszny, M., 2002. Bézier and B-Spline Techniques. Springer-Verlag Berlin Heidelberg.
R Core Team, 2017. R: A Language and Environment for Statistical Computing. R Foundation for Statistical Computing, Vienna, Austria.
URL `https://www.R-project.org/`
Rabl, A., 1988. Parameter estimation in buildings: methods for dynamic analysis of measured energy use. Journal of Solar Energy Engineering 110 (1), 52–66.
Roels, S., Bacher, P., Bauwens, G., Castaño, S., Jiménez, M. J., Madsen, H., 2017. On site characterisation of the overall heat loss coefficient: Comparison of different assessment methods by a blind validation exercise on a round robin test box. Energy and Buildings 153, 179–189.
Ruiz-Arias, J., Alsamamra, H., Tovar-Pescador, J., Pozo-Vázquez, D., 2010. Proposal of a regressive model for the hourly diffuse solar radiation under all sky conditions. Energy Conversion and Management 51, 881–893.
Sauer, T., 2006. Numerical Analysis. Pearson.
Schoenberg, I. J., 1946. Contributions to the Problem of Approximation of Equidistant Data by Analytic Functions. Quart. Appl. Math. 4, 45–99; 112–141.
Socolow, R. H., 1977. The Twin Rivers Program on Energy Conservation in Housing: Highlights and Conclusions*. Energy and Buildings 1 (3), 207–242.
Zastawniak, T., Brzezniak, Z., 1998. Basic stochastic processes. Springer.
Zeifman, M., Roth, K., 2016. Residential remote energy performance assessment: estimation of building thermal parameters using interval energy consumption data. In: ACEEE Summer Study on Energy Efficiency in Buildings. pp. 1–12.

Article

METHOD FOR SCALABLE AND AUTOMATISED THERMAL BUILDING PERFORMANCE DOCUMENTATION AND SCREENING

Christoffer Rasmussen [1]*, Peder Bacher [1], Davide Calì [1], Henrik Aalborg Nielsen [2] and Henrik Madsen [1]

[1] Department of Applied Mathematics and Computer Science, Technical University of Denmark, 2800 Kgs. Lyngby, Denmark
[2] ENFOR A/S, Lyngsø Allé 3, 2970 Hørsholm, Denmark
* Correspondence: chrras@dtu.dk

Version May 29, 2020 submitted to Energies

Abstract: In Europe, more and more data on building energy use will be collected in the future as a result of the energy performance of buildings directive (EPBD), issued by the European Union. Moreover, both at European level and globally it became evident that the real energy performance of new buildings and the existing building stock needs to be documented better. Such documentation can, for example, be done with data-driven methods based on mathematics and statistical approaches. Even though the methods to extract energy performance characteristics of buildings are many, they are of varying reliability and often associated with a significant amount of human labour, making them hard to apply on a large scale. A classical approach to identifying certain thermal performance parameters is the energy signature method. In this study, an automatised, non-linear and smooth approach to the well-known energy signature is proposed, to quantify key thermal building performance parameters. The research specifically aims at describing the linear and non-linear heat usage dependency on outdoor temperature, wind and solar irradiation. To make the model scalable, we realised it so that it only needs the daily average heat use of buildings, the outdoor temperature, the wind speed, and the global solar irradiation. The results of applying the proposed method on heat consumption data from 16 different and randomly selected Danish occupied houses are analysed.

Keywords: Thermal building performance; Energy documentation and screening; Energy signature; Occupants effect on heat consumption

1. Introduction

The energy efficiency directive (EED) of the European Union [1] states that all member states are responsible for installation of individual energy meters, including heat meters, on all buildings to the extend that it is technically possible and economically feasible. Furthermore, the new energy performance of buildings directive (EPBD) states a list of requirements which should boost a technical and economical national renovation strategy [2]. With the current data collection requirements and the new EPBD, the relevancy of data-driven methods for screening and documentation of the thermal performance of buildings become more relevant than ever.

Several method for evaluating thermal energy performance of buildings exists. That being from pure deterministic white box models — as TRNSYS, Modelica or IDA ICE models — where building parameters are tuned such that the simulation output corresponds to the observations, to fully statistical black-box models. Typically a neural network, support vector machines, k-nearest neighbours algorithms, etc. are considered black-box approaches. The latter models are, however,

typically only used for prediction, control, and clustering as the internal dynamics are physically non-interpretable.

A third category of models is grey-box models. This kind of models is a hybrid of the before mentioned white and black-box models. As the white and black-box models are the extremes of the model spectrum, examples of grey-box models are in the form of stochastic differential equations based on physics [3] to auto-regressive moving average model with exogenous inputs (ARMAX) for time series data [4]. The latter kind of models can be explained in physical terms, by first formulating a thermal lumped resistance-capacity (RC) model, and from that deriving an ARMAX or ARX representation, as done in e.g. [5,6].

Other approaches in the literature includes time varying parameter estimation related to thermal building performance. In [7] each parameters of interest is treated as time varying states in a neural network, while an alternative approach based on multivariate kernel estimation for estimating time varying parameters is presented in [8].

In general it can be said that the category of supervised machine learning techniques can be used for performance parameter estimation, prediction, and control, whereas unsupervised techniques are suitable for prediction and control only, as the inseparability is lacking.

Common for most methods is that they require human interaction for model selection and validation. For large scale application they are therefore not feasible. There is in other words a need for methods which are robust, scalable, automatic and methods which only requires generally available data such as heat metering and weather data.

1.1. Energy Signature Methods

For a long time, energy signature models has been studied and applied in order to quantify the energy performance of buildings. A few of the early examples can be found in [9–11] with the earliest known, dated all the way back to 1951 [12].

The dominant principle of the methods is to apply linear regression on e.g. outdoor temperature in order to explain the heat demand, and consequently extract information about heat transfer coefficient.

In one of the simplest models [13], the heat consumption as a function of the outdoor temperature is described with a slope and an intercept in the heating period. During the weather independent period the heat consumption is modelled as a constant. The change points for the weather dependent period (heating period) to the weather independent period is described with a base outdoor temperature T_{b_0} at which the building is in thermal balance. For a fixed value of T_{b_0}, this is similar to the well-known degree-day method, see e.g. [14,15].

In the *ASHRAE Guideline 14-2002 – Measurement of Energy and Demand Savings* [13] seven different energy signature models are proposed depending on different factors concerning if the building is equipped with heating, cooling, heat recovery or different combinations of such systems.

Common for all the methods in the ASHRAE Guideline is that the heat usage is a function of the outdoor temperature alone, contrary to e.g. [10,16].

In [16] it was found that the heat loss coefficient is fairly insensitive ($\pm 5\,\%$) to solar gain and electricity use. The estimated base temperature were more sensitive to these two factors. Since both electricity and solar gain is an additive term to the heat demand (i.e. a functional offset), this seems like a reasonable finding.

More recent studies like [17,18] shows that the energy signature method is still used in research. However, only minor advances on this technique have been reported since the earliest applications of the method.

1.2. Motivation

For all of the above energy signature methods, it is assumed that the transition from a weather dependent heat consumption to a weather independent heat consumption is instantaneous. However, this simplification does not match the reality. Hence, we propose an advancement of the traditional

energy signature models, by formulating it as a smooth non-linear model, from which the transition period can be determined. Furthermore, by reformulating the traditional energy signature model as a smooth, i.e. fully differentiable, model, the estimation procedure can be made more efficient and more advanced modelling approaches, which require full differentiability can be applied.

Finally, it is well known that *all models are wrong, but some are useful* (quote by George E. P. Box). It is therefore such that the non-modelled effects on the heat consumption are part of the model errors. We utilise this fact to form a method to quantify the occupants' effect on the heat consumption, based on the model residuals.

The overall aim of this work is to establish a robust and scalable method for thermal energy performance estimation. The focus in this article is on buildings without secondary heat sources (e.g. wood stoves) and cooling systems, however, it would be possible to extend the model to include mechanical cooling.

2. Method

2.1. Heat Demand Formulation

The energy signature models presented in the introduction all share a common feature. Namely that the transition from one regime to the next happens instantaneously. The mathematical formulation of a model for a building with heating only is thus, according to the e.g. ASHRAE Guideline [13], expressed as:

$$\Phi_{\text{heat}} = \max(f(T_{\text{a}}, \dots),\, g(T_{\text{a}}))\,, \tag{1}$$

where $f(T_{\text{a}}, \dots)$ is the heat consumption in the heating period as a function of the outdoor temperature and other potential explanatory variables, and $g(T_{\text{a}}) = \Phi_0$ is the constant heat consumption for periods outside the heating season.

No matter which mathematical representation one use to model the heat demand in Equation (1), the function is not differentiable for all values of T_{a} as it has an instantaneous change point where $f(T_{\text{a}}, \dots)$ becomes $g(T_{\text{a}})$. Besides potential optimisation issues with a non-differentiable function, for example if the optimiser relies on automatic differentiation, a sudden change between the two regimes is a rough simplification for simple models like the energy signature which typically used daily averaged data. Instead we propose a smooth transition between the two regimes in Section 2.2.

First, different formulations of $f(T_{\text{a}}, \dots)$ are proposed in Sections 2.1.1 and 2.1.2. Furthermore, throughout this article $g(T_{\text{a}})$ is defined as a constant:

$$g(T_{\text{a}}) = \Phi_0 + \varepsilon\,, \tag{2}$$

where ε is normal distributed noise with mean zero.

2.1.1. Heating Degree Day Approach

The simplest approach to model the total heat demand Φ_{total} of a building in the heating season is by using the Fourier's law on steady state form:

$$\Phi_{\text{total}} = \text{UA}\,(T_{\text{i}} - T_{\text{a}}) + \varepsilon\,, \tag{3}$$

where UA is the heat loss coefficient, T_{i} and T_{a} are the in- and outdoor temperature, and $\varepsilon \sim N(0, \sigma^2)$ is the system and observation noise. Furthermore, Φ_{total} consists of space heating, internal heat gains, solar gain, heat transmission to surroundings and ventilation heat loss. For daily average values, the heat exchange with the internal thermal mass (e.g. exterior and interior walls or furniture) is assumed negligible.

Equation (3) can be rewritten as:

$$\begin{aligned} \Phi_{\text{total}} &= \Phi_{\text{heat}} + \Phi_{\text{x}} = \text{UA}\,(T_{\text{i}} - T_{\text{a}}) + \varepsilon \Rightarrow \quad (4)\\ \Phi_{\text{heat}} &= \text{UA}\,(T_{\text{i}} - T_{\text{a}}) - \Phi_{\text{x}} + \varepsilon \\ &= \text{UA}\,(T_{\text{i}} - \Phi_{\text{x}}\text{UA}^{-1} - T_{\text{a}}) + \varepsilon \Rightarrow \\ \textbf{M1:} \quad \Phi_{\text{heat}} &= \text{UA}\,(T_{\text{b}_0} - T_{\text{a}}) + \varepsilon\,, \quad (5) \end{aligned}$$

where M1 refers to the model name, Φ_{heat} is the space heating and Φ_{x} is the remaining constant heat gain which are not explicitly included in the model. Finally,

$$T_{\text{b}_0} = T_{\text{i}} - \frac{\Phi_{\text{x}}}{\text{UA}} \quad (6)$$

is the base temperature, i.e. the outdoor temperature at which the heat losses and gains are in balance, under the assumption that Φ_0 is zero. Hence, for outdoor temperatures above T_{b_0}, the heat consumption is independent of the weather conditions.

Note: Φ_{x} is the remaining heat gains which are not explicitly included in the model. It will therefore change from model to model as it depends on the included heat gains and heat losses.

As many heat gains are infeasible to measure; the indoor temperature often is not readily available; and because a representative indoor temperature is not trivial to measure, $T_{\text{b}_0} = T_{\text{i}} - \Phi_{\text{x}}\text{UA}^{-1}$ can be fixed or estimated as a constant.

It should be noticed that $T_{\text{b}_0} \to T_{\text{i}}$ for $\text{UA} \to \infty$ and/or $\Phi_{\text{x}} \to 0$. Hence, T_{b_0} will approach T_{i} for poorly insulated buildings with small internal and external heat gains.

For daily averaged input values and a fixed value of the base temperature, Equation (5) can be directly related to the commonly known heating degree days (HDD) method, as $\text{HDD} = T_{\text{b}_0} - T_{\text{a}}$.

Often a base temperature is given in the building codes or by other national or regional institutions. In Denmark the base temperature is 17 °C [19]. Using the Danish standard base temperature, Equation (5) becomes:

$$\textbf{M0:} \quad \Phi_{\text{heat}} = \text{UA}\,(T_{\text{b}_0} - T_{\text{a}}) + \varepsilon = \text{UA}\,(17\,^{\circ}\text{C} + \frac{\Phi_0}{\text{UA}} - T_{\text{a}}) + \varepsilon\,. \quad (7)$$

2.1.2. Model Extensions

The model in (5) simply assumes that the heat balance is solely a function of the temperature difference between in- and outside. The solar irradiation, the heat convection of the envelope, the air exchange of the building with the outside, and the outgoing long-wave radiation are therefore indirectly assumed constant (not considered in the model). Hence, the estimated UA values with the simplistic model results in weather biased parameters estimates. For example, for a particular windy and cold heating season, the UA value will be overestimated by applying Equation (5). Likewise, a sunny transition period between the weather dependent and weather independent season results in an overestimated UA value. The model definition is therefore not reliable for estimating thermophysical parameters of buildings [10].

In the following sections, a number of model extensions is proposed to overcome this weather related bias.

Convection and Infiltration

Wind has two main effects on the heat consumption. Increased wind will increase the external convection on the building facade and the infiltration rate — i.e. the unintended air exchange between inside and outside. Moreover, the infiltration dependence on both wind speed and thermal stack effects. The literature provide several empirical formulas for describing the convection and infiltration, see for example [10,20].

For simple steady state models like those presented here, we aim for a simplified formulation for the combined wind effect on the heat consumption. Hence, we propose that the convection and infiltration due to increased wind speed can be treated as proportional to the temperature difference between in- and outside. Equation (5) can then be extended to:

$$\begin{aligned}\Phi_{\text{heat}} &= (\text{UA}_0 + W_\text{s}\,\text{UA}_\text{W})\,(T_\text{i} - T_\text{a}) - \Phi_\text{x} + \varepsilon \\ &= (\text{UA}_0 + W_\text{s}\,\text{UA}_\text{W})\,(T_\text{i} - \Phi_\text{x}(\text{UA}_0 + W_\text{s}\,\text{UA}_\text{W})^{-1} - T_\text{a}) + \varepsilon\,,\end{aligned} \tag{8}$$

where W_s is the wind speed, UA_0 is the heat loss coefficient for wind speeds equal to zero, and UA_W is the additional heat loss due to increments in the wind speed. As seen in the Equation (8), the base temperature is now $T_\text{i} - \Phi_\text{x}(\text{UA}_0 + W_\text{s}\,\text{UA}_\text{W})^{-1}$. In order to keep the model simple, the base temperature is instead kept constant as in Equation (6), rather than wind speed dependent, as in Equation (9),:

$$\textbf{M2:} \qquad \Phi_{\text{heat}} = (\text{UA}_0 + W_\text{s}\,\text{UA}_\text{W})\,(T_{\text{b}_0} - T_\text{a}) + \varepsilon\,, \tag{9}$$

which indirectly mean that Φ_x is equal to $(\text{UA}_0 + W_\text{s}\,\text{UA}_\text{W})\,(T_\text{i} - T_{\text{b}_0})$.

Solar Radiation

The solar gain Φ_sol can be characterised by the product of global solar irradiation I_g and a constant solar transmission coefficient gA. The previous model from Equation (9) can therefore be extended with an explicit solar gain term:

$$\begin{aligned}\textbf{M3:} \qquad \Phi_{\text{heat}} &= (\text{UA}_0 + W_\text{s}\,\text{UA}_\text{W})\,(T_{\text{b}_0} - T_\text{a}) - \text{gA}\,I_\text{g} + \varepsilon \\ &= (\text{UA}_0 + W_\text{s}\,\text{UA}_\text{W})\,(T_{\text{b}_0} - T_\text{a}) - \Phi_\text{sol} + \varepsilon\,.\end{aligned} \tag{10}$$

As mentioned before, Φ_x (which is embedded in $T_{\text{b}_0} = T_\text{i} - \Phi_\text{x}\text{UA}^{-1}$) represents the remaining heat gains and losses which are not explicitly modelled. Φ_x is therefore decreased compared to the previous models, as the solar gain now is modelled explicitly as $\text{gA}\,I_\text{g}$.

If the gA value depend on e.g. time-of-year, the model can further be extended by modelling the functional relation between that and the solar gain similar to what is shown in [21]. That is however out of scope in this article.

Thermal Radiation

Another contribution to the total heat loss is the long wave radiation between the building surface and its surroundings.

The long wave radiation heat loss to the sky Φ_rad can be formulated as:

$$\Phi_\text{rad} = \varepsilon A\,\sigma(T_\text{sky}^4 - T_\text{surf}^4)\,, \tag{11}$$

where εA is the emissivity of the building surfaces multiplied with projected exposed surface area, and σ is the Stefan–Boltzmann constant. T_sky and T_surf are the temperatures of the sky dome and of the building surface in kelvin, respectively [22].

In order to keep the model simple and applicable, the unknown temperature of the outer envelope of the building is assumed to be equal to the ambient outdoor temperature T_a.

Variations between T_surf and T_a, as well as T_surf and the actual surrounding radiant temperature are assumed constant.

The full model is now:

$$\begin{aligned} \textbf{M4:} \qquad \Phi_{\text{heat}} &= (\text{UA}_0 + W_\text{s}\,\text{UA}_\text{W})\,(T_{\text{b}_0} - T_\text{a}) - \Phi_\text{sol} + \varepsilon A\,\sigma(T_\text{sky}^4 - T_\text{surf}^4) + \varepsilon \\ &= (\text{UA}_0 + W_\text{s}\,\text{UA}_\text{W})\,(T_{\text{b}_0} - T_\text{a}) - \Phi_\text{sol} + \Phi_\text{rad} + \varepsilon\,. \end{aligned} \tag{12}$$

Notice that εA is a parameter while ε is the noise term. They are therefore not related.

2.2. Smooth maximum with LogSumExp

In the following sections we explain the theory behind the smooth maximum function, *LogSumExp* as an alternative to the model in Equation (1), where $f(\cdot)$ is a model for the weather dependent heat consumption outlined above and $g(\cdot)$ is the weather independent heat consumption which in this case is as in Equation (2). Furthermore, we show how it can be applied, and how we use of the LogSumExp function to quantify the transition between two functions.

2.2.1. Definition and Intuition of LogSumExp

The LogSumExp (LSE) function is a smooth maximum approximation function often used in machine learning and as activation function in artificial neural networks. It is defined as:

$$\begin{aligned} \text{LSE}(\boldsymbol{y}) &= \text{LSE}(y_1, \ldots, y_n) \\ &= \log\left[\exp(y_1) + \cdots + \exp(y_n)\right]\,. \end{aligned} \tag{13}$$

In essence, the inner part of the log operator in Equation (13) amplifies the differences between the individual values of $\boldsymbol{y}$ exponentially. For a large value of $\boldsymbol{y}$, such as $y_1 \gg y_2, ..., y_n$, we see that $\sum_{i=1}^{n} \exp(y_i) \approx \exp(y_1)$. In order to get back to the original domain we take the logarithm of the sum. In conclusion it can be said that Equation (13) approximates the maximum of the values in $\boldsymbol{y}$:

$$\text{LSE}(y_1, \ldots, y_n) \approx \max(y_1, \ldots, y_n)\,. \tag{14}$$

2.2.2. Derivatives

By applying the chain rule for differentiation, the partial derivative of Equation (13) can be shown to be the *softmax* function,

$$\frac{\partial}{\partial y_i}\text{LSE}(y_1, \ldots, y_n) = \frac{\exp(y_i)}{\sum_{j=1}^{n}\exp(y_j)}\,, \tag{15}$$

which essentially is the multivariate version of the logistic function [23]. With $n = 2$ and by differentiating w.r.t. y_1 we get:

$$\frac{\partial}{\partial y_1}\text{LSE}(y_1, y_2) = \frac{\exp(y_1)}{\sum_{j=1}^{2}\exp(y_j)}\,. \tag{16}$$

By further defining $y_1 = x$ and $y_2 = 0$, the standard logistic function is obtained:

$$\frac{\partial}{\partial x}\text{LSE}(x, 0) = \underbrace{\frac{\exp(x)}{\exp(x) + 1}}_{\substack{\text{The standard} \\ \text{logistic function}}}\,. \tag{17}$$

The complimentary logistic function is obtained by differentiating Equation (15) w.r.t. $y_2 = 0$.

2.2.3. LogSumExp as a Function of $g(x)$ and $f(x)$

For y_1 and y_2 being the two functions $f(x) > g(x)$ for $x \to -\infty$ of zeroth or first order, and by introducing the logistic growth rate k, Equation (16) can be rewritten as:

$$\frac{\partial}{\partial f(x)}\mathrm{LSE}(f(x), g(x)) = \underbrace{f'(x)\frac{\exp(f(x)\,k)}{\exp(f(x)\,k) + \exp(g(x)\,k)}}_{\text{The logistic function}}\,. \tag{18}$$

The indefinite integral of Equation (18) shown in (19), can now approximate the model in Equation (1) with a smooth transition between the two functions described by the hyperparameter k:

$$\mathrm{LSE}(f(x), g(x)) = \underbrace{\log\left[\exp(f(x)\,k) + \exp(g(x)\,k)\right]k^{-1}}_{\text{Smooth approximation of } \max((f(x),\, g(x))} \tag{19}$$

The logistic function in Equation (18) is monotonically increasing and describes the smooth transition between the slopes of $f(x)$ and $g(x)$. Hence, Equation (18) approaches the numeric larger slope of the two as $x \to -\infty$, and the smaller slope as $x \to \infty$.

2.2.4. Transition Interval

As Equation (19) only approach $f(x)$ and $g(x)$ asymptotically, it is not possible to define a finite transition interval between the two functions.

Instead, the transition interval can be defined as the interval of x for which Equation (18) is between $p \cdot 100\,\%$ and $(1-p) \cdot 100\,\%$ of the right-hand side asymptotic limit of the function, where $p \in [0, 1]$.

The transition interval can be found by solving for x in Equation (20) where $f(x) > g(x)$ for $x \to -\infty$:

$$lb < f'(x)\,\frac{\exp(f(x)\,k)}{\exp(f(x)\,k) + \exp(g(x)\,k)} < ub\,, \tag{20}$$

where lb and ub is:

$$lb = f'(x) + p(g'(x) - f'(x))\,, \tag{21}$$

$$ub = f'(x) + (1-p)(g'(x) - f'(x))\,. \tag{22}$$

In this study the values of p is fixed as $p = 0.1$

Figure 1 summarises the concepts explained in Section 2.2. The upper plot shows the logistic function associated with the smooth maximum function shown in the lower plot. In the specific case p in Equation (21) and (22) is chosen to be 0.1, $f(x) = -x$, $g(x) = 0$, and $k = 1$. The red part of the curves shows the transition between $f(x)$ and $g(x)$, and $f'(x)$ and $g'(x)$ in the lower and upper plot, respectively.

2.3. Unmodelled Heat Gains

Notice that in the following there will not be distinguished between the constant UA value in e.g. Equation (3) and the wind dependent UA value as in Equation (9). All UA values will from now on be stated as $\mathrm{UA}(\cdot)$, where $\cdot$ is the wind speed which may or may not be specified.

So far the models considered have treated the sum of a number of heat gains and losses as the constant Φ_x. This is of course a crude simplification. However, instead of modelling the remaining heat gains explicitly, we propose a method where the heat gains are derived from the time ordered model residuals e_t.

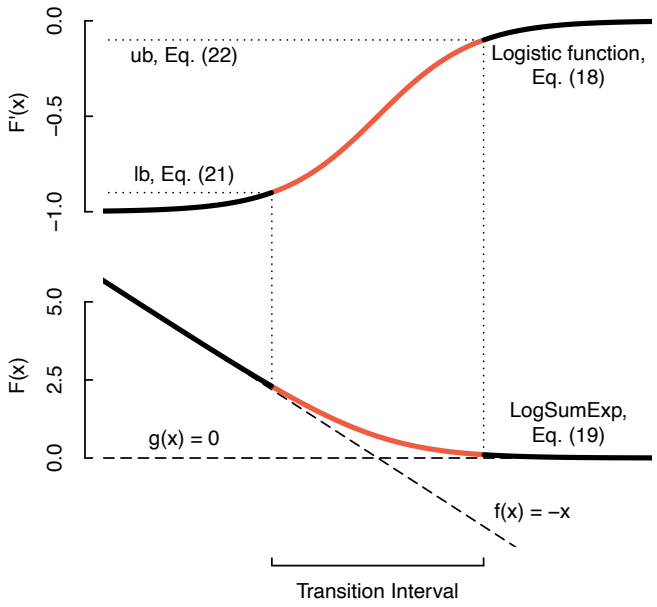

Figure 1. Conceptual diagram of transition interval.

The assumption here is that the thermal dynamics (i.e. the absorption and release of heat in the thermal mass) are filtered out by using daily average values. Furthermore, latent heat exchange and heat exchange to the ground and to adjacent rooms located outside the thermal zone are assumed to be neglectable. Consequently, Φ_{x} is related to the building usage and therefore mainly the sum of ventilation losses and internal heat gains, such as electrical power usage and and the heat produced by the occupants through metabolism, domestic hot water usage and cooking.

From the auto-correlation in Figure 4 in Section 4.2 it is clear that the day-to-day residuals are correlated. Given the above assumptions, it can be concluded that $T_{\mathrm{b}_0} = T_{\mathrm{i}} - \Phi_{\mathrm{x}}\mathrm{UA}^{-1}$ is not constant.

To model the variation of T_{b_0} over time t, we can set up the following model:

$$T_{\mathrm{b}_0}(t) = T_{\mathrm{i}} - \frac{\Phi_{\mathrm{x}} + \Delta\Phi_{\mathrm{x}}(t)}{\mathrm{UA}} + \varepsilon_t = T_{\mathrm{i}} - \frac{\Phi_{\mathrm{x}}(t)}{\mathrm{UA}} + \varepsilon_t\,, \tag{23}$$

where $\Delta\Phi_{\mathrm{x}}(t)$ is the time varying heat contribution to maintain the thermal balance.

The residuals e_t from the earlier stated heat demand models can now be described as:

$$e_t = \Delta\Phi_{\mathrm{x}}(t) + \varepsilon_t\,. \tag{24}$$

An estimate of the underlying function of e_t — namely $\Delta\Phi_{\mathrm{x}}(t)$ — can be found by kernel estimation. Kernel estimation is a non-parametric method used to determine hidden non-linear functional relations. The kernel estimate is shown to be equal to the locally weighted least squares estimate in [24]. Hence, the time varying model parameters $\hat{\beta}(t)$ is obtained by:

$$\hat{\beta}(t) = \arg\min_{\beta} \frac{1}{N}\sum_{i=1}^{N} w_i(t)(Y_i - X_i\,\beta)^2\,. \tag{25}$$

In the equation above i refers to the i^{th} vector element or matrix row, and $w_i(t)$ is the kernel weights:

$$w_i(t) = \frac{k[h^{-1}(t_i - t)]}{\frac{1}{N}\sum_{i=1}^{N} k[h^{-1}(t_i - t)]}\,, \tag{26}$$

where k is the Epanechnikov kernel [25] with bandwidth h. The bandwidth is found by leave-one-out cross validation as described in [24].

Substituting Y with the model residuals e_t we obtain an estimate of $\Delta\Phi_{\mathrm{x}}(t)$, and by inserting in Equation (23), a corrected time varying estimate of the base temperature $T_{\mathrm{b}_0}(t)$ is obtained.

2.3.1. Thermal Performance Evaluation

It is clear from Equation (23) that it is not possible to estimate the indoor temperature T_{i} and the heat gains $\Phi_{\mathrm{x}} + \Delta\Phi_{\mathrm{x}}(t)$ separately. However, to evaluate a building's thermal performance with a given design temperature, the resulting heat gain related to the building use and its occupants can be estimated by rearranging Equation (23):

$$\Phi_{\mathrm{x}}(t) = \Phi_{\mathrm{x}} + \Delta\Phi_{\mathrm{x}}(t) = \mathrm{UA}(\cdot)\left(T_{\mathrm{i}} - T_{\mathrm{b}_0}(t)\right). \tag{27}$$

The estimate of $\Phi_{\mathrm{x}}(t)$ can now be compared with the sum of heat gains related to metabolism and electricity consumption; and ventilation losses from an energy performance calculation.

It should, however, be noticed that the results only are valid for days with weather dependent heat consumption.

3. Experimental Setup

3.1. Data

16 random selected houses in Sønderborg in Southern Denmark have been used as demonstration case. The built year of the houses ranges from 1937 to 1996, and the heated floor area from 86 to 173 m^2. All houses are heated by district heating only, i.e. there is no additional and unmeasured heat sources in the houses except from internal gains. Finally, four of the houses have night-setback on the temperature set point.

The only measurement used from the houses is the total heat consumption provided by Sønderborg Fjernvarme — a consumer owned district heating company in Sønderborg. In addition, outdoor temperature, wind speed and global solar irradiation is measured at the district heating plant which is within 10 km of the houses.

The sky temperature estimates are obtain from the freely available reanalysis data set *ERA5-Land* provided by the Copernicus Climate Change Service [26]. The full documentation on the ERA5-Land can be found in [27].

The heat consumption were measured every 10^{th} minute, and the weather data is obtained for every hour. In the analyses, only daily averaged values are used from a period from January 2, 2009 to May 1, 2011.

The original heat consumption data consists of both domestic hot water consumption and space heating. Before the analyses in this article the hot water consumption has been separated from the space heating by means of kernel smoothing as described and done in [28]. Hence, the estimated space hating has been used, rather than the total heat consumption.

3.2. Software

Each of the models tested has been set up in *Template Model Builder (TMB)* (version 1.7.16) [29] fitted with the global optimisation algorithm, *Multi-Level Single-Linkage (MLSL)*, along side with the local optimiser *Limited-memory BFGS*, which is implemented in the *R* package for nonlinear optimisation, *R Interface to NLopt (nloptr)* (version 1.2.1) [30]. Version 3.5.1 of *R* [31] has been used throughout the study.

Despite the choice of software in this article, the models can be estimated by using a broad range of optimisers and softwares.

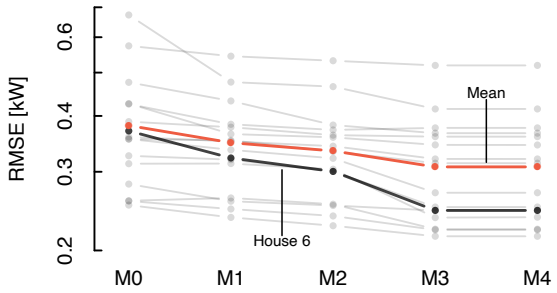

Figure 2. Slope chart of root mean squared error (RMSE) of the seven models test on 16 houses. The RMSE is based on a 20 % cross validation data set. Notice that the logarithmic scale is used meaning that the slopes between the points indicates the relative change in RMSE.

4. Results

In Sections 2.1.1 and 2.1.2 a series of model candidates for the weather dependent heat consumption were presented. The model for the weather independent heat consumption were defined in Equation (2). In Table 1 each model tested in this section is outlined and references to the specific equations are stated.

Table 1. Model name overview and equation references. The bullet (•) indicates that the given inputs are included in the specific model. Equations numbers under $f(\cdot)$ and $g(\cdot)$ refers to which models that have been used in Equation (19). Model M0 distinguish itself from the remaining models, as the base temperature T_b is fixed at 17 °C.

Model	Input				Eq.	
	T_a	W_s	I_g	T_{sky}	$f(\cdot)$	$g(\cdot)$
M0	•	–	–	–	(7)	
M1	•	–	–	–	(5)	
M2	•	•	–	–	(9)	(2)
M3	•	•	•	–	(10)	
M4	•	•	•	•	(12)	

4.1. Model Validation

All models were fitted and validated by means of a five-fold cross validation where the hyperparameter k in Equation (19) was tuned. The training and validation data was splitted randomly in a 80/20 ratio. The root mean squared error (RMSE) on the validation set is shown in the slope chart in Figure 2, and each of the model names on the x-axis is found in Table 1.

The corresponding RMSE for each house is given as a grey or black dot. The red line indicates the mean RMSE across all of the houses and the black indicates House 6 which we will study in details within this work. Notice that the RMSE is plotted on a logarithmic scale, i.e. the slopes of the lines between the points express the relative change in model error.

Extending the very simple model, M0, with an extra degree of freedom (T_{b_0}) shows a very clear general model improvement as expected.

Model M2 and M3 are the model extensions which include wind and solar irradiation, respectively. For both models we see a decrease of the RMSE meaning that both wind and solar irradiation has a significant effect on the heat consumption. However, including solar gain has the largest positive effect on the model errors across all model extensions when the models are evaluated in a successive manner. This is also referred to as type I partition [32].

Finally, the heat loss related to long wave radiation (M4) does not affect any of the model predictions. The parameter εA in Equation (11) is simply estimated as such a low and insignificant value that it does not affect the RMSE.

4.2. Residual Analysis

In Figure 3 the residual analysis plot for House 6 is shown. Each row consists of three plots. 1) Model residuals of a given model, 2) the fit of its model extension, and 3) the residuals after the model extension.

In the top-left plot in Figure 3 the residuals are shown for model M0. From the plot, a series of systematic errors around 8.0 to 17 °C, and a negative trend in the residuals is seen.

The negative trend in the residuals is diminished after the M0 model is extended to the M1 model (top-right). However, the systematic errors are still present. The systematic error means that model M0 and M1 are not capable of describing the days without space heating in the transition period.

Lastly, in the residuals for temperatures below 8.0 °C a slight concave trend is seen for both M0 and M1. These two patterns indicate that the heat consumption is not only a function of the outdoor temperature.

In the second row of plots to the left, the residuals of M1 as a function of the wind speed are shown. The red dashed line indicates that the M1 model tends to underestimate the heat demand for wind speeds above ca. 2.5 m/s and overestimate the the heat demand for wind speeds below 2.5 m/s. Modelling the wind dependent heat loss as in M2 makes this tendency disappear.

In the third row of plots to the left, the model residuals of M2 are compared to the global solar irradiation. In this case we see a negative linear trend in the residuals. This means that for days with high levels of solar irradiation the model overestimates the the space heating demand — simply because the model does not include the effect of solar gain. After implementing the solar gain in model M3 the residuals flattens out.

It can be seen that the solar irradiation explains a lot of the variance in the transition period around 5 to 15 °C (third row, second column). In contrast to this, we see that the wind speed in the M2 model (second row, second column) mainly explains the variance in the lower outdoor temperature range. As the heat loss due to wind is proportional to the outdoor temperature, and due the fact that the daily mean outdoor temperature is correlated with the solar irradiation, this is a reasonable result.

Additionally, Figure 3 shows the residuals of the M3 model as a function of the outdoor temperature in row four, column three. Compared to the residuals of the previous models, we now see that the systematic error in the transition period disappears. Only a changing variance between weather dependent and weather independent days are seen. Hence, the solar gain is the main reason for the heating system turning on and off in the transition period.

In the last row of plots the effect of long wave radiation between the building and its surroundings is shown. As expected, based on the unaffected RMSE in Figure 2, the residuals remains unaffected.

Finally, the residuals as a function of time is shown in Figure 4 for model M3. A clear auto-correlation is found, and as argued for in Section 2.3, this is likely due to time correlated occupants behaviour. The time dependence is further modelled as described in Section 2.3 and is shown in Figure 5.

4.3. Parameter Sensitivity

We demonstrated that the model including outdoor temperature, global solar irradiation and wind speed can describe the actual energy use of the buildings rather accurate. In this section, we will take a look at how two of the common parameters across all models (UA$(\cdot)$ and the base temperature T_{b_0}) are affected by the different model formulations.

In Figure 6 (top) the estimated UA$(\overline{W}_s)$ value for each house and model is shown. The UA$(\overline{W}_s)$ value is the UA value under influence of the mean wind speed (2.5 m/s) observed in the measurement period.

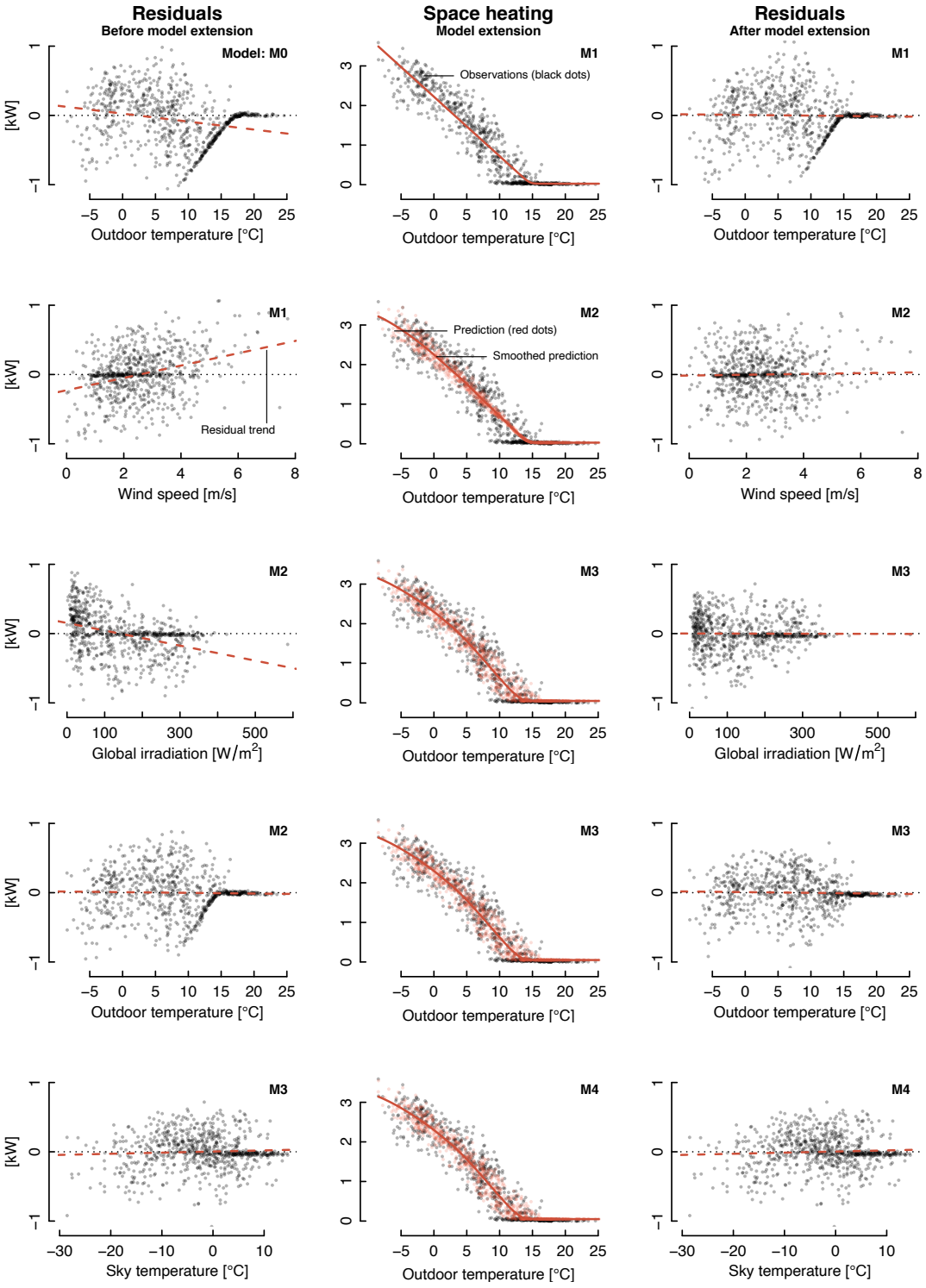

Figure 3. Forward model extension for House 6. The figure shows the effect of a particular model extension, starting with the model residuals of Model M0 in the top-left corner. The figure is read row-wise and each row represents a model extension. The models names in the top-left corner of the individual plot can be found in Table 1. Notice that the x-axes of the residuals plots change depending on the model extension.

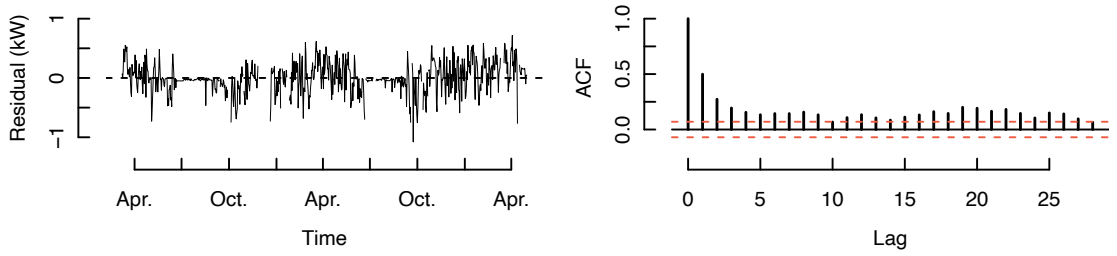

Figure 4. Analyses plots of auto-correlation in residuals of model M3 on House 6. The red dashed lines in the ACF plot indicates the 95 % confidence limits.

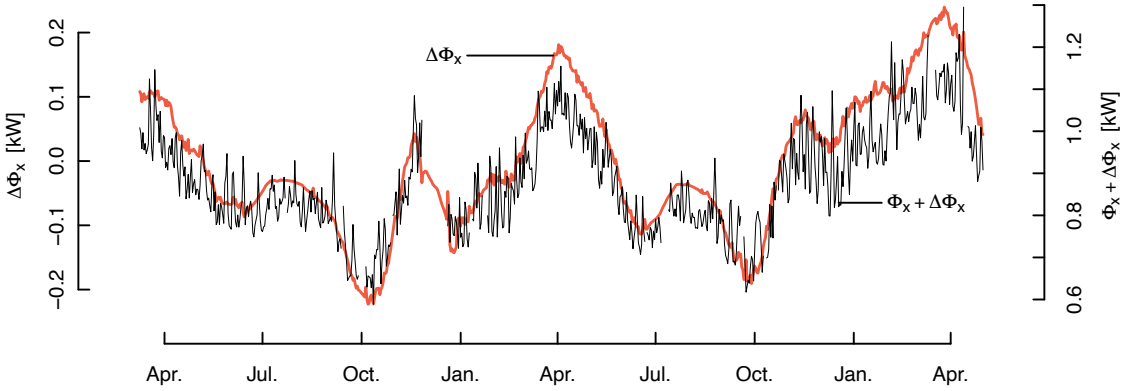

Figure 5. Kernel estimation of $\Delta\Phi_x(t)$ (red line) in Equation (23) and $\Phi_x + \Delta\Phi_x(t)$ (black line) in Equation (27) provided an indoor temperature of 20 °C.

Going from model M0 to M1 gives rise to both increments and reductions in the estimate of $\mathrm{UA}(\overline{W}_s)$ and T_{b_0}. It is therefore not possible to state any general bias by fixing T_{b_0}; it depends on the building and the occupants.

Including the effects of the wind speed as done in M2 increase the estimated $\mathrm{UA}(\overline{W}_s)$ value significantly and consistently for all houses. The effect on the base temperature T_{b_0} is more moderate and reduce it slightly.

On the other hand, including solar gain in model M3 creates a small decrease in the $\mathrm{UA}(\overline{W}_s)$ value, as well as in the base temperature.

The introduction of long wave radiation is not affecting $\mathrm{UA}(\overline{W}_s)$ nor T_{b_0}, and is totally irrelevant for the heat consumption as it is implemented in the M4 model.

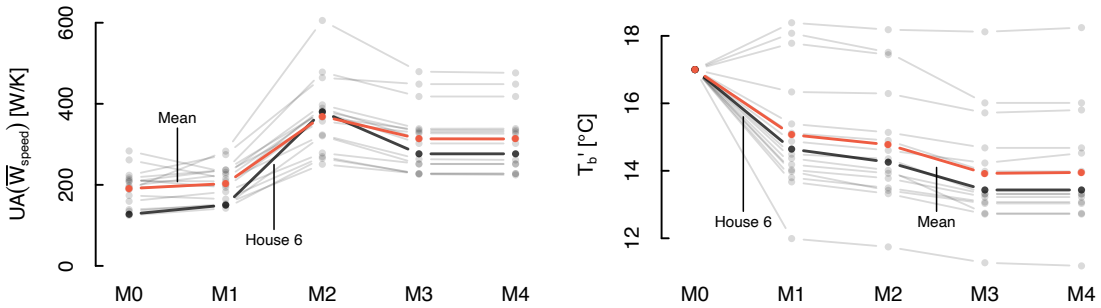

Figure 6. Slope chart of $\mathrm{UA}(\overline{W}_s)$ value and base temperature T_{b_0} of the six models on 16 different houses. The $\mathrm{UA}(\overline{W}_s)$ values are the heat loss under wind speed conditions corresponding to the mean wind speed observed in the measurement period (2.5 m/s).

Going from the simplest reasonable model (M1) to the best model (M3) gives an average change in the estimated $\mathrm{UA}(\overline{W}_\mathrm{s})$ value of $+54\,\%$ for all the 16 considered buildings, with the smallest and largest change of $+26\,\%$ and $+84\,\%$, respectively.

The base temperature changes in average from M1 to M3 by $-8\,\%$, with the smallest and largest change of $-1\,\%$ and $-11\,\%$, respectively.

4.4. Thermal Performance Characterisation

Based on the finding in the previous sections the M3 model has been chosen as the most general and best performing model. In this section we will use that model and estimate the key thermal performance parameters for all of the 16 different houses.

Table 2. Estimated performance parameters for 16 houses in Denmark. The number in parentheses states the standard error of the parameters. UA_0 is the heat loss coefficient under wind free conditions, and UA_W is the wind dependent increment in the UA value. The column for $T_\mathrm{transition}$ states the range of outdoor temperatures at which the building is in transition from heating to non-heating period, given no wind and solar irradiation.

House	Year	Floor area [m^2]	U_0 [$\mathrm{W/(K\,m^2)}$]	UA_0 [W/K]	UA_W [W/K per m/s]	gA [m^2]	Φ_0 [W]	T_b [°C]	$T_\mathrm{transition}$ [°C]	$\Phi_\mathrm{x}(t)$ [W]	$\sigma_{\Phi_\mathrm{x}(t)}$ [W]
1	1970	151	1.25 (0.03) *	189 (4) *	58 (7) *	2.5 (0.3) *	676 (84) *	16.5 (0.5)	12.1 – 21.0	702	157
2	1969	163	1.25 (0.02) *	204 (4) *	39 (8) *	3.7 (0.3) *	340 (47) *	14.2 (0.4) *	9.5 – 18.9	1246	194
3	1963	140	1.28 (0.02) *	179 (2) *	32 (5) *	2.5 (0.1) *	141 (30) *	15.7 (0.2) *	11.9 – 19.5	810	103
4	1952	86	1.45 (0.03) *	125 (2) *	41 (5) *	1.5 (0.2) *	215 (19) *	12.8 (0.3) *	10.2 – 15.4	971	118
5	1966	111	1.54 (0.03) *	171 (3) *	61 (7) *	1.6 (0.2) *	110 (63)	16.6 (0.3)	9.6 – 23.6	643	155
6	1963	119	0.97 (0.02) *	115 (2) *	65 (6) *	2.8 (0.2) *	47 (19) *	13.3 (0.3) *	10.2 – 16.4	880	129
7	1947	119	2.17 (0.04) *	258 (5) *	72 (13) *	1.2 (0.4) *	6 (50)	13.5 (0.3) *	6.9 – 20.0	1810	243
8	1965	160	1.24 (0.04) *	199 (6) *	57 (14) *	2.2 (0.4) *	376 (45) *	12.6 (0.5) *	8.9 – 16.4	1569	258
9	1965	173	1.21 (0.02) *	210 (3) *	42 (6) *	1.2 (0.2) *	523 (62) *	18.2 (0.3) *	15.8 – 20.6	389	275
10	1996	135	0.90 (0.02) *	121 (2) *	51 (6) *	2.5 (0.2) *	106 (25) *	14.1 (0.4) *	10.2 – 18.0	786	193
11	1966	122	1.09 (0.04) *	133 (4) *	31 (11) *	1.2 (0.3) *	108 (46) *	14.7 (0.5) *	10.5 – 18.9	751	96
12	1975	136	1.05 (0.02) *	143 (2) *	31 (4) *	1.9 (0.1) *	644 (17) *	13.4 (0.3) *	11.3 – 15.4	1001	94
13	1937	86	2.67 (0.06) *	229 (5) *	92 (14) *	4.4 (0.4) *	45 (31)	11.2 (0.3) *	7.6 – 14.8	2227	431
14	1965	123	1.36 (0.02) *	167 (2) *	57 (6) *	2.4 (0.2) *	356 (22) *	14.1 (0.3) *	11.8 – 16.4	1068	203
15	1953	127	1.65 (0.03) *	209 (4) *	80 (10) *	3.1 (0.3) *	166 (35) *	13.0 (0.3) *	7.0 – 19.1	1593	210
16	1967	137	1.22 (0.02) *	167 (3) *	34 (7) *	1.3 (0.2) *	193 (26) *	13.5 (0.3) *	8.1 – 18.9	1137	143
H_0 :			$\mathrm{U}_0 = 0$	$\mathrm{UA}_0 = 0$	$\mathrm{UA}_\mathrm{W} = 0$	$\mathrm{gA} = 0$	$\Phi_0 = 0$	$T_\mathrm{b} = 17$			

Significance code '*': p-value < 0.05

As an example, we see that House 6 has a UA_0 value of 115 W/K in Table 2. The UA_0 value represents the heat loss coefficient under weather conditions with a wind speed of 0 m/s. Even though House 6 has the smallest UA_0 value estimated, the heat loss related to convection and infiltration (UA_W) is the fourth highest among the 16 houses. This indicates that House 6 house potentially has some serious issues with air leakages.

Looking at all the estimated UA_W values all houses seems to be significantly affected by the wind. Furthermore, it is reasonable to believe that a high standard error (e.g. House 8) is a result of different wind effect from different wind directions, or by the fact that people often open and close the windows. Both scenarios will result in a high standard error.

The base heat load Φ_0 is the most varying parameter from house to house. If the heat consumption used to train the model only accounts for space heating this value tells if there is an unreasonable high base load. If it includes on the other hand the heating energy for hot water consumption as well, and the hot water consumption is known, a reasonable estimate of the base heat losses can be estimated.

T_b tells at which outdoor temperature the house is in thermal balance, given the average of the other explanatory variables. Notice that the base temperature in $f(\cdot)$ is the base temperature under the assumption that the $\Phi_0 = 0$. T_b which is presented in Table 2 is the actual base temperature under average weather conditions. The base temperature varies from 11.2 °C to 18.2 °C. A low T_{b_0} can — as stated in the Section 2.1.1 — mean three things. Either the internal gains are high, or the

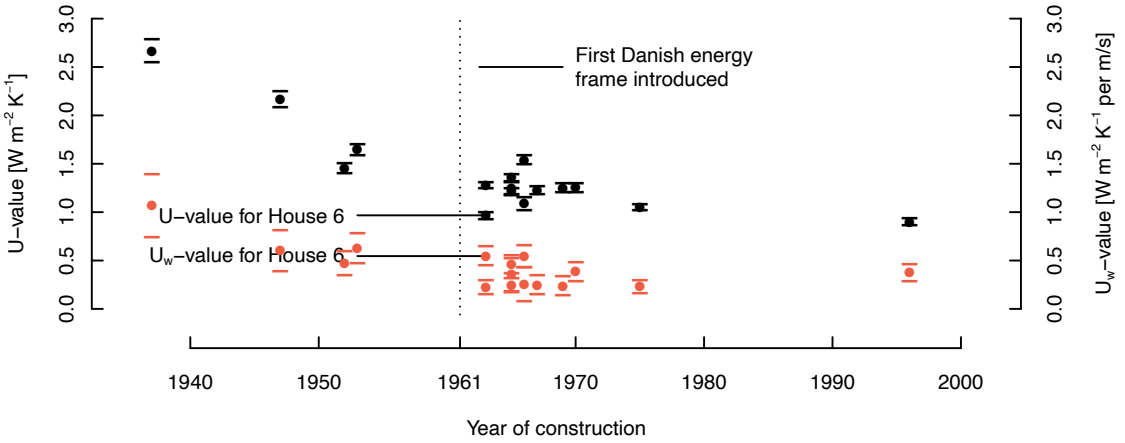

Figure 7. Illustration of UA and UA(W_s) per heated floor area as function of construction year. The black dots (left axis) show a clear increment in insulation level as the year of construction becomes more recent. The red dots (right axis) show the sensitivity to wind. I.e. the level of air leakage.

indoor temperature is low, or the house is poorly insulated, or some sort of combination. The opposite it true for a high value of T_{b_0}.

As the heat loss of the houses are based on daily averages input values, but do not know the indoor temperature and the heat gains related to the building use, we are not able to deduct the two latter. However, fixing the indoor temperature to e.g. the design temperature, we can estimate the remaining unobserved heat gains needed to obtain the design temperature. This is described in Section 2.3. The mean ($\Phi_x(t)$) and standard deviation ($\sigma_{\Phi_x(t)}$) of the stochastic process $\Phi_x(t)$ is stated in the two last columns of Table 2.

The transition period $T_{\text{transition}}$ also shows varying spans over the considered buildings. The spans indicate, indirectly, to which extend the heating system is affected by the weather. I.e. a narrow band tells us that the building or the heating system is insensitive to rapid changing weather conditions, and visa versa.

In Figure 7 the estimated U_0 value and the wind dependent increment of the U value (UA_W per m^2 heated floor area) are plotted as a function of the year of construction. The bars around the dots indicates a 95 % confidence interval of the estimate.

Regarding both U_0 and U_W the Figure shows that there is a negative trend in the estimates, which indicates that the thermal performance has increased during the years. Despite the sample is rather small, it seems like there is a significant difference between houses build before 1961, which is the year where the first energy frame came in force in Denmark, and after.

Even though the negative trend is the same for the U_0 and the U_W values, the reduction of U_0 for the individual houses does not necessarily lead to a reduction in U_W. One example of this is shown for House 6, which has the lowest U_0 value of the houses build between 1961 and 1980, but the one of the highest U_W values in the same cluster.

5. Discussion

The key to minimise the model's uncertainty is to model as many heat gains as possible. Hence, the inclusion of the readings of the electricity usage will improve the model accuracy further. Also readings of the heat consumption only would lower the uncertainty: At the same time, the readings from domestic hot water energy usage could be used an extra source of heat gain.

However, for estimation of the two most important thermal performance parameters in this paper — the UA and UA(W_s) value — the above mentioned missing heat gains affect the estimates to a minor extend, as long as the heat gains are of approximately equal magnitude for all weather conditions. The reason for this is that such heat gains are additive terms in the model formulations,

and therefore do not influence the slope of the models. Therefore, to keep the models flexible and scalable, as few as possible measurements are preferred, as long as they do not introduce a serious bias to the estimated model parameters.

In Section 2.3 we have shown how it is possible to model the residuals and estimate the required additional heat gain over time to obtain a specific indoor temperature. In Table 2, the mean and the standard deviation of the heat gain to maintain an indoor temperature of 20 °C is given for all 16 houses.

From the investigation of the residuals of model M3 (Figure 3) there is no clear sign for any missing effects that are a function of outdoor temperature, wind speed, global solar irradiation or long wave radiation. However, there is a correlation over time. Consequently, we have some time dependent dynamics which are not captured by the model.

For a sample rate of one day or longer, the dynamics related to the heat capacities of the building should be averaged sufficiently out even though the long time constants often exceeds 24 h [10]. We can hence believe that the dynamics (which create the auto-correlation) consist of two main effects: changing temperature set-points and ventilation rates. I.e. both effects which are directly related to the building use (occupant behaviour).

However, as a further development of the proposed model, the correlation of the residuals should be checked, and the heat capacity should eventually be modelled. One approach to this can be found in [8].

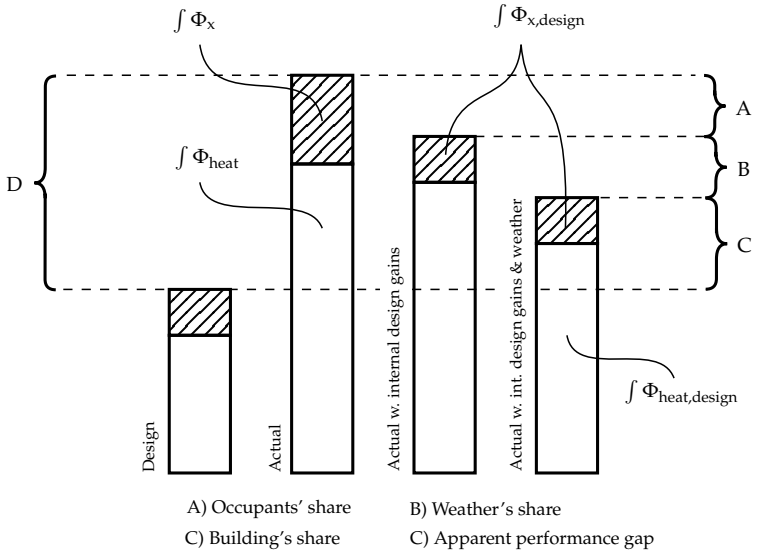

Figure 8. Conceptual illustration of performance gap and three causes of the discrepancy. Point A, B and C are further explained in the following list.

In general, to document the actual energy performance of a building under usage (including the way the occupants affect this performance), a few design parameters used as input for the calculation of the building energy performance are required. Those include: the weather data (e.g. the design reference year (DRY) weather data), the design indoor temperature, internal heat gains, and ventilation losses. The actual energy performance evaluation can hence be done in several ways, to illuminate the different reasons causing the discrepancy between expected and realised energy use. In Figure 8 we illustrate the apparent performance gap and the three possible causes of discrepancy:

A *Unintended occupants' related differences* in the energy consumption can be estimated as the difference between the estimated user related heat gain $\Phi_x(t)$, and:

$$\Phi_{x,design}(t) = UA\,(T_{i,design} - T_{b_0}(t)) + \Phi_{vent,design} + \Phi_{int,design}\,, \tag{28}$$

where the subscript *design* refers to design values, and $\Phi_{\text{vent,design}}$ and $\Phi_{\text{int,design}}$ is the intended design ventilation loss, and the intended internal heat gain, respectively.

If $\Phi_{\text{x}}(t) - \Phi_{\text{x,design}}(t) < 0$ the ventilation loss is higher than expected in the design phase; the internal heat gains are lower than expected in the design phase; the indoor temperature is higher than the design temperature, or a combination. On the other hand, if $\Phi_{\text{x}}(t) - \Phi_{\text{x,design}}(t) > 0$ the ventilation losses, the indoor temperature or a combination is lower, or the internal heat gains are higher than assumed in the design phase.

B *Weather related differences* in the energy use can be estimated by comparing the predicted energy use with the actual weather conditions, and the predicted energy use with the outdoor temperature, wind speed, and global solar irradiation used in the design phase. The model in (19) is used for prediction, where f and g is stated in (10) and (2), respectively.

C *Building envelope related differences* in the energy use can be estimated as the difference between the predicted energy use (obtained using (19), (10) and (2)) and the weather and occupants corrected energy use obtained from point A and B, above.

This kind of documentation can be valuable in building energy screenings, as those mentioned in the EPBD [2].

6. Conclusion

This study has shown that the typical linear energy signature methods fund in literature can be significantly improved by applying a non-linear and smooth model formulation.

Only daily average heat consumption and measurements of outdoor temperature, wind speed and global solar irradiation were used as model input. From that, several measures for the thermal building performance were estimated, including: heat loss coefficients, heat losses related to convection and infiltration, solar transmittance, base heat load and transition periods. The use of so few variables as input makes the proposed method highly scalable and easily automatised. In the present study all of the 16 random selected houses were evaluated automatically.

The proposed model showed that it is capable of describing the variance and non-linearities in the heat consumption data to a much greater extend than a simple energy signature with only the outdoor temperature as the explanatory variable.

Based on the model residuals, the heat gains related to the building usage were estimated by means of non-parametric kernel estimation methods. The estimation of building use related heat consumption opens up for detailed building performance documentation and screening as outlined in the current energy performance of buildings directive (EPBD) [2]. For example, the impact on energy use related to weather, building use, and the building envelope itself can be estimated separately.

The novel heat demand formulation using a smooth maximum function (LogSumExp) does not only provide a way of estimating the transition period where the energy consumption goes from weather dependent to weather independent. It also make it possible to make more advances model — such as state space models with hidden states — as the model is fully differentiable contrary to the traditional energy signature model.

In the future three main issues should be addressed:

1. In the present paper, only 24 hour average values were used with the argument that the effects of the heat capacities were averaged out as stated in [10]. Several tests on parameter sensitivity could be done with input variables averaged over longer and shorter periods than 24 h.

   Furthermore, the heat capacity could be modelled to account for potential dynamics related to the heat capacities of the building. Residuals (e_t) with no cross-correlation in the differentiated outdoor temperature ($\text{corr}(e_t,\ T_{a,t} - T_{a,t-1}) \approx 0$), will indicate that no thermal dynamics are left unmodelled. However, auto-correlation in the residuals might still appear, which will indicate time correlated building use. E.g. the building use in one time step is correlated with the next.

2. In Figure 6 it was shown that the wind speed had a tremendous effect on the estimated heat loss. Even though the model predictions improved, it might be worth investigating other ways of modelling the wind's effect on the heat consumption. As the effects are highly dependent on surroundings, building geometry and other unknown factors, it is suggested to model the wind dependence by means of non-parametric methods such as kernel estimation.
3. As the variance of the model residuals are highly dependent on the outdoor temperature they are seemingly heteroskedastic, i.e. not constant. The implication of that is that the standard errors of the model parameters are biased. To improve that, the model should be formulated as a weighted least square problem where the weights are the inverse of the error variance.

Acknowledgments: The authors would like to thank the three projects which have made this research possible by providing financial support: SmartTune founded by The Research Council of Norway [296345]; Renovating Buildings Sustainably (REBUS) [5151-00002B]; and Centre for IT–Intelligent Energy Systems in Cities (CITIES) founded by the Danish Innovation Fund [DSF1305-00027B–CITIES]. Finally, an acknowledgement is given to Sønderborg Fjernvarme for providing the data.

1. Directive 2012/27/EU of the European Parliament and of the Council of 25 October 2012 on energy efficiency (EED). http://data.europa.eu/eli/dir/2012/27/2020-01-01, 2012. Accessed: 2020-04-12.
2. Directive (EU) 2018/844 of the European Parliament and of the Council of 30 May 2018 amending Directive 2010/31/EU on the energy performance of buildings and Directive 2012/27/EU on energy efficiency. http://data.europa.eu/eli/dir/2018/844/oj, 2018. Accessed: 2020-04-12.
3. Madsen, H.; Holst, J. Estimation of continuous-time models for the heat dynamics of a building. *Energy and buildings* **1995**, *22*, 67–79.
4. Madsen, H. *Time series analysis*; CRC Press, 2007.
5. Jiménez, M.J.; Madsen, H.; Andersen, K.K. Identification of the main thermal characteristics of building components using MATLAB. *Building and Environment* **2008**, *43*, 170–180.
6. Madsen, H.; Bacher, P.; Bauwens, G.; Deconinck, A.H.; Reynders, G.; Roels, S.; Himpe, E.; Lethé, G. IEA EBC Annex 58-Reliable building energy performance characterisation based on full scale dynamic measurements. Report of subtask 3, part 2: Thermal performance characterisation using time series data-statistical guidelines, 2016.
7. Lundin, M.; Andersson, S.; Östin, R. Development and validation of a method aimed at estimating building performance parameters. *Energy and Buildings* **2004**, *36*, 905–914.
8. Nielsen, H.A.; Mortensen, S.B.; Bacher, P.; Madsen, H. Analysis of energy consumption in single family houses. DYNASTEE International Workshop on Dynamic Methods for Building Energy Assessment, 2010.
9. Fels, M.F. PRISM: An introduction. *Energy and Buildings* **1986**, *9*, 5 – 18. doi:https://doi.org/10.1016/0378-7788(86)90003-4.
10. Hammarsten, S. A critical appraisal of energy-signature models. *Applied Energy* **1987**, *26*, 97 – 110. doi:https://doi.org/10.1016/0306-2619(87)90012-2.
11. Hammarsten, S. *Estimation of energy balances for houses*; National Swedish inst. for building research, 1984.
12. Dick, J.B.; Thomas, D.; others. Ventilation Research in Occupied Houses. *Journal of the Institution of Heating and Ventilating Engineers* **1951**, *19*, 306–26.
13. ASHRAE. *ASHRAE Guideline 14-2002 – Measurement of Energy and Demand Savings*; American Society of Heating, Refrigerating and Air-Conditioning Engineers (ASHRAE), 2002.
14. Spinoni, J.; Vogt, J.; Barbosa, P. European degree-day climatologies and trends for the period 1951–2011. *International Journal of Climatology* **2015**, *35*, 25–36.
15. Verbai, Z.; Lakatos, Á.; Kalmár, F. Prediction of energy demand for heating of residential buildings using variable degree day. *Energy* **2014**, *76*, 780–787.
16. Sjögren, J.U.; Andersson, S.; Olofsson, T. Sensitivity of the total heat loss coefficient determined by the energy signature approach to different time periods and gained energy. *Energy and Buildings* **2009**, *41*, 801–808.

17. Eriksson, M.; Akander, J.; Moshfegh, B. Development and validation of energy signature method Case study on a multi-family building in Sweden before and after deep renovation. *Energy and Buildings* **2020**, p. 109756.
18. Rohdin, P.; Milic, V.; Wahlqvist, M.; Moshfegh, B. On the use of change-point models to describe the energy performance of historic buildings. The 3rd International Conference on Energy Efficiency in Historic Buildings (EEHB2018), Visby, Sweden, September 26th to 27th, 2018. Uppsala University, 2018, pp. 182–190.
19. Graddage - Hvad er graddage? https://www.teknologisk.dk/ydelser/graddage/hvad-er-graddage/492,3. Accessed: 2020-03-18.
20. Roels, S.; Langmans, J. Highly insulated pitched roofs resilient to air flow patterns: Guidelines based on a literature review. *Energy and Buildings* **2016**, *120*, 10–18.
21. Rasmussen, C.; Frölke, L.; Bacher, P.; Madsen, H.; Rode, C. Semi-parametric modelling of sun position dependent solar gain using B-splines in grey-box models. *Solar Energy* **2020**, *195*, 249–258.
22. Cengel, Y. *Heat and mass transfer: fundamentals and applications*; McGraw-Hill Higher Education, 2014.
23. Bishop, C.M. *Pattern Recognition and Machine Learning (Information Science and Statistics)*; Springer-Verlag: Berlin, Heidelberg, 2006.
24. Madsen, H.; Holst, J.; Lindström, E. *Modelling non-linear and non-stationary time series*; Technical University of Denmark, Department of Informatics and Mathematical Modelling, 2000.
25. Epanechnikov, V.A. Non-parametric estimation of a multivariate probability density. *Theory of Probability & Its Applications* **1969**, *14*, 153–158.
26. Copernicus Climate Change Service. https://climate.copernicus.eu, 2020. Accessed: 2020-04-02.
27. ERA5-Land: data documentation. https://confluence.ecmwf.int/display/CKB/ERA5-Land%3A+data+documentation, 2020. Accessed: 2020-04-02.
28. Bacher, P.; de Saint-Aubain, P.A.; Christiansen, L.E.; Madsen, H. Non-parametric method for separating domestic hot water heating spikes and space heating. *Energy and Buildings* **2016**, *130*, 107–112.
29. Kristensen, K.; Nielsen, A.; Berg, C.W.; Skaug, H.; Bell, B. TMB: automatic differentiation and Laplace approximation. *arXiv preprint arXiv:1509.00660* **2015**.
30. Ypma, J.; Borchers, H.W.; Eddelbuettel, D.; Ypma, M.J. Package 'nloptr', 2020.
31. R Core Team. *R: A Language and Environment for Statistical Computing*. R Foundation for Statistical Computing, Vienna, Austria, 2018.
32. Madsen, H.; Thyregod, P. *Introduction to general and generalized linear models*; CRC Press, 2010.

Characterization of energy dynamics of residential buildings with scarce data

Jaume Palmer Real[a,*], Christoffer Rasmussen[a], Rongling Li[b], Kenneth Leerbeck[a], Ole Michael Jensen[c], Kim B. Wittchen[c], Henrik Madsen[a]

[a] *Department of Applied Mathematics and Computer Science*
Technical University of Denmark

[b] *Department of Civil Engineering*
Technical University of Denmark

[c] *Danish Building Research Institute (SBi)*
Aalborg University

Abstract

Buildings represent a large portion of the total energy consumption and they will serve as a significant thermal storage capacity that can be advantageous for the future energy grid. To utilise this capacity it is necessary to understand building dynamics and develop strategies that could use it. In addition, the methods need to be general enough to be applicable to a significant share of the building stocks. This work proposes a model to characterise the thermal dynamics of thermostatically controlled buildings. The method builds on stochastic differential equation models of the heat transfer in buildings. By selecting the relevant data periods, we are able to reduce the system dimensions while keeping its physical interpretation. Then we use these periods to summarize building heat dynamics into two parameters. This method works with limited data and shows promising results that could be used for categorizing buildings according to their thermal response. Finally, we study how the model output reveals information about the energy flexibility potential of the building.

Keywords: Building characterisation, data analysis, modelling, energy flexibility, demand response

1. Introduction

In order to successfully introduce *demand response* policies that support a large scale transition from fossil fuel to renewable energy based energy supply, there is a need for understanding buildings' thermal dynamics as they will be a key asset in the future flexible energy systems [1].

There are several approaches for estimating the main indicators of the building energy performance: the *heat loss coefficient* (or its inverse, the thermal *resistance*) and the thermal capacity [2]. One option is to estimate them using numerical tools, such as the finite volume methods (FVM)[3]. This approach is computationally expensive, and relies either on simulated data or complex experimental assemble. A different approach was presented as the *co-heating* method [4]. This method is based on simplified heating dynamic equations describing the heat transfer inside a building. This method showed accurate results assessing the energy performance of buildings; however, it needs a meticulous experimental set up to control and measure the temperature, and the experiment can take multiple days. In addition, the measurements are bound to the external conditions during the experimental period. Finally, due to the necessary infrastructure for the assessment, it can only be performed in empty houses. Alternatively, in [5], a new method is introduced that could evaluate the building thermal response in a two days experiment. This represents an improvement from the traditional co-heating method. Nevertheless, it still requires an extensive experimental set up. In addition, there often exists a performance gap between the model prediction using thermal parameters estimated with the above methods and the real operational energy performance of the building [6][7].

For existing buildings, the grey-box model approach is often used, as it takes into account building physics in data-driven modelling. In [8] multiple variations of the lumped resistance-capacity (RC) model are presented and it is shown that such models make it possible to estimate the heat resistance and capacity for different components of the house. This method allows the use of in-situ measures of operative houses. However, this approach still needs a considerable amount of data to decouple the different processes that are part of the energy flow. Also, the complexity of these models can easily grow, burdening the computation. For this reason, and specially when working with large data sets, it is important to use strategies to reduce the order of the models, as suggested in [9]. Even with high quality data, it could be difficult to gain insights into the building dynamics. For instance, during the periods where the building is thermostatically controlled, the impact of external variables over the indoor air temperature might be masked by the effects of the controller, which makes it impossible to estimate the thermal capacities.

*Corresponding Author
Email address: jpre@dtu.dk
Postal Address: Anker Engelunds vej 1, Building 101A, 2800 Kongens Lyngby, Denmark

In this study, we suggest a simple and efficient method to scan buildings and retrieve their thermal characteristics. Specifically, we compute *time constants* of the dynamics of the buildings, which show how fast the heat loss is. Thus, these parameters reveal the potential of that particular building to be used as a flexible storage unit for thermal energy. In order to do so, we identify the night periods with no heat input and fit an auto-regressive model given the measurements from those periods. It is important to emphasize that this method does not require a particular experimental set up: the measurements are taken with in-use buildings.

The considered method is built upon the well known RC models that often are used to describe the thermal dynamics in buildings. There are many studies developing complex RC model configurations as they try to fit in all building components taking part in the heat transfer of buildings [8]. Such studies are based on data sets with a large number of variables, e.g. temperatures of all components, which are not commonly measured in existing buildings. In this work, in an effort to pursue generality, we take the opposite direction to build simple models using scarce data measured in buildings.

Our method is general enough to be applied in a significant portion of the current building stocks. The only requirement is that the buildings follow a *night setback* schedule. This schedule is a commonly used strategy to decrease the energy consumption during night with a lower temperature setpoint than during daytime. Given that Danish buildings are well insulated in general, indoor temperatures do not decrease to the level of causing discomfort to residents during night-time. During these hours, it can be assumed that there is no influence on the indoor temperature from the users as they most likely are asleep. There is also no solar irradiation affecting the indoor temperature. Thus, the pattern of temperature decreasing during nights can be understood as a building fingerprint that explains its energy storage performance.

1.1. Outline

This study is divided in three sections, followed by a conclusion. In Section 2, the mathematical background of the applied method is explained; the model structure and its physical interpretation are discussed, and the method for data selection and the concepts used in the flexibility analysis are described. Section 3 describes the data used in the study. Section 4 shows the modelling results, an interpretation of the system dynamics and the estimated values of time constant for a number of buildings. In Section 5, a simulation framework is used to show how the building intrinsic parameters affect the time constants, and how the time constants provide information about the flexibility potential of the building.

2. Method

In this section, it is shown how an auto-regressive model is derived from a stochastic RC model. The purpose of this approach is to offer a physical interpretation of the parameters. Then, it is explained how the time constants are computed using the *transfer function* form of the auto-regressive model.

Our proposed method only works for specific periods of time; here, the method to select the relevant data periods is presented.

Finally, the concepts of *flexibility index* (FI) and *flexibility function* (FF) that we use in section 5 are presented.

2.1. Building as a second order dynamical system

Equation (1) describes a general continuous time model for heat dynamics inside of a building. It tracks the temporal evolution of two main variables inside the building: the indoor air temperature, T_i, and the thermal mass temperature, T_m. The model is represented as a second order linear stochastic differential equation (*SDE*) system. This system has three main external inputs: the outdoor temperature, T_a, the global solar irradiation, I_g, and the space heating input, Φ_h. This model has five parameters $\{R_i, R_a, C_i, C_m, A_w\}$ that are described in Table 1. The uncertainty in the system is captured by the stochastic term, $d\omega_i \ \forall i \in [1, 2]$. This term represents a Wiener process with incremental variances $\sigma_i^2 \ \forall i \in [1, 2]$.

The external inputs affect only the indoor air temperature; in turn, there is a heat transfer between the indoor air and the thermal mass. For a detailed description of the model, see [10].

$$\begin{cases} dT_i = \dfrac{1}{C_i}\left(\dfrac{1}{R_i}(T_i - T_m) - \dfrac{1}{R_a}(T_i - T_a) + \Phi_h + I_g A_w\right)dt + \sigma_1 d\omega_1 \\ dT_m = \dfrac{1}{R_i C_m}(T_m - T_i)\,dt + \sigma_2 d\omega_2 \end{cases} \tag{1}$$

Since the system in Equation (1) is linear, it can be re-written using the following matrix form,

$$\begin{pmatrix} \frac{dT_i}{dt} \\ \frac{dT_m}{dt} \end{pmatrix} = \begin{pmatrix} \frac{1}{R_i C_i} & -\left(\frac{1}{R_a C_i} + \frac{1}{R_i C_i}\right) \\ \frac{-1}{R_i C_m} & \frac{1}{R_i C_m} \end{pmatrix} \begin{pmatrix} T_i \\ T_m \end{pmatrix} + \begin{pmatrix} \frac{1}{R_a C_i} & \frac{1}{C_i} & \frac{A_w}{C_m} \\ 0 & 0 & 0 \end{pmatrix} \begin{pmatrix} T_a \\ \Phi_h \\ I_g \end{pmatrix} + \begin{pmatrix} \sigma_1 & 0 \\ 0 & \sigma_2 \end{pmatrix} \begin{pmatrix} \frac{d\omega_1}{dt} \\ \frac{d\omega_2}{dt} \end{pmatrix}. \tag{2}$$

Now, the model variable is a vector: $\boldsymbol{T}(t) = (T_i(t),\ T_m(t))^\top$, and $\boldsymbol{U}(t) = (T_a(t),\ \Phi_h(t),\ I_g(t))^\top$ is the vector of external inputs. We can write Equation (2) in a compact form as

$$\frac{d}{dt}\boldsymbol{T}(t) = \boldsymbol{A}\boldsymbol{T}(t) + \boldsymbol{B}\boldsymbol{U}(t) + \boldsymbol{\Sigma}\frac{d}{dt}\boldsymbol{\omega}(t)\,, \tag{3}$$

where $\boldsymbol{A}$ is the design matrix describing the dynamic characteristics of the building, and $\boldsymbol{B}$ describes how the input variables enter the system. Finally, $\boldsymbol{\omega}(t) = (\omega_1(t),\ \omega_2(t))^\top$ is the stochastic term, and $\boldsymbol{\Sigma}$ is the matrix of incremental variances.

In this work, only the indoor air temperature, T_i is observed. It is important to notice that the system described in Equation (1) has no measurement equation. Thus, we assume that the error measurements for T_i are small enough to be disregarded.

	Description	Units
R_i	Thermal resistance: indoor air ↔ thermal mass	[K/kW]
R_a	Thermal resistance: indoor air ↔ outdoor air	[K/kW]
C_i	Thermal capacity of the indoor air	[kWh/K]
C_m	Thermal capacity of the thermal mass	[kWh/K]
A_w	Effective window area	[m^2]
σ_1	Incremental variance of T_i	[K]
σ_2	Incremental variance of T_m	[K]

Table 1: Model parameters

2.2. From SDEs to auto-regressive

As shown in [10], the system in Equation (3) can be discretized by integrating over a sample interval, $[t, t+s)$, where s is the *sampling time* of the system. Then, assuming that the input ($U(t)$) is constant in the sampling interval, the system can be re-written as

$$\boldsymbol{T}(t+s) = \boldsymbol{\Phi}(s)\boldsymbol{T}(t) + \boldsymbol{\Gamma}(s)\boldsymbol{U}(t) + \boldsymbol{\nu}(t,s)\,. \tag{4}$$

If the sampling time is small enough, the discrete time model structure will capture the relevant dynamics described in the continuous case. We can fix the sampling time to an arbitrary time unit, $s = 1$, and find he explicit expression for the elements describing Equation (4):

$$\boldsymbol{\Phi}(s=1) = \exp(\boldsymbol{A}\cdot 1) = \begin{pmatrix} \phi_{11} & \phi_{12} \\ \phi_{21} & \phi_{22} \end{pmatrix} \tag{5}$$

$$\boldsymbol{\Gamma}(s=1) = \int_0^{s=1} \exp(\boldsymbol{A}\cdot r)\boldsymbol{B}dr = \begin{pmatrix} \Gamma_{11} & \Gamma_{12} & \Gamma_{13} \\ \Gamma_{21} & \Gamma_{22} & \Gamma_{23} \end{pmatrix} \tag{6}$$

$$\boldsymbol{\nu}(t, s=1) = \begin{pmatrix} \nu_t^{(1)} \\ \nu_t^{(2)} \end{pmatrix} \text{ with } \nu_t^{(i)} = \mathcal{N}(0, \varsigma_i^2)\ \ \forall i \in [1,2]\,. \tag{7}$$

In this case, $\boldsymbol{\Phi}$ describes the discrete dynamics of the system and $\boldsymbol{\Gamma}$ the effect from the external inputs. The vector $\boldsymbol{\nu}$ is normally distributed white noise with zero mean and variance $\varsigma_i^2\ \forall i \in [1,2]$, and it accounts for the stochastic part of the system.

This study is focused on the dynamics of buildings with a night heating setback. Thus, if there is no solar irradiation and the space heating is turned off, the input term can be simplified to $\boldsymbol{U} = (T_a, 0, 0)^\top$. It is then possible to write discrete explicit expressions for the indoor air temperature and the thermal mass:

$$\begin{cases} T_{t+1}^i &= \phi_{11}T_t^i + \phi_{12}T_t^m + \Gamma_{11}T_t^a + \nu_t^{(1)} \\ T_{t+1}^m &= \phi_{21}T_t^i + \phi_{22}T_t^m + \Gamma_{21}T_t^a + \nu_t^{(2)}\,, \end{cases} \tag{8}$$

where the notation has been changed to highlight the discrete nature of the expression.

Now, we want to remove the thermal mass variable from the model, since we do not have access to its associated temperature measurements. In order to do this, the equations from Equation (8) have been merged, adjusting the index t,

$$T_{t+1}^i = \phi_{11}T_t^i + \phi_{12}\overbrace{(\phi_{21}T_{t-1}^i + \phi_{22}T_{t-1}^m + \Gamma_{21}T_{t-1}^a + \nu_{t-1}^{(2)})}^{T_t^m} + \Gamma_{11}T_t^a + \nu_t^{(1)}\,. \tag{9}$$

For houses with regular heating schedules that have not been ventilated recently, the temperature of the thermal mass should be very similar to the temperature of the indoor air [11]. Assuming that $T_{t-1}^i \approx T_{t-1}^m$, it is possible to reduce the expression to Equation (10), where all variables are observed

$$\begin{aligned} T_{t+1}^i = \phi_{11}T_t^i + (\phi_{12}\phi_{21} + \phi_{12}\phi_{22})T_{t-1}^i + \\ \Gamma_{11}T_t^a + \phi_{12}\Gamma_{21}T_{t-1}^a + \nu_t^{(1)} + \phi_{12}\nu_{t-1}^{(2)}\,. \end{aligned} \tag{10}$$

During winter, the outdoor temperature varies slowly during night, as shown in Figure 1. For a small enough time step, there is little change from one measurement to the next one, i.e. $T_t^a \approx T_{t-1}^a\ \forall t$. This simplification allows us to reduce the system complexity:

$$T_{t+1}^i = \overbrace{\phi_{11}}^{\theta_1}T_t^i + \overbrace{(\phi_{12}\phi_{21} + \phi_{12}\phi_{22})}^{\theta_2}T_{t-1}^i + \overbrace{(\Gamma_{11} + \phi_{12}\Gamma_{21})}^{\omega}T_t^a + \nu_t^{(1)} + \phi_{12}\nu_{t-1}^{(2)}\,, \tag{11}$$

where the final model parameters, $\{\theta_1, \theta_2, \omega\}$, have been introduced.

Finally, a new stochastic variable is defined, $\nu_t = \nu_{t-1}^{(1)} + \phi_{12}\nu_{t-2}^{(2)}$. Since $\nu_t^{(1)}$ and $\nu_t^{(2)}$ are independent and normally distributed with zero mean $\forall t$; the new variable, ν_t, is also normally distributed with zero mean. Thus, it is possible to write the final model as the following *auto-regressive* model,

$$T_t^i = \theta_1 T_{t-1}^i + \theta_2 T_{t-2}^i + \omega T_t^a + \nu_t\,, \tag{12}$$

where the time index, t, has been adjusted for clarity.

2.3. A system with two time constants

In order to study the heat loss between the indoor air and the outdoor air, we focus on the interaction between T_t^i and T_t^a from model (12) using the *transfer function* as shown in Equation (13),

$$T_t^i = \underbrace{\frac{\omega}{1 - \theta_1 B - \theta_2 B^2}}_{H(B)} T_t^a\,, \tag{13}$$

where B is the *backshift operator* defined as $B^j X_t = X_{t-j}$ for an arbitrary dynamic random variable $\{X_t\}$, and $H(B)$ is the transfer function of the system (12). As described in [12], in order to compute the time constant of the system (12) it is necessary to find the roots of the denominator of $H(B)$, i.e., the *poles* of the system. In this case, there are two poles, q_1 and q_2, as the

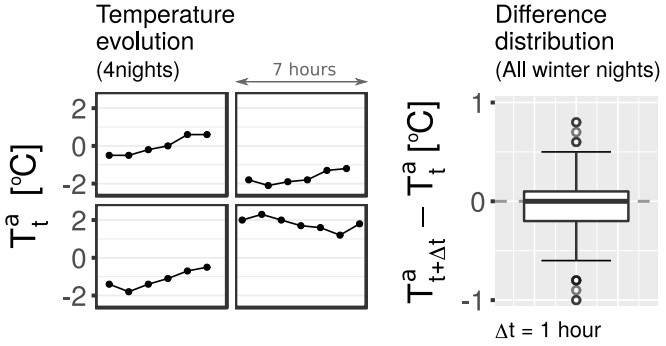

Figure 1: The lattice on the left shows the temporal evolution of the outdoor temperature for 4 different nights. The hourly evolution reveals a slow variation of the temperature. On the right, the temperature hourly differences for all winter nights is shown. The differences are always mild and concentrated around 0.

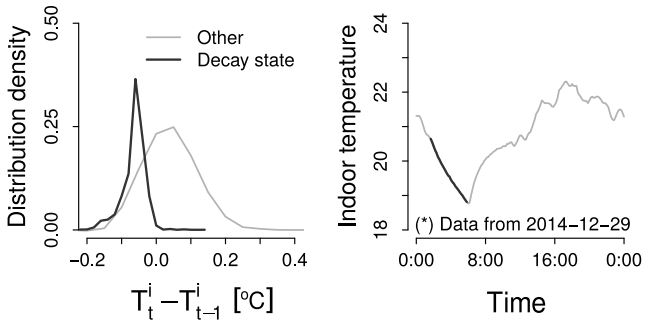

Figure 3: An example of the distribution of decay points for one arbitrary building with night setback. The figure on the left shows the distribution of data points d_t. It shows that the decay states distribute different from other states. The figure on the right shows the indoor temperature of a day with the thicker curve indicating the decay period selected using the HMM method.

polynomial in the denominator is order two. Finally, each pole has an associated time constant which can be computed as:

$$\tau_j = \frac{s}{\ln|q_j|} \quad \forall j \in [1,2]\,. \tag{14}$$

iHence, in this case there are two different time constants that characterize the heat flow between indoor air and outdoor air. Each of these time constants has time units and they reveal information about the two processes described by the initial system (2) as illustrated in Figure 2. In general, when the heating is shut down, there is a quick heat transfer between the indoor air and the thermal mass due to the low thermal capacity of the air. As described in [10], the initial heat transfer is captured by the parameter τ_1. The heat transfer between indoor air and outdoor air is the second process, which is characterized by τ_2, is slower and will dominate the dynamics as indoor temperature keeps decreasing [10].

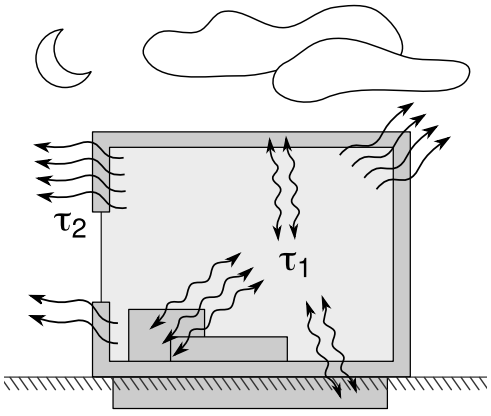

Figure 2: This figure shows a schematic of the two main processes governing the heat flow between indoor air and outdoor air. First, the heat transfers from the indoor air to the thermal mass, which is characterized by τ_1. Meanwhile, the heat is transferred from the indoor air to the outdoor air; this is characterized by τ_2.

2.4. Identification of night setback temperature curves

All studied houses showed a temperature decay of the indoor air during night hours. There are multiple methods to detect decaying behaviours. One example is the use of statistical change point detection of the transformed signal of interest as done in [13]. In the present work, we use hidden Markov model (HMM) on the indoor temperatures observations to identify the periods of night setback. The same method was used in [14] to detect various human activities using CO_2 concentration data.

HMM consists of two components: an observed sequence of states and a corresponding hidden state sequence. The current state only depends on the state of the previous observation. The states change according to a fitted transition matrix, which is a matrix providing the probability of a state change. For each state, the observations are Gaussian, and the mean and variance depends on the state. In order to identify the states, a new variable was created to be used as an input for the model:

$$d_t = T^i_t - T^i_{t-1}\,. \tag{15}$$

Tracking the distribution of d_t we were able to spot the periods where the temperature is decaying. The Viterbi algorithm is used to find the most likely sequence of states given a sequence of observed data points. A mathematical representation of HMM and the Viterbi algorithm are provided in [15].

The data points corresponding to times when temperature is continuously dropping are distributed differently from the rest, as can be seen in Figure 3. For some houses, the selected periods are not only the long night decaying periods, but also shorter decays during the day time due to the dead-band of the controller. The long night decays are selected with a threshold. This threshold was computed by clustering all d_t data points into two based on the length of the period. In general, it is concluded that this process is sufficient to reveal the natural split between short daytime decays (unwanted) and long night decays, although the time spans vary from house to house because of their different time constants.

2.5. Flexibility index (FI) and Flexiblity Function (FF)

In order to gain insights into the relationship between the time constant and the flexibility of a building, the concepts of the Flexibility Index (FI) [16] and the Flexibility Function (FF) [17] are used. The FI quantifies the savings caused by allocating energy consumption in a flexible way. This is done by comparing the cost of the consumption adapted to a flexible control signal (*flexible cost*) and the cost of the consumption if the system was unaware of the price signal (*ignorant cost*). The idea behind the FI can be seen in equation (16). FI = 1 characterizes a building with an extreme flexibility potential, and FI = 0 the opposite.

$$\mathrm{FI} = 1 - \frac{\text{Flexible cost}}{\text{Ignorant cost}} \tag{16}$$

The *flexibility function* (FF) describes the energy that is available at a particular moment, or *state of charge*; and the resources it can allocate and how it can allocate them before reaching the system limits. This function provides information about how an energy system would adapt to changes in the control signal or changes in its state of charge. Moreover, an energy system has limited resources that can be turned on/off in case of need, and the rate at which it is able to move those resources depends on the dynamic characteristics of each system. The theoretical foundation for these two concepts, FI and FF can be found in [16] and [17].

When calculating the FI and FF in this work, the energy systems are buildings that have their indoor air temperature controlled with an MPC controller. Then, the state of charge translates into the room temperature: the building is completely charged when the indoor temperature reached its daily maximum inside the comfort boundaries and vice-versa. The heating input is controlled by a price signal which is built using the wind speed data. This price signal can also be based on other data and be used for other purposes such as peak shaving, or lowering CO_2 emissions.

3. Data description

This study is based on measurements from a set of 39 Danish single family houses in the Middelfart region in Denmark. All of the buildings were built between 1960s and 1980s. In this paper they are identified by 5 digit numbers. There are two data sets. The first data set contains the indoor temperature measurements from December 2014 to December 2015. We used only the winter data between December 2014 and March 2015 and with a 10 min resolution. The second data set consists of hourly outdoor temperature values. This data set has been selected to match the dates of the indoor temperature data. In order to compensate the lower resolution, the hourly values are interpolated using linear interpolation. This interpolation are carried under the assumption that, during winter nights the fluctuations in outdoor temperature are slow.

For better presentation and visualization of the work, the rest of this work focuses on three buildings with representative decay patterns, as shown in Figure 4. It can be noticed that building B shows a sharp decay at the beginning and then a slower decaying trend; building A has a fast temperature drop; and building C has a shorter decay curve, but still steeper than the curve in B. For all the three example buildings, the decaying patterns are consistent during different nights. For instance, it can be noticed that in building C, the decaying trend is similar in every case even though the initial indoor temperature varies.

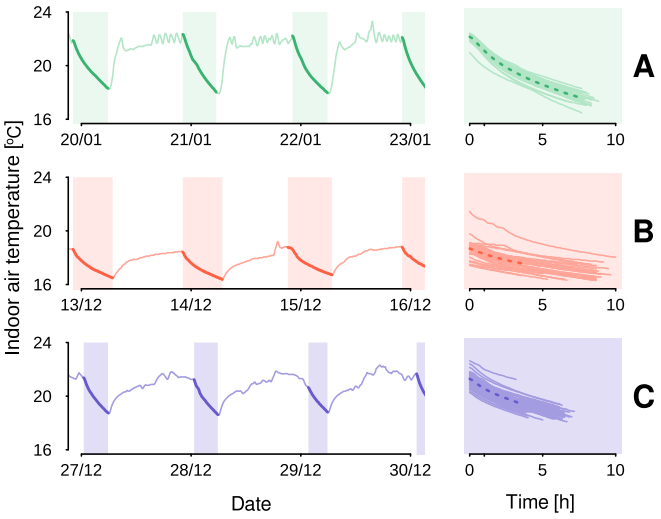

Figure 4: Temperature decays of three example houses. On the left it can be seen a 4 day period for three different households (A, B, C). The area corresponds to the decay hours is highlighted. On the right, the lines corresponding to all decay periods present in the time series of three month data are shown. This visualization reveals that each building has its clear decay pattern. The mean of every decay pattern is plotted as the darker dashed line.

4. Results and discussions

This section presents the results from the modelling process. These results are also discussed to understand how the thermal dynamics are captured. Afterwards, this section offers a classification of the buildings based on their time constants.

4.1. Model validation

The parameters from the model in Equation (12) were estimated using *ordinary least squares* (OLS) method in the first place, since the model is linear and the noise is supposed to be normally distributed. This revealed that the term related to the outdoor temperature, ω, was not significant in most of the tested buildings. However, as presented in Section 2, the outdoor air temperature affects the heat loss dynamics. This impact is more noticeable at the end of the decaying curve, when the heat exchange with the outdoor air is more significant than the heat exchange with the thermal mass. In addition, at the beginning of the decay trend, the assumption that $T_t^i \approx T_t^m$ is less accurate, since in reality both temperatures converge over time. Lastly, at the beginning of the decaying curve there is a higher chance than the users might be awake. All these reasons suggest that the noise over time, $\{\nu_t\}$, might not be independent. In fact, the

system noise is expected to be at its maximum at the beginning of the decay and then continuously decrease over time. In order to cope with this, the *weighted least squares* (WLS) method was used, where the models is fitted giving a specific weight to each observation. These weights are proportional to the time since the temperature decay started, given that the observations become more reliable as time moves forward. The following equation was used for the weighting process,

$$w(k) = 1 - \frac{1}{\alpha + (1-\alpha)k} \quad \text{with } 0 \leq \alpha \leq 1\,, \tag{17}$$

where k is an integer counting the number of measurements since the beginning of the decay period and α is a tuning parameter. Notice that $w \in [0, 1]$, it is minimum right at the beginning of the decay period, $w(1) = 0$, and then grows monotonically. The parameter α defines how fast is this growth; i.e. how the weights are distributed along the decay period. Notice that this parameter depends on the time constants of the building and it could be fine-tuned in a recursive method in order to fit a particular building. Thus, it is important to remark that this weighting function is not unique and it could be adapted to each case.

		Estimate		**Std. error**		**p-value**	
		OLS	WLS	OLS	WLS	OLS	WLS
Building **A**	$\hat{\theta}_1$	1.768	1.779	0.016	0.017	<1E-16	<1E-16
	$\hat{\theta}_2$	-0.769	-0.781	0.016	0.017	<1E-16	<1E-16
	$\hat{\omega}$	4.3E-4	3.3E-4	2.5E-4	2.9E-4	0.09	0.26
Building **B**	$\hat{\theta}_1$	1.111	1.273	0.024	0.023	<1E-16	<1E-16
	$\hat{\theta}_2$	-0.113	-0.275	0.024	0.023	<1E-16	<1E-16
	$\hat{\omega}$	1.8E-3	1.5E-3	2.4E-4	2.6E-4	<1E-16	<1E-16
Building **C**	$\hat{\theta}_1$	1.624	1.707	0.015	0.015	<1E-16	<1E-16
	$\hat{\theta}_2$	-0.625	-0.708	0.015	0.015	<1E-16	<1E-16
	$\hat{\omega}$	2.8E-4	1.3E-4	1.4E-4	1.7E-4	0.05	0.45

Table 2: Table comparing the parameter estimates for each example building. The table shows the results using WLS using function in (17) compared with the OLS.

Table 2 compares the results after fitting the model with OLS and WLS. Notice how, after using WLS, the p-values of the parameter estimates are below 0.1, confirming that the parameters are highly significant. It can also be noticed that the estimate of the contribution of the outdoor temperature, $\hat{\omega}$, increased significantly using the WLS, especially for houses A and C, which confirms the influence of the external conditions.

Figure 5 reveals that the ordinary residuals, after using the WLS, behave like white noise regardless of the outdoor conditions. It also can be seen that most of the residuals are in the $[-0.1, 0.1]$ range, which show the accuracy of the one-step prediction. The values that fall outside of this range are from the beginning of the decaying periods when it is expected to be noisy, as explained previously. The distribution of residuals can be seen in Figure 6, which shows that the errors are small and centered around zero.

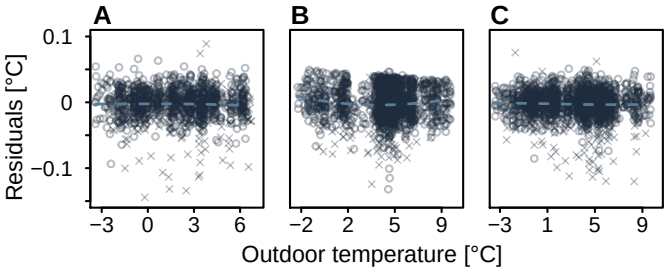

Figure 5: The figure shows the relationship between the outdoor air temperature and the residuals using the WLS model. The residuals from the first hour of each decay are marked with an x. The trend of all residuals is plotted as a dashed line. It is shown that there is no effects from the outdoor air to the residuals, since all residuals are centered around 0 and evenly spread across all temperature range.

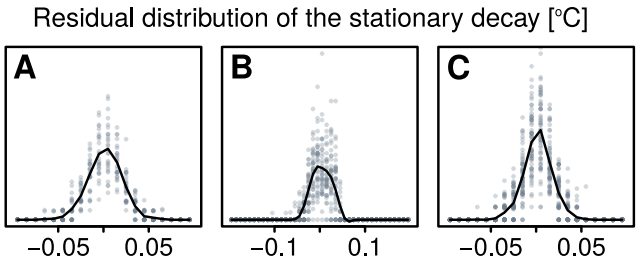

Figure 6: Distribution of residuals after using the WLS model. The figures include all the decays in the time span of interest ignoring the first hour of each decay. For each building a smooth curve was plotted for better visibility.

In Figures 5 and 6 it is not possible to see if the residuals are biased on a daily basis. For this reason, the evolution of residuals are plotted for 3 arbitrary days picked at random for each example building in Figure 7. It can be seen from this figure that in all cases the prediction follows the same pattern. At the beginning of the decay period, the model is over-predicting so the residuals are negative and larger. This bias comes from the simplification $T_t^i \approx T_t^m$, since it forces the stochastic part to account for the changes in T_t^m. However, shortly after the start the residuals converge to white noise, since $T_t^i \to T_t^m$ quickly [10]. These transient periods are the cause of the larger residuals seen in Figure 5.

4.2. Time constant of 39 houses

The time constants of the three example buildings are shown in Table 3; it is important to notice that τ_1 is expressed in minutes, whereas τ_2 is expressed in hours. These results can be compared with the qualitative behaviour observed in Figure 4. In comparison with the other two, building B shows a flatter decay trend at the end of each night. This translates into having $\tau_2^{(B)} > \tau_2^{(C)} > \tau_2^{(A)}$. In addition, the numerical results in Table 3 reveal that building B loses energy swiftly at the beginning of the decay, which is different from house A where the heat transfer between the indoor air and thermal mass also has a significant contribution to the decay period.

Moreover, the results of house A were compared with the results computed using a different method presented in [18], where a more complex auto-regressive model (including heating data) was fitted using a time span of 11 days. The difference

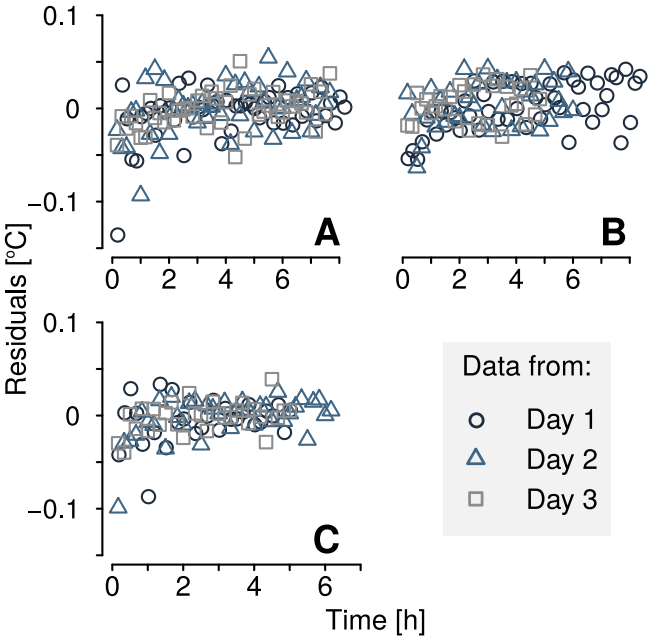

Figure 7: Temporal evolution of the residuals during each decay period. Only 3 decays are plotted for better visibility. It can be seen that the ordinary residuals are larger at the beginning of the decay period, but shortly after there is no observable trend.

	τ_1 [min]	τ_2 [hour]
Building **A**	38.8	36.7
Building **B**	4.6	65.6
Building **C**	21.5	49.7

Table 3: Results for the example houses. For house A the results are compared with the results obtained using a different model described in [18] which are shown in brackets.

between results were smaller than an 8%. In addition, it is important to remark that it is possible to further reduce the difference between the results by fine-tuning the weighting function (17), specifically for house A.

The simplicity and generality of this method has allowed us to use it in the total pool of 39 buildings and to categorize their parameters τ_1 and τ_2. Figure 8 shows the distribution of the time constants for all 39 buildings. It can be observed that: i) the long time constant, τ_2, has the same order of magnitude as the time constant one would expect from Danish family houses [19, 20]; ii) for the short time constant, τ_1, all values are shorter than one hour, which highlights the importance of a small time step to capture this part of the dynamics. From Figure 8 it can be seen that the 39 buildings are clustered in groups. K-means clustering method [21] was used and as the result three clusters are marked in the figure. Note that each of the three selected buildings falls in different categories, confirming the qualitative differences in their heat loss dynamics spotted at the beginning of this work.

In figure 8, one can get a clear picture at the available classes of buildings in the studied set. On the short time constant axis,

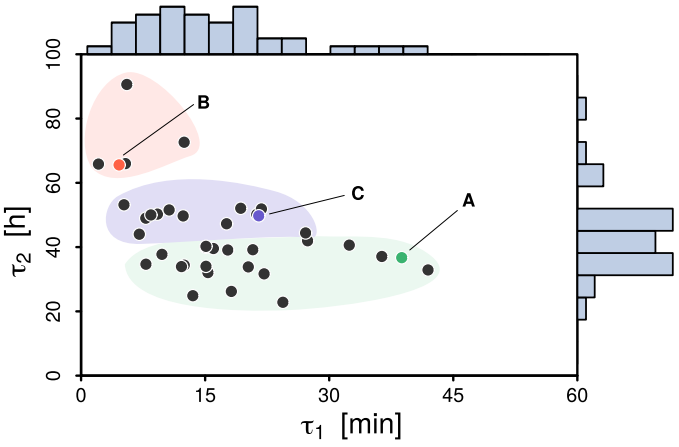

Figure 8: Scatter plot of the two time constants for 39 buildings. As the result of a K-means clustering, three regions are marked in the figure. In each cluster, the example house is highlighted.

τ_1, the time values are mostly scattered, contrarily to the τ_2 where most of the values lie around the bottom half of the plot. Furthermore, it can be seen how the main driver for clustering comes from the long time constant τ_2, i.e., the three main regions reveal three different steps along the y-axis. The difference among three clusters could be due to the difference in insulation level, house size, the amount of thermal mass, etc. However, to investigate this level of detail would require more information about these houses which we do not have, thus it was left out of the current study.

5. Flexibility assessment

This section shows the application of using the computed time constants of the house to reveal its energy flexibility potential based on simulations.

The simulations are based on the model described in (2) and carried out using different parameter values to gain an overview of their impact. Specifically, the parameters of the indoor air heat resistance, R_i, and the capacity of the indoor air, C_i, were fixed; while the heat resistance between the indoor and outdoor air, R_a, and the capacity of the thermal mass, C_m, were changed in each simulation. The first two parameters depend on intrinsic magnitudes of the air; meanwhile, the last two parameters are easier to interpret and they characterize magnitudes from a building that are easier to correct through renovation. Finally, the only external output of the model, the outdoor temperature, follows an arbitrary pattern that matches the order of magnitude of danish winter time.

For each combination of parameters, a time series of four days was simulated with a night-setback schedule. Using those values, the time constants were computed, and the results can be seen in Figure 9. It can be seen that both parameters are directly proportional to the value of the time constants, as expected. Three cases have been highlighted (H1, H2 and H3) to represent three buildings with a different parameter combination. These have been chosen to further assess the effects of the parameters on the building thermal performance.

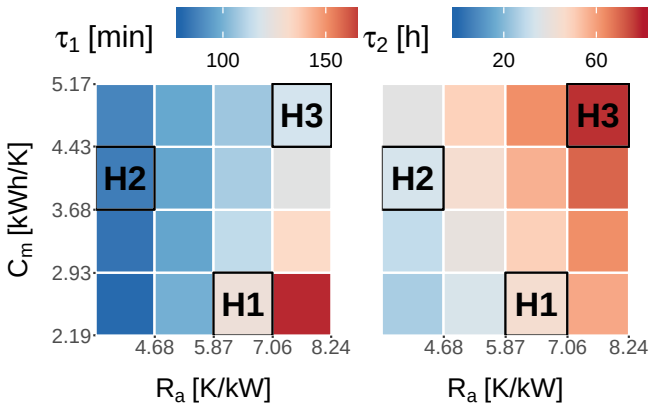

Figure 9: Heat map of the resulting time constant values for different values of C_m and R_a. The increase of R_a yields higher values of both time constants. The increase of C_m benefits only τ_2. H1, H2 and H3 represent three different houses with different characteristics.

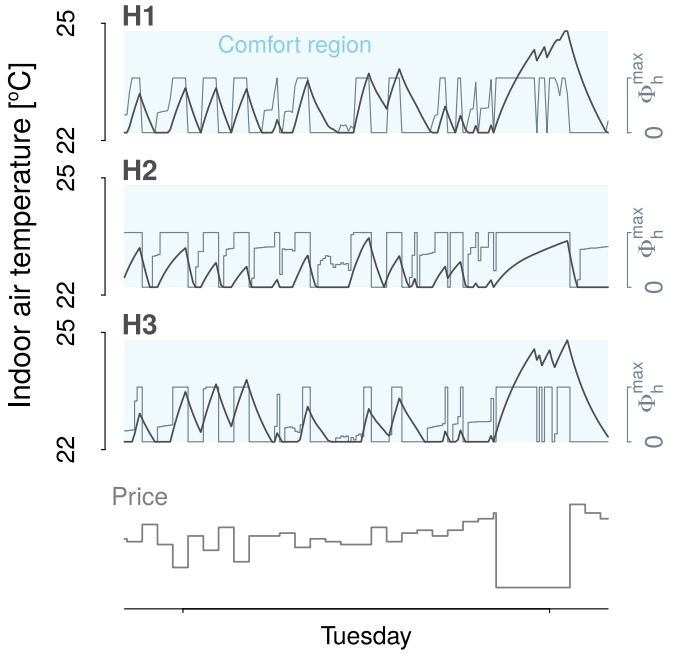

Figure 10: Simulation of the flexible control scenario for the representative houses. The indoor temperature follows the schedule of the heat supply, which is controlled by the price signal at the bottom of the plot. It can be seen that H3, due to its high thermal resistance and capacity, is able to keep indoor temperature within the comfort region with the heating system running for a shorter time comparing to other two houses.

Figure 11: Heat map of the resulting Flexibility Index value for different values of C_m and R_a. It can be noticed that the main driver for the FI is the thermal resistance. H1, H2 and H3 represent three different houses with different characteristics.

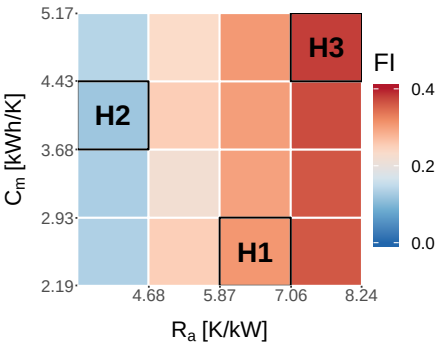

For each combination of parameters shown in Figure 9, we simulated four days using two different control strategies: one ignores the price signal and only tries to keep the indoor temperature inside a defined comfort region. In the other simulation, the heating system is controlled using *Model Predictive Control* (MPC), where the control signal is the price of energy. The MPC controller tries to minimize the operation cost using the aforementioned price signal, while also keeping the indoor temperature within the comfort region. These two strategies represent the *Ignorant Cost* and *Flexible Cost* as described in Section 2.

For the simulations, we created a price signal that depends on the wind speed during an arbitrary period of time, to simulate a system powered by wind energy. The energy price decreases as the wind speed increases, assuming that energy supply is always sufficient.

The results of the controlled simulation for the three highlighted cases (H1, H2, H3) are presented in Figure 10. It can be seen that when the price is low, the heating is switched on and when the price increases the heating is turned off until the temperature approaches the lower boundary. It can be noticed that the heating in H3 could be turned off for a longer time due to the building's higher time constants. The indoor air temperature in building H2 never reached the upper boundary of the comfort region due to higher heat losses.

It can be seen in Figure 11 that the resistance R_a is the key parameter to increase savings using the flexibility of the building.

Lastly, the results of the flexibility function of the three houses can be seen in Figure 12. This figure summarizes how the three different houses react to a change in the two main drivers of the energy consumption: the room temperature and the energy price. This reaction is presented as the deviation from the ignorant consumption; i.e. the consumption of the system ignoring the flexible price signal. The three houses display a similar response to the state of charge: a flat section, where the system ignores the variations of the indoor temperature, and two steep curves at the ends of the temperature range. When the room temperature reached the low boundary, the system was forced to increase consumption to maintain comfort; similarly, the system decreases consumption when the room temperature reached the high boundary. It can be noted that H3 is able to stay on the flat region for a wider temperature range than the other two. This suggests that H3 is more resilient to changes in the room temperature than the H1 and H2.

The response to energy price follows a decreasing curve for the three houses. For lower prices, the power demand of H1 is below H2 and H3. As the price increases, H3 consumption gets below H1 and H2. This result is in line with the results in Figure 11, and confirms that the high value of the FI of H3 is the result of avoiding expensive prices. The savings of H1 compared to H2 come mainly from decreasing consumption during cheaper hours.

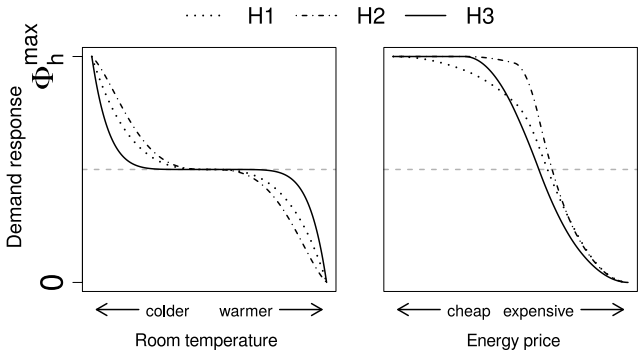

Figure 12: Results of the flexibility function. The figure shows that the energy demand is affected by changes on the state of the system (room temperature) and the variations in the control signal (energy price). The dashed line represents the regular consumption if it was not affected by the price signal and indoor temperature; the scale is normalized so this dashed line lies right in the middle. The curve above the dashed line means that the consumption is increased, and vice-versa. It can be seen that H3 is more resilient to changes in the room temperature, and it is able to consume less during the most expensive hours.

6. Conclusions

This study shows how one can obtain insights from the thermal characteristics of a building with limited data. First of all, Hidden Markov Models were used to select the relevant periods to extract measurements from the periods with a night-setback. By focusing on these long decaying periods, it has been possible to transform a complete physical system to a simple autoregressive structure. This model structure only uses the indoor air temperature and the outdoor air temperature, which are normally easy to measure.

It is important to use a high resolution sampling to capture the fast dynamics inside the building. In this study, 10-minute time interval data was used. This small time step made it possible to reduce the model structure by taking advantage of the slow changes and small variations of the outdoor temperature. Additionally, the resulting time constants highlighted the importance of choosing a small time step. The only external input of our model, the outdoor temperature, was measured hourly and was transformed to 10-minute data using linear-interpolation taking advantage of its slow dynamics.

It is critical to understand the physical meaning of the model. In order to fit the model, it was necessary to take into account the decreasing trend of the system noise during the night by using the WLS method. Only by doing this, all parameters in the model became significant. This is important because the temperature decay inside of a building could potentially be caused by other factors: such as the air mixing in the same room, or a heat transfer to a much colder contiguous room. The significance of the parameter corresponding to the outdoor air confirms that the indoor air decreases due to a heat loss to the outdoor air, which validates our model assumptions.

This method offers a general and computationally light model that can be scaled to a large portion of the existing building stocks. By visualizing the two time constants for all 39 buildings as shown in Figure 8, three clusters of buildings with similar characteristics could be easily found. In this study, we used a simple clustering method to identify those building clusters.

The usability of each time constant depends on the specific problem. The long time constant is the one that gives a clearer picture of buildings' characteristics for thermal storage and it is also closely related to the classical time constant used in building physics. However, the short time constant could be relevant for studying short term flexibility and indoor comfort.

Finally, it is confirmed that there is a clear connection between the time constants and the flexibility potential of buildings. It is shown that the long time constant dominates the potential usage of a house as a energy storage unit in a flexible energy grid. Moreover, using the FF, it is possible to assess qualitatively the flexible response of the simulated houses. In conclusion, the results show that a house with higher values of τ_1 and τ_2 can implement more flexible strategies.

Acknowledgements

This work is part of the CITIES project (nr. DSF1305-00027B) as well as the *Smart Energi i Hjemmet* project. I would like to thank my colleague Rune G. Junker for many valuable discussions and for sharing his work and vision on the future of flexible energy systems.

Bibliography

[1] K. Foteinaki, R. Li, A. Heller, and C. Rode. Heating system energy flexibility of low-energy residential buildings. *Energy and Buildings*, 180:95–108, 2018.

[2] V. Dimitriou, S. K.Firth, T. M.Hassan, T. Kane, and M. Coleman. Data-driven simple thermal models: The importance of the parameter estimates. *Energy procedia*, 78:2614–2619, 2015.

[3] C. Luo, B. Moghtaderi, H. Sugo, and A. Page. A new stable finite volume method for predicting thermalperformance of a whole building. *Building and Environment*, 43:37–43, 2008.

[4] G. Bauwens and S. Roels. Co-heating test: A state-of-the-art. *Energy and Buildings*, 82:163–172, 2014.

[5] F. Alzetto, G. Pandraud, R. Fitton, I. Heusler, and H. Sinnesbichler. Qub: A fast dynamic method for in-situ measurement of the whole building heat loss. *Energy and Buildings*, 225:175–182, 2018.

[6] S. Roels, P. Bacher, G. Bauwens, S. Castano, M. J. Jiménez, and H. Madsen. On site characterisation of the overall heat loss coefficient: Comparison of different assessment methods by a blind validation exercise on a round robin text box. *Energy and buildings*, 153:179–189, 2017.

[7] D. Cali, T. Osterhage, R. Streblow, and D. Müller. Energy performance gap in refurbished german dwellings: Lesson learned from a field test. *Energy and buildings*, 127:1146–1158, 2016.

[8] P. Bacher and H. Madsen. Identifying suitable models for the heat dynamics of buildings. *Energy and Buildings*, 43:1511–1522, 2011.

[9] S. Goyal and P. Barooah. A method for model-reduction of non-linear thermal dynamics of multi-zone buildings. *Energy and Buildings*, 47:332–340, 2012.

[10] H. Madsen and J. Holst. Estimation of continuous-time models for the heat dynamics of a building. *Energy and buildings*, 22:67–79, 1995.

[11] K. Foteinaki, R. Li, A. Heller, M. H. Christensen, and C. Rode. Dynamic thermal response of low-energy residential buildings based on in-wall measurements. *E3S Web of Conferences*, 111, 2019.

[12] H. Madsen. *Time series analysis*. Chapman Hall, 2008.

[13] C. Rasmussen, R. Relan, and H. Madsen. Identification of Occupancy Status by Statistical Change Point Detection of CO_2 Concentration. In *2018 IEEE Conference on Control Technology and Applications (CCTA)*, pages 1761–1766. IEEE, 2018.

[14] S. Wolf, J. Kloppenborg Møller, M. A. Bitsch, J. Krogstie, and H. Madsen. A markov-switching model for building occupant activity estimation. *Energy and Buildings*, 183:672–681, 2019.
[15] C. Bishop. *Pattern Recognition and Machine Learning*. Springer, 2006.
[16] R. Gronborg Junker, A. Gashem Azar, R. Amaral Lopes, K. Byskov Lindberg, G. Reynders, R. Relan, and H. Madsen. Characterizing the energy flexibility of buildings and districts. *Applied energy*, 225:175–182, 2018.
[17] R. G. Junker, C. S. Kallesøeb, J. Palmer Real, B. Howard, A. Lopes, and H. Madsen. Stochastic nonlinear modelling and application of price-based energy flexibility. submitted, 2020.
[18] S. Nordli. Statistical methods for optimizing renovation projects. Master's thesis, DTU Compute, 2018.
[19] P. Bacher, H. Madsen, H. A. Nielsen, and B. Perers. Short-term heat load forecasting for single family houses. *Energy and Buildings*, 65:101–112, 2013.
[20] J. Le Dréau and P. Heiselberg. Energy flexibility of residential buildings using short term heat storage in the thermal mass. *Energy*, 111:991–1002, 2016.
[21] T. Hastie, R. Tibshirani, and J. Friedman. *The elements of statistical learning*. Springer, 2009.

Technical University of Denmark
Department of Applied Mathematics and Computer Science

Richard Petersens Plads, Building 324
2800 Kgs. Lyngby
Tel.: +45 4525 3031

www.compute.dtu.dk